ABSTRACT

Title of dissertation: MODELING CRUTCH COMPENSATION OF HIP ABDUCTOR WEAKNESS AND PARALYSIS

James Rocco Borrelli, Doctor of Philosophy, 2011

Dissertation directed by: Henry W. Haslach Jr.
Department of Mechanical Engineering

Hip abductor weakness or paralysis is prevalent in the half a million cases of low level spinal injuries in the United States alone. Crutches are often used as an ambulatory aid by individuals with this type of permanent disability. This study investigates whether using a crutch with a wide stance, as opposed to a conventional vertical stance, returns the hip rotation and pelvic obliquity to a more normal range of motion for individuals with weak or paralyzed hip abductors.

An inverse dynamics six link model of the body with ten degrees of freedom and a forward dynamics six link model with six degrees of freedom were used to simulate the swing and stance phases of gait with hip abductor weakness/paralysis while using either compensatory motions (hip hiking or lateral displacement of the torso) or crutches. The forward dynamics model characterizes the effect of hip abductor weakness on the gait kinematics hip rotation and pelvic obliquity. The model also characterizes the effect of compensatory motions and crutch use on gait with paralyzed hip abductors. The inverse dynamics model calculates the time

varying body weight that must be supported on a contralateral crutch to achieve normal gait kinematics even with paralyzed hip abductors.

The forward dynamics model predicts that hip abductor paralysis reduces the range of pelvic obliquity and increases the range of hip rotation. The model also predicts that compensatory motions and crutch use restore the range of motion of hip rotation and pelvic obliquity in gait with paralyzed hip abductors to more normal. The inverse dynamics model predicts that the portion of body weight that must be supported on a crutch for normal gait kinematics with paralyzed hip abductors is lowered by using a wide crutch stance.

This study suggests that contralateral crutch use replaces the need for the compensatory motions hip hiking and lateral displacement of the torso while restoring the range of hip rotation and pelvic obliquity to more normal ranges in an individual with weak or paralyzed hip abductors. Furthermore, angling the crutch side-to-side restores the range while supporting less body weight on a contralateral crutch.

MODELING CRUTCH COMPENSATION OF HIP ABDUCTOR WEAKNESS AND PARALYSIS

by

James Rocco Borrelli

Dissertation submitted to the Faculty of the Graduate School of the
University of Maryland, College Park in partial fulfillment
of the requirements for the degree of
Doctor of Philosophy
2011

Advisory Committee:
Dr. Henry Haslach Jr.
Dr. Balakumar Balachandran
Dr. Amr Baz
Dr. Bongtae Han
Dr. Adam Hsieh
Dr. Arthur Johnson

Table of Contents

List of Figures

Chapter 1

Introduction

A crutch was developed based on the observation that people with weak or paralyzed hip abductors and other muscle disabilities use a wide base of support when using crutches to provide a horizontal force on the body. This raises the question, can crutches lower the energy cost of gait for those with permanent gait related muscular disabilities. This thesis develops a framework for characterizing pathological motions associated with a specific muscle weakness, identifying compensatory motions that may reverse the effects and evaluating whether a crutch works in the same way.

Supporting weight on a contralateral crutch at an angle is hypothesized to reduce pathological gait kinematics, reduce compensatory motions and/or reduce the work required in the gait of individuals with weak or paralyzed hip abductors more than a vertical crutch. Hip abductor weakness is exhibited by an individual with low-level spinal damage and spina bifida. In addition to varying degrees of hip abductor paralysis, these individuals also typically have other muscle weakness. In order to investigate the effect of only hip abductor weakness or paralysis on gait kinematics, several mathematical models are developed. Models are used as opposed to a human study because hip abductor weakness or paralysis does not occur without other accompanying muscles weakness.

When a person is disabled their walking pattern is changed. Some of these changes in the walking pattern may be compensatory. Individuals with weak hip abductors, exhibit the compensatory motions of excess lateral trunk movement and hip hiking. Hip hiking raises the swing-side hip right before swinging their leg. Lateral displacement of the trunk, compensates for a hip stabilization deficiency and both are less desirable motions because they lead to back and knee pain.

Three models, one static planar model and two three-dimensional dynamics models, are used to investigate the hypothesis. The models are used to characterize the effect of hip abductor weakness on gait motions and calculate the work done. The effect of the compensatory motions, torso tilting and hip hiking, on gait motions and the work done on a gait with weak or paralyzed hip abductors is characterized. Then the effect of crutch use and angled crutch use on a gait with weak or paralyzed hip abductors are compared. The work done is the metric used to compare angled (side-to-side) crutch use versus vertical crutch use.

1.1 Background

Walking is a complex coordination of motions and while there is still some debate over the relative importance of the various motions, the most important motions of walking have been identified. These motions are referred to as the determinants of gait and are reviewed in this section. The determinants of gait identify important motions, especially of the pelvis, that should be included in the models developed in chapter 2. The effect of hip abductor weakness on gait is reviewed.

Existing dynamic models of normal walking and crutch walking are reviewed and discussed in the context of determinants of gait.

1.1.1 Determinants of Gait

Normal walking is a periodic motion in which the three phases: stance, double support and swing are repeated. The phases of gait are classified by whether or not a foot is in contact with the ground. Double support is the brief period in the gait cycle when both feet are on the ground. Following double support one limb is in its stance phase while the other limb is in its swing phase. Then another period of double support follows and the limbs reverse roles. Walking is the repetition of the aforementioned motions (Fig. 1.1a). Figure 1.1b shows, in order, double support, left leg stance, double support, left leg swing and double support. The scale on the x-axis in Fig. 1.1b is the percent of one gait cycle.

The three planes that divide the body front to back, left to right and top to bottom are the frontal, sagittal and horizontal planes, respectively. The three planes are shown in Fig. 1.2.

Although the majority of the walking motions occur in the sagittal plane, normal walking occurs in three-dimensions simultaneously. In fact, Eng and Winter show that significant work is done by the pelvis in the frontal plane [20] and Apkarian et al. [5] highlight the importance of three-dimensional analysis in the study of pathological gait.

There are few walking models and no crutch walking models that take into

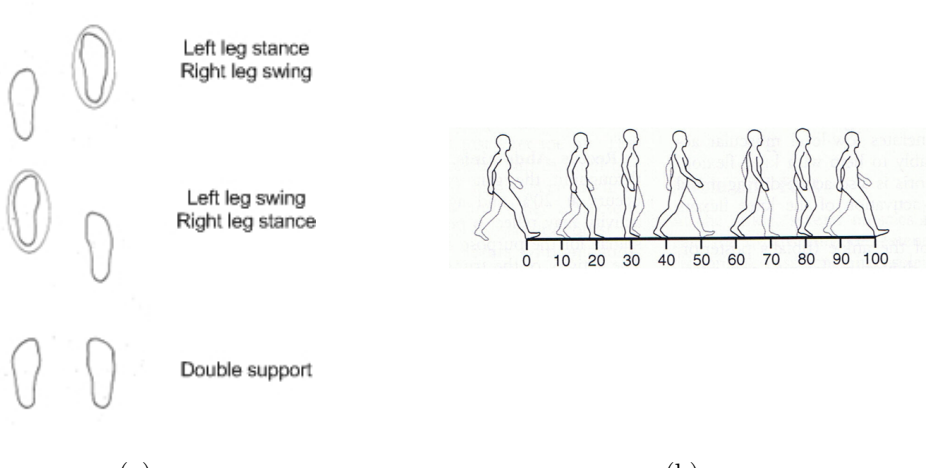

(a) (b)

Figure 1.1: (a) Coordination of the feet during normal walking. The circled foot is in the air at the time. Normal gait is a cyclic repetition of the three phases shown [37]. (b) Profile of normal walking [48].

account all the motions that have been identified as key walking motions. Saunders et al. [63] define the fundamental determinants of normal human gait as body motions that minimize the displacement of the center of gravity (COG) of the body. Saunders et al. hypothesize that the body attempts to follow the most energy efficient trajectory of the COG. The most energy efficient trajectory of the COG, assumed by Saunders et al., is a sinusoidal pathway of low amplitude in the frontal and sagittal planes.

Ignoring all determinants of gait leads to compass gait, the simplest model of bipedal gait without any determinants of gait is called compass gait. Compass gait models bipedal walking with two massless links representing the legs. The links are pinned at one end and there is a mass at the pin representing the COG. When the system "walks" the trajectory of the "hip", viewed as the point where the legs are

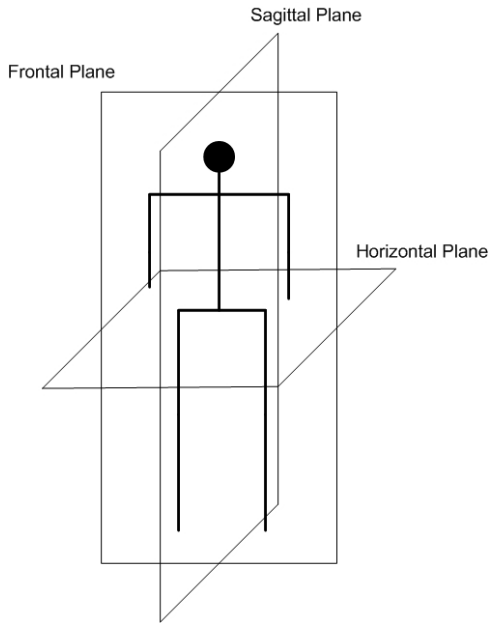

Figure 1.2: The body is divided into three planes. Diagram of the sagittal, horizontal and frontal planes.

joined, follows a sinusoid that abruptly changes direction half-way through the gait cycle (Fig. 1.3). Saunders et al. [63] claim that the addition of determinants of gait to "compass gait" decreases the energy necessary to walk by minimizing the undulation of the COG.

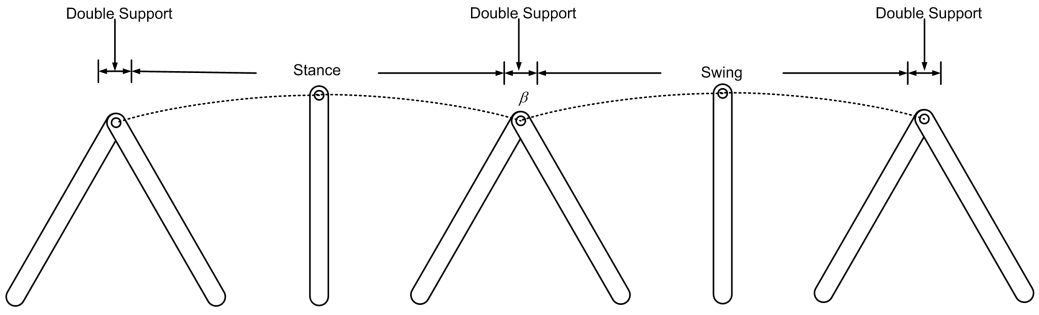

Figure 1.3: One complete gait cycle performed by a model with a so-called compass gait.

The first determinant, pelvic rotation, refers to the pelvis rotating around the

vertical axis in the horizontal plane. The pelvis rotates alternately to the left and to the right during gait resulting in an increase in stride length. Pelvic rotation reduces the angle of the intersecting arcs of the trajectory of the COG at β (Fig. 1.3). Pelvic rotation is thought to reduce the energy required for walking by making the change in direction of the COG less abrupt during double support.

The second and third determinants, pelvic list (or pelvic obliquity) and knee flexion in the stance phase, reduce the height of the COG during the stance and swing phases of gait. Pelvic list or obliquity refers to the pelvis rotating around the axis that coincides with the direction of travel in the frontal plane. During normal gait the pelvis tilts downward on the side opposite of the weight bearing limb, thus lowering the COG. Knee flexion in the stance phase is simply a bending of the knee thereby reducing the height of the COG.

The fourth and fifth determinants, foot and knee interactions (counted twice), increase the vertical displacement of the COG at double support and during the middle of the swing and stance phases. The last determinant of gait, lateral displacement of the pelvis, does not reduce the vertical displacement of the COG. Lateral displacement of the pelvis moves the COG over top of the stance leg, balancing the body. The theory of Saunders et al. assumes a redundancy of motions that accomplish the same goal. That is, if one determinant of gait is lost, exaggeration of another can compensate for the change in gait because of the redundancy of the determinants.

1.1.2 Compensation

Individuals with spinal injuries in the lower region of the spine have weak or paralyzed hip abductors as well as other muscle weakness. Hip abductor weakness affects the muscles that control the lateral displacement of the pelvis. The energy expenditure required for gait with this type of disability is greater than for a non-disabled individual who walks upright [72]. The increase in energy expenditure is attributed to excessive trunk and pelvic motion in addition to excessive knee flexion compared to normal gait [17], [18]. Duffy et al. [17], [18], Pandy and Berm [55], [57] and Rose [61] highlight the importance of functioning hip abductors in non-disabled individuals. Duffy et al. speculate that the increase in energy expenditure in individuals with weak or paralyzed hip abductors is due to excessive pelvic and trunk motions which are thought to be an attempt to compensate for weak or paralyzed hip abductors (Fig. 1.4a). The excessive motions are called compensatory motions. These deviations from normal gait put excess stress on the knee in the frontal plane by inducing a varus moment, shown in Fig. 1.4b and consequently these individuals frequently develop knee pain [73]. The aim of a crutch designed for this weakness is to modify a gait with weak or paralyzed hip abductors so the compensatory motions are not needed.

Neumann [47], [48] develops simple static planar model that explains the mechanism behind torso tilting, hip hiking and crutch use. Figure 1.5b idealizes the forces on the pelvis while standing still and tilting over the stance leg. The forces are from the hip abductor (HAF), the joint reaction force (JRF) and five-sixth of the body

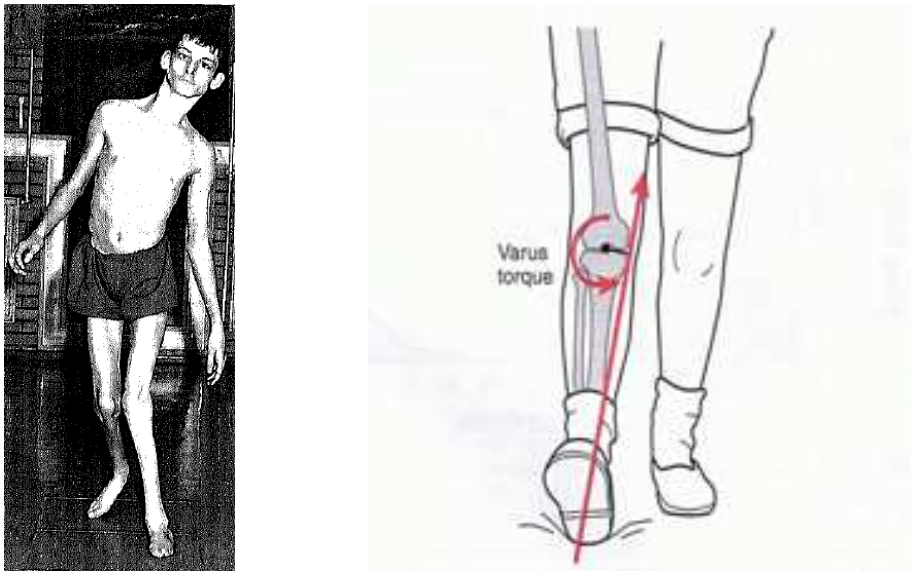

(a) (b)

Figure 1.4: (a) Picture of an individual with weak hip abductors exhibiting the characteristic gait utilizing a hiked up hip and excessive lateral torso displacement [18]. (b) A varus moment at the knee in the frontal plane [48].

weight (BW), assuming the stance leg weight one-sixth of the body's total weight.

Summing the moments around the point where the femur meets the pelvis allows computation of the hip abductor moment required for equilibrium, with positive couples shown clockwise,

$$\sum M_o = 0 : HAF \cdot D_1 - \frac{5}{6} BW \cdot D_2 = 0. \tag{1.1}$$

The distance between the point where the HAF is applied and where the femur meets the pelvis is D_1 and the distance between where the femur meets the pelvis and the line of action of the BW is given by D_2.

This model explains the mechanism of compensation in individuals with weak or paralyzed hip abductors. Hiking up the pelvis and tilting the torso moves the

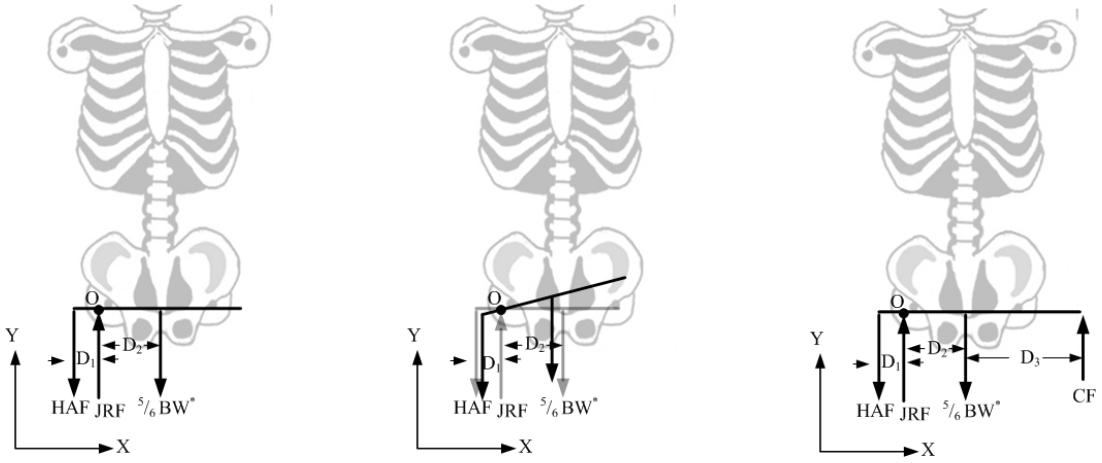

(a) (b) (c)

Figure 1.5: (a) Force balance of the pelvis while standing still. (b) Force balance of the pelvis while standing still and tilting over the stance leg. (c) Static model while using a contralateral cane. The weight of the stance leg is not included and its weight is assumed to be 1/6 of the total body weight, leaving 5/6 BW acting through the COG. Skeleton picture from the web [29].

COG over the stance leg which reduces the hip abductor moment and the muscle force. By moving the trunk over the stance leg, the moment arm, D_1 in Fig. 1.5b, is reduced. A reduction in the moment arm that the BW acts through reduces the couple that must be developed by the hip abductors for static equilibrium. Johnson [31] comes to the same conclusion through an analysis of the stance leg.

The inclusion of a contralateral cane modeled as an external cane force (CF). The force is assumed to be a distance D_3 from where the femur meets the pelvis. The moment balance including a crutch force is given by

$$\sum M_o = 0 : HAF \cdot D_1 - \frac{5}{6} BW \cdot D_2 + CF \cdot D_3 = 0. \tag{1.2}$$

There is an inversely proportional relationship between the crutch force and the hip

abductor force. The more weight supported by a contralateral crutch, the lower the moment that must be generated by the hip abductors.

This model predicts a contralateral cane can reduce the need for the hip abductor muscles while standing still but really any assistive device such as a crutch would suffice. The model predicts almost a 50% reduction in the hip abductor moment necessary to stabilize the pelvis when supporting 10% of the body weight on a contralateral cane while standing still compared to not using a cane. This model shows the importance of the moment arm through which relevant forces act and any increase in CF or D_3 reduces the hip abductor moment for constant $BW \cdot D$. Cane use, which creates a similar loading as forearm or crutches, has been shown to reduce the moment needed by the hip abductors to stabilize the hip in the frontal plane. Vankoski et al. [71] show a decrease of excessive or unnecessary pelvic motions among individuals with low level spina bifida who use forearm crutches resulting in a more "normal" gait compared to those who do not.

1.1.3 Crutches

Crutches are used when a person is unable to walk normally or support the weight of their body. Before discussing walking models and crutch walking models, some crutch terminology is presented. The two main types of crutches are axillary (Fig. 1.6a) and forearm crutches (Fig. 1.6b). The user supports him or herself by carrying weight through the hands and bracing the device against their body. The axillary support of axillary crutches is braced against the ribs. The forearm cuff of

forearm crutches is braced against the forearm (Fig. 1.6). Supporting weight by resting the underarm on the axillary support can result in axillary nerve damage and so is not recommended by physical therapists.

(a) (b) (c) (d)

Figure 1.6: Pictures of an axillary crutch (a), a forearm crutch (b) and the *Strutter*© (c). The new crutch (d) has a novel footpad and axillary support. The footpad and axillary support (4) allow the support tube (1) to rotate around a longitudinal pin (2) in the frontal plane. A torsional spring (3) provides a restoring force to return the device to the vertical [32], [33].

Except when completely vertical, crutch and cane footpads are constantly deformed while in use. Too wide a crutch angle in the frontal plane may cause the footpad of axillary or forearm crutches to deform, altering the contact pattern, and slip. This problem is overcome through a novel improvement on conventional crutch design, [32], [33] shown in Fig. 1.6d. The footpad and axillary support are

implemented on the *Strutter*© (Fig. 1.6c). The Strutter has shown some promise in reducing energy expenditure compared to axillary crutches for individuals who had undergone knee or hip replacement [50].

The improved device (Fig. 1.6d) maintains a constant orientation between the footpad and the ground because the support shaft pivots about the footpad in the forward and side-to-side directions. The device also maintains a constant orientation between the axillary pad and the body because the axillary pad rotates around the forward and side-to-side directions also. Internal springs and dampers provide a restoring force which returns the device to the vertical position. A benefit of the the axillary pad maintaining a constant orientation with the body is reduced chaffing where the axillary pad on a normal crutch is slipping and sliding between the arm and ribcage.

1.1.3.1 Crutch Gait

Crutch gaits are characterized by the way the legs and crutches are coordinated. A crutch gait is chosen depending on the level of the difficulty a person has walking. A person who needs minor weight bearing assistance would use a two-point alternating gait, shown in Fig. 1.7a. A two-point alternating gait moves pairs of contralateral leg and crutch, left leg with right crutch and right leg with left crutch.

A person who has very limited weight supporting ability might use an ankle-knee-foot orthosis (AFKO) or some other type of orthosis in order to successfully

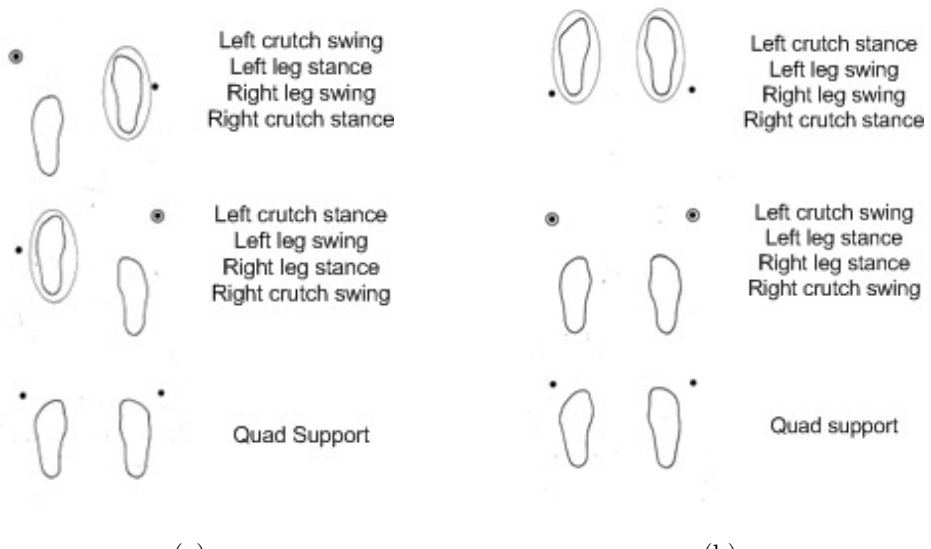

(a) (b)

Figure 1.7: (a) Coordination of the feet and crutches of a two-point alternating crutch gait. The circled foot or crutch is in the air at that time. (b) Coordination of the feet and crutches of a two-point alternating crutch gait. The circled foot or crutch is in the air at that time [37].

walk with crutches. AFKOs and other orthoses lock various lower body limbs in place. AFKOs for example prevent the ankle and knee from rotating. AFKOs compensate for a lack of weight bearing ability and crutches are used for stability. The most common crutch gait used with AFKO type orthoses is a swing-through gait (Fig. 1.7b).

1.1.4 Walking Models

The models analyzed in the following sections, despite having shortcomings, are able to model some feature of gait. The models are all rigid link systems, the dynamics of which are dealt with in chapter 2. The literature survey indicates that

the more links contained in the model, the more determinants of gait the model represents. The few studies of crutch walking are overly simplified and employ swing-through crutch gait which effectively eliminates most determinants of gait. Normal walking models are summarized because of the lack of crutch models, and solution techniques for the models are reviewed.

1.1.4.1 Crutch Walking Models

The majority of studies of crutch walking focus on a type of swing-through gait used by individuals with a short-term disability such as an ankle sprain or broken leg [40], [16], [24], [62]. In addition, these are empirical studies using human subjects but the overall conclusion of these studies is that crutch use results in a decreased speed of locomotion and an increase in energy expenditure. Shoup et al. [64] compared the motions of various body segments when using axillary crutches with a swing-through gait to the motions of normal walking and found that the vertical fluctuations of the joints in normal walking, are smallest for those joints that are the closest to the floor. The opposite is true for swing-through crutch gait. Noreau et al. [49] developed a dynamic model describing walking with forearm crutches to determine the joint torques at various joints in the body during swing-through crutch gait. To ease solution of the model, the gait is assumed to be bilaterally symmetrical so that the use of constraint equations are avoided. The gait is assumed to be planar, meaning that there is no side to side undulation. The forearm crutches are modeled as rigid links that are fixed to the forearm.

These studies showed that paraplegic users exhibit different kinematic and kinetic profiles from normal walking. Using a swing-through gait imposes a loss of the determinants of gait, pelvic rotation and list, and lateral displacement of the pelvis. However, it is unlikely that crutches can compensate for lost determinants when using a swing-through gait. This is because swing-through effectively eliminates pelvic rotation, tilt and lateral displacement of the pelvis.

1.1.4.2 Passive/Ballistic Walking

Passive and ballistic models of walking typically model no more than three (four with some creative assumptions) determinants of gait. The models generally have no more than four rigid links, up to two for the stance leg and up to two for the swing leg. These types of models are unactuated and only model the swing/stance phases of gait. Double support is assumed to happen instantaneously. Passive and ballistic models are differentiated by the source of the energy used by the model for locomotion. In passive walking, the model walks/falls down a gentle slope, the energy is input by gravity. The energy is supplied by the initial velocities in ballistic walking. One interesting conclusion from ballistic modeling is that as the number of determinants of gait represented in the model is increased, the walking speed/step period relationship becomes more realistic. An interesting conclusion from passive walking is that the models settle into a stride length depending on the slope of the walkway. This suggests that a model should be sufficiently complex and that even the simplest of models have some optimal gait rhythm.

McMahon [43] and Mochon and McMahon [45] analyze the contribution of four of the determinants of gait by developing a ballistic model with only one determinant of gait, hip flexion and then add three more (knee flexion, knee and ankle interaction and pelvic rotation). Mochon and McMahon claim hip flexion is a determinant of gait but hip flexion is not one given by Saunders et al. [63]. Mochon and McMahon also assert that pelvic rotation only affects gait by increasing step length if the pelvic rotation is slow enough. The two models are shown in figs. 1.8a and 1.8b.

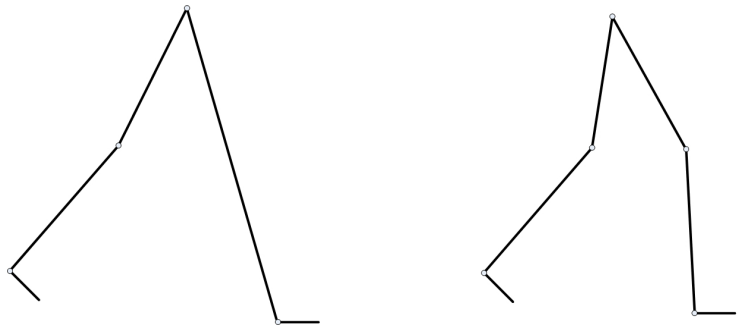

(a) (b)

Figure 1.8: (a) Triple inverted pendulum model of the swing phase of gait used by Mochon and McMahon [45] in their ballistic walking model. (b) Triple inverted pendulum model of the swing phase of gait used by Mochon [45].

The initial joint angles and velocities are chosen so that the swing-leg comes to full extension at the moment the heel strikes the ground. The model with only one determinant (Fig. 1.8a) predicts step period, joint angles and horizontal ground reaction forces (GRF) that are in reasonable agreement with experiment. The GRFs are the reaction forces between the foot and the ground. The GRF in the vertical direction could be described as the vertical reaction force of an inverted pendulum swinging freely through an unstable equilibrium. These results suggest that the

horizontal GRFs are influenced in part by the motion of the swing leg and that the lack of determinants of gait affect the model's ability to predict the vertical GRF. Mochon and McMahon conclude that introducing pelvic list and stance-leg plantar flexion would improve the model's agreement with experimental results by increasing the predicted vertical GRF right after toe-off and just before heel-strike.

McGeer [41] shows that a passive walking machine can produce a periodic gait when walking down a slope by using gravity to make up for the energy lost at heel strike. The model by McGeer is an inverted double pendulum. McGeer concludes that the model approaches a velocity that is a function of the slope the model is walking down irrespective of the initial conditions. McGeer concludes that the addition of an extended torso can assist with postural control and stability. For example the torso can be held in a backward recline to provide a braking torque while traveling down a steep incline. Passive and dynamic models provide only a peek into gait because they can be used to explain the increase in step period in the absence of determinants of gait.

1.1.4.3 Normal Walking Models

Almost all gait models assume the body is comprised of segments that are modeled as rigid links connected by joints. The joint torques are modeled as instantaneously available torque generators. In normal and crutch walking models, an important factor is the number of links included in the model. The more links a model contains, the more determinants of gait that are modeled. The explanation

given by researchers for the discrepancy between their models and experimental results is commonly as proposed by Saunders et al. [63] that the loss of a determinant of gait results in an exaggeration of the remaining determinants of gait.

Chow and Jacobson [11] develop a planar walking model with seven segments that includes swing, stance, and double support. The model is two-dimensional so it does not model pelvic obliquity, rotation, or lateral displacement of the pelvis. Chow and Jacobson claim their model predicts results that agree well with the kinematics found in experiments by the Eberhart-Inman group at Berkeley [19].

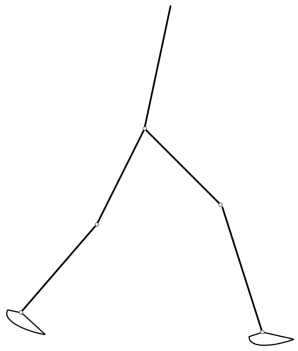

Figure 1.9: Five link planar dynamic model of walking used by Chow and Jacobson [11] and Ren et al. [59].

Ren et al. [59] model normal human walking as a two-dimensional seven segment configuration similar to that of Chow and Jacobson [11], Fig. 1.9. Ren et al. also consider the double support portion of gait. The model predicts motions that are in good agreement with experimental data over most of the gait cycle. However the model predicts a greater range of pelvic rotation before and after double support compared to experiments reported in literature. Ren et al. hypothesize that the difference in results from the model and experiment is caused by the model being

limited to the sagittal plane and because the arms and pelvis are not included in the model.

The previously mentioned two-dimensional models all lack at least three determinants of gait, pelvic list, pelvic rotation, and lateral motion of the pelvis. The lack of a pelvis and the accompanying determinants of gait cause an exaggeration of foot and knee interaction and knee flexion. It is clear that a pelvis must be included to more accurately model normal or disabled human gait.

Anderson and Pandy [3] develop a three-dimensional dynamic optimization model which consists of 10 segments with 23 degrees of freedom (Fig. 1.10). The 10 segments include two thighs, two shanks, two feet, and a pelvis. The mass of the head, arms, and torso are lumped in one mass above the pelvis. The pelvis is a single rigid link with the torso pinned in the middle of it. The ankle is represented as two links. The ankle first rotates about rear link then the front link. This approximates how a person's foot rolls on the heel then the ball of the foot.

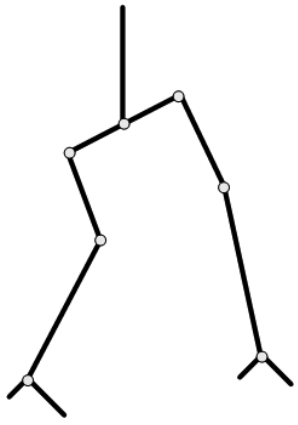

Figure 1.10: Ten link dynamic model of walking used by Anderson and Pandy [3].

Anderson and Pandy's [3] model includes all of the determinants of gait except

lateral displacement of the pelvis. However discrepancies remain between the model predictions and experimental gait results. The rotation of the pelvis about the vertical axis is exaggerated near heel-strike, a motion not demonstrated by subjects in experiment. The model includes additional motions such as lateral bending, axial rotation, and flexion and extension of the torso which are not included in other models. An interesting feature of the model is that it predicts axial rotation of the torso opposite to that of the pelvis as if the model had arms even though the model has no arms to create such a rotation.

Chow and Jacobson and Ren et al. [59] assume that the muscles are instantaneously available actuators. This means that the torque at a joint can go from no torque to an arbitrary value with no transition. Hill [28] showed that there is a problem with modeling muscles as immediately available actuators because muscle response is better modeled as a differential equation, to capture the transient effects. However the increase in complexity may not justify the numerical cost. Anderson and Pandy [3] model the muscles of their walking model as differential equations and the simulation time is in hundreds of hours. Ren et al. [59] assume that muscles are instantly available and their simulation times were in tens of minutes. The simplifying assumption of muscles being instantaneously available actuators turns out to be a more conservative estimate [12]. Davy and Audu [12] analyze the swing phase of normal walking using a three link swing-leg model with three degrees of freedom (Fig. 1.11). The system is actuated by nine muscles that are modeled by a contractile element in series with an elastic element. The contractile element is the active part of the model to correspond to muscle contraction. Davy and Audu solve

the model using two methods, the muscle force is modeled as an instantaneously available actuator or as a differential equation for comparison. Their findings indicate that assuming the joint torques are instantaneously available actuators results in higher joint torques, which can be viewed as a conservative approach.

Figure 1.11: Dynamic model used by Davy and Audu [12]. This model is only valid for the swing phase.

1.1.5 Solution Techniques

The equations of motion that govern model behavior relate the configurations history, i.e. the kinematics, to the external force-couple system, i.e. the system kinetics. In order to solve the equations of motion, either the kinematics or the kinetics must be known and the other quantity is solved for. These two techniques are called inverse and direct dynamics, respectively. When the external force-couple system is known and the configurations history is solved for, this method is called forward dynamics. The next two sections give examples of the solution technique

used later in the thesis.

1.1.5.1 Forward Dynamics

A model of the swing leg with actuation is shown in Fig. 1.12. Defining the

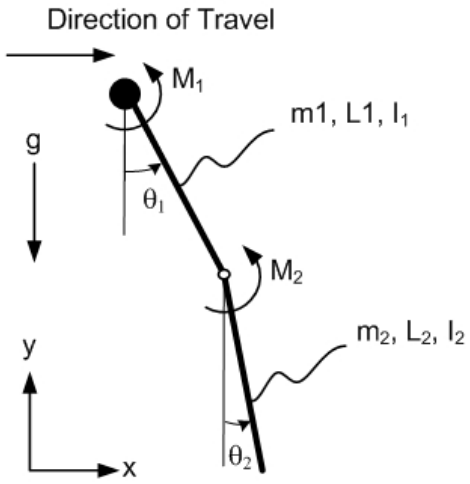

Figure 1.12: Double pendulum model of the swing leg.

torque at the hip by M_1 and the torque at the knee by M_2, the equations of motion are

$$\left(I_1 + m_1 a^2 + m_2 L_1^2\right)\ddot{\theta}_1 + m_2 b L_1 \cos\left(\theta_1 - \theta_2\right)\ddot{\theta}_2 + m_2 b L_1 \sin\left(\theta_1 - \theta_2\right)\dot{\theta}_2^2$$

$$+ \left(m_2 L_1 + m_1 a\right) g \sin\theta_1 = M_1 - M_2 \tag{1.3}$$

and

$$m_2 b L_1 \cos\left(\theta_1 - \theta_2\right)\ddot{\theta}_1 + \left(I_2 + m_2 b^2\right)\ddot{\theta}_2 - m_2 b L_1 \sin\left(\theta_1 - \theta_2\right)\dot{\theta}_1^2$$

$$+ m_2 g b \sin\theta_2 = M_2 \tag{1.4}$$

where θ_1 and θ_2 are the angle of the thigh and shank relative to the vertical. The mass and length of the thigh and the shank are m_1, m_2, L_1, and L_2 respectively. The mass moment of inertia of the thigh and shank are I_1 and I_2. The distance from the "hip" to the middle of the thigh is given by a and the distance from the knee to the mid-point of the shank is b. Average joint torques at the hip and knee, taken from Neumann [48], are curve fit with a 4^{th} order Fourier series for the purpose of substituting into eqns (1.3) and (1.4), which gives the joint angles for the hip and knee shown in figs. 1.13a and 1.13b.

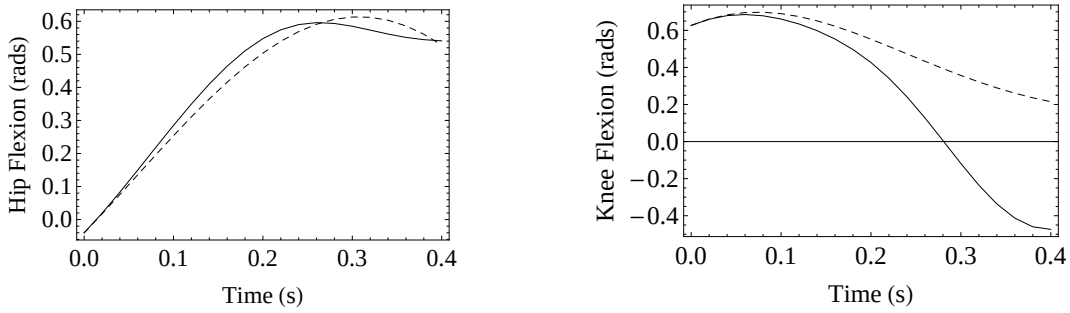

(a) (b)

Figure 1.13: Comparison of the angle of the hip (a) and knee (b) predicted by the forward dynamics solution of equations of motion (dashed) with experimental results from Neumann [48] shown with a solid line.

During the swing phase of gait, the swing thigh is accelerated forward by the torque at the hip joint. The shank is raised for toe-clearance by the torque at the knee and then at about mid stance, the hip torque decelerates the thigh and the knee torque extends the shank. A portion of the torque generated at the swing hip and knee, is a result of interactions with other body segments that are not present in this model. As a consequence, the torques for a non-disabled individual, when applied

to this model, result in the swing leg reaching a maximum step length prematurely and then falling backwards because the knee begins to flex, Fig. 1.14. Even with a more sophisticated model of walking, it is not uncommon for the model to make predictions that differ significantly from what has been measured in experiment without manipulating the inputs [51].

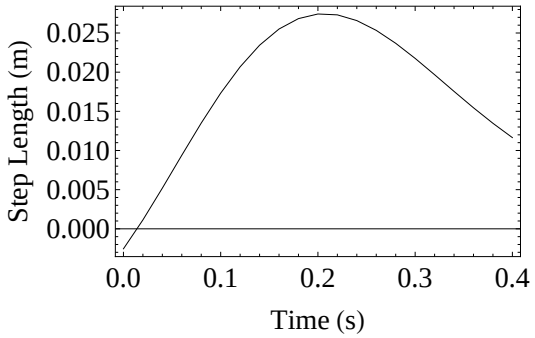

Figure 1.14: Position of the foot as a function of time.

1.1.5.2 Inverse Dynamics

To solve the model using inverse dynamics, the joint angles, velocities and accelerations are assumed known. The hip and knee angles (from Neumann [48]) are curve fit with a four-term Fourier series, and the equation is substituted in eqns 1.3 and 1.4. The model predicts the following torques at the hip and knee, shown in figs. 1.15a and 1.15b respectively. The predicted kinetics are different from what has been measured in experiments. The only explanation is that more components of gait must be included to accurately model walking [75], [60]. Inverse dynamics is a common solution technique used in modeling walking, discussed later. A comprehensive uncertainty analysis [60] shows error as high as 200%, an estimate

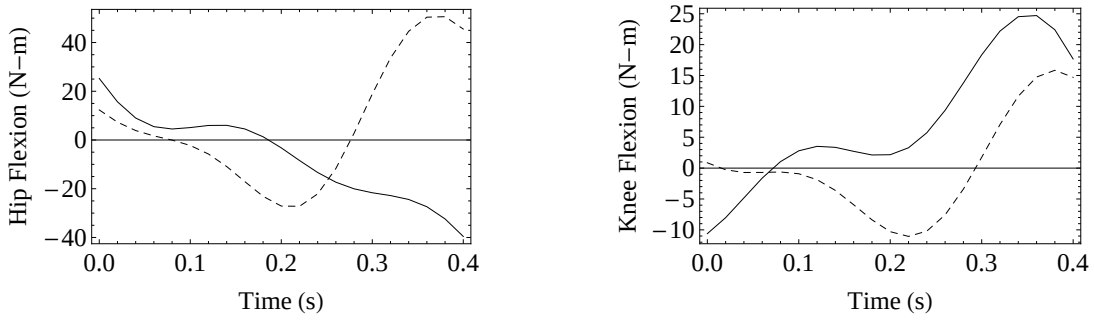

(a) (b)

Figure 1.15: Comparison of torque at the hip (a) and knee (b) predicted by the inverse dynamics solution of the equations of motion (dashed) with experimental results from Neumann [48] shown with a solid line.

that does not take into account a lack of sufficient motions included in the model.

1.1.5.3 Optimization

In inverse and direct dynamics, either the kinematics or the kinetics must be known in order to determine the other quantity. When both the movement and internal forces and moments are desired to be calculated, there are more unknowns that there are independent equations. Optimization techniques can be used to generate the extra equations.

Several of the previously mentioned models by Chow and Jacobson [11], Koopman et al. [35], Ren et al. [59], utilize this technique to reduce the reliance on the assumed known inputs needed to solve the model. Other models use optimization to estimate the muscle forces, which is also an indeterminant problem, [3], [12]. The optimal solution is one for which the partial derivatives of the augmented Lagrangian function with respect to the kinematic and/or kinetic variables are zero.

The augmented Lagrangian is the sum of the integrand of an objective function and the product of the equations of motion and a Lagrange multiplier. The objective function is a mathematical representation of some physical quantity to be optimized. The objective functions used by [11], [35] and [59] are time integrals of some measure of the work or energy done by the muscles or by the muscles in aggregate as joint torques. Any objective function can be used but is preferable to use an objective function that has a physically relevant interpretation, such as minimization of mechanical work or total joint torque.

Chow and Jacobson [11] assume that during the normal range of activity, the sum total of mechanical energy expenditure by the muscle-activating system is proportional to the integral of the square of the net moment, M_i of the i^{th} link

$$J = \frac{1}{2}\int_{t_0}^{t_f} r|M_i(t)|^2 dt, \quad r \geq 0, \tag{1.5}$$

where r is the weighting factor. The objective function, J, allows the model to have only one input, the trajectory of the hip, which is assumed to be a periodic function of time.

Ren et al. [59] use minimization of mechanical work as the objective function, J, in their model. The objective function is given by,

$$J = \int_{t_0}^{t_f} \left| M_i(t) \left(\omega_p^i(t) - \omega_d^i(t)\right)\right| dt, \tag{1.6}$$

where M_i is the net muscle moment at the i^{th} joint and ω_p and ω_d are the angular velocities of the proximal and distal segments. Distal refers to a point that is furthest from the body and proximal refers to a point that is closest to the body. The inputs

of the Ren et al. model are average walking velocity, cycle period and double support duration.

Ren et al. found many solutions, but based on the major features of the gait patterns, they appeared to fall into four distinct families of solutions. The four families are believed to represent four local minima of the solution manifold. The most realist gait pattern is the one with the lowest energy consumption. This suggests that deviation from a normal gait pattern leads to increased energy cost, further suggesting the use of energy consumption as an objective function of gait to be minimized.

The unit-less objective function used by Koopman et al. [35] is a slight modification of the objective function used by Chow and Jacobson [11],

$$J = \frac{1}{T} \int_{t_0}^{t_f} \frac{M_i}{M_{max}} dt \tag{1.7}$$

where M_i is the joint torque at the i^{th} joint, and M_{max} is the maximal positive or negative torque at the i^{th} joint. These studies all share the fact that the objective function they chose was a function of the moment acting on the various joints. The Koopman et al. model uses the ankle, knee and hip angles as inputs and predicts hip rotation and tilt as well as torso rotation

The objective functions used by Anderson and Pandy [3] and Davy and Audu [12] are functions of muscle force whereas the objective functions of Chow and Jacobson [11], Ren et al. [59] and Koopman et al. [35] are functions of the moment at the joints. The selection of an objective function is an implicit assumption or constraint placed on the solution and should be carefully selected. Each of the

objective functions discussed previously are various forms of minimization of energy expenditure. Using minimization of energy expenditure as an objective function is an intuitive choice for non-disabled walking but may not be for disabled walking. There may be a more dominant performance objective or competing one such as minimization of joint pain. This concept is discussed later in section 5.

1.2 Summary

The determinants of gait were reviewed, and available models of walking with and without crutches were reviewed. The conclusion is that current models of walking do not include motions of the pelvis that have been identified as important in section 1.1.1. Further, all models of walking with crutches do not include a pelvis. This implies that a pelvis must be included in a three-dimensional model if a realistic model of human walking with crutches is to be obtained.

The model of Neumann was used to explain how leaning over the stance leg, a compensatory motion, reduces the demand on the hip abductor muscles. The model was also used to explain how a contralateral assistive device, a cane in this case, can completely compensate for paralyzed hip abductor while standing still. The level of activation required by the hip abductors is a function of the load applied to the cane. As the load applied to the cane is increased, the level of activation required by the hip abductor decreases. Vankoski [71] has shown that contralateral crutch use reduces compensatory motions or returns a pathological gait to a more normal one, these simple models provide a way to explain this phenomena. Compensatory

motions, such as excessive lateral displacement of the torso and hip hiking, reduce the moment needed by the hip abductor. The less the hip abductors are needed, the less compensatory motions are needed and the lower the energy cost of gait.

Chapter 2

Dynamic Modeling

2.1 Deriving Characteristic Equations

Two methods for deriving the equations of motion are those using Euler's or Lagrange's equations. Since the forces on the bones are not of interest in a gait model, Lagrange's equations are the focus. The preliminary steps in the assembly of Lagrange's equations include deriving the velocity of the center of mass, angular velocity and the vector of the generalized forces. This chapter goes through these steps, first by deriving a relationship for the orientation of a rigid body in three-space, finding its angular velocity and then an example is presented that demonstrates how to derive the vector of generalized forces as well as the center of gravity velocity and the angular velocity. The method shown here is general and can be extended to describe a multiple rigid-link system that will be used in later chapters to model walking and walking with crutches.

2.1.1 Relative Motion of a Rigid Link

Three translational coordinates of the center of gravity (COG) and three coordinates that describe the orientation of the body are needed to characterize the position of a rigid body in three-dimensions. There are several ways to describe the orientation of a rigid body in three-dimensions, Cardan angles are used because this

ordered sequence, ϕ, ψ, θ around the y_1, x_2, z-axes corresponds to flexion/extension, ab/adduction and internal/external rotation [21]. Given a rigid body, S^*, is given the local coordinate system of body coordinates with origin at the center of gravity, G, as shown in Fig. 2.1. The inertial coordinates system is given by X, Y, Z.

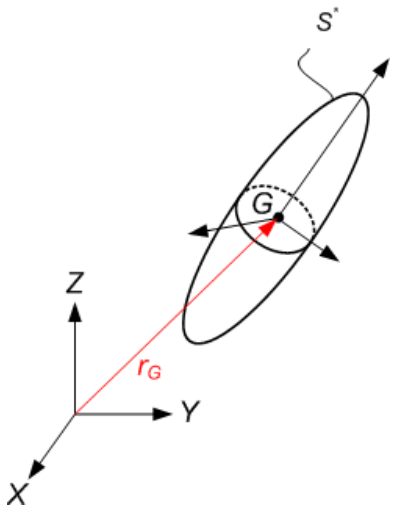

Figure 2.1: Rigid body, S^*, with a local coordinate system embedded at the center of gravity, G.

2.1.2 Position of the Center of Mass

Cardan angles correspond to an ordered sequence of three rotations which occur about three separate axes. These angles are used to describe the rotation of coordinate systems and the rates of change of the rotations. Consider the three rotations, ϕ around the inertial Y-axis which yield the new coordinate system, x_1, y_1, z_1, ψ around the x_1-axis yielding the x_2, y_2, z_2 system and finally θ around the z_2-axis which gives the final body fixed system, x, y, z, embedded in S^* at G.

The body coordinate system is initially coincident with the inertial frame. The

first rotation, ϕ, around the inertial Y-axis is shown in Fig. 2.2. After the rotation,

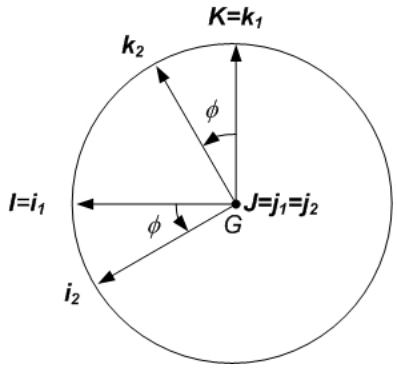

Figure 2.2: Rotating the body embedded coordinate frame through the angle ϕ about the inertial y coordinate gives the new body embedded frame, x_1, y_1, z_1.

the body frame (x_1, y_1, z_1) is related to the inertial frame as follows,

$$\boldsymbol{i_1} = \cos\phi \boldsymbol{I} - \sin\phi \boldsymbol{K}, \tag{2.1}$$

$$\boldsymbol{j_1} = \boldsymbol{J}, \tag{2.2}$$

$$\boldsymbol{k_1} = \sin\phi \boldsymbol{I} + \cos\phi \boldsymbol{K}. \tag{2.3}$$

The unit vectors in the inertial frame are $\boldsymbol{I}$, $\boldsymbol{J}$, and $\boldsymbol{K}$. The relationship between the body and inertial frames can also be expressed as

$$\begin{pmatrix} x_1 \\ y_1 \\ z_1 \end{pmatrix} = R_{y,\phi} \begin{pmatrix} X \\ Y \\ Z \end{pmatrix}, \tag{2.4}$$

or more compactly as

$$\boldsymbol{x_1} = R_{y,\phi} \boldsymbol{X}, \tag{2.5}$$

where $R_{y,\phi}$ is given by

$$R_{y,\phi} = \begin{pmatrix} \cos\phi & 0 & -\sin\phi \\ 0 & 1 & 0 \\ \sin\phi & 0 & \cos\phi \end{pmatrix}. \tag{2.6}$$

Rotating the x_1, y_1, z_1 system by ψ around the x_1-axis yields the x_2, y_2, z_2 system, shown in Fig. 2.3. The x_1, y_1, z_1 system is related to the x_2, y_2, z_2 coordinates

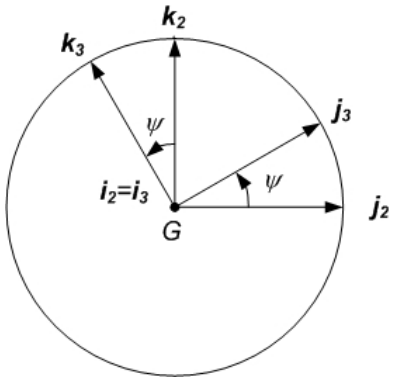

Figure 2.3: Rotating the body embedded coordinate frame through the angle ψ about the body embedded x_1 coordinate gives the new body embbedded frame, x_2, y_2, z_2.

by,

$$\boldsymbol{i_2} = \boldsymbol{i_1}, \tag{2.7}$$

$$\boldsymbol{j_2} = \cos\psi \boldsymbol{j_1} + \sin\psi \boldsymbol{k_1}, \tag{2.8}$$

$$\boldsymbol{k_2} = -\sin\psi \boldsymbol{j_1} + \cos\psi \boldsymbol{k_1}. \tag{2.9}$$

The current coordinate system is related to the previous one by

$$\boldsymbol{x_2} = R_{x,\psi} \boldsymbol{x_1}, \tag{2.10}$$

where

$$R_{x,\psi} = \begin{pmatrix} 1 & 0 & 0 \\ 0 & \cos\psi & \sin\psi \\ 0 & -\sin\psi & \cos\psi \end{pmatrix}. \tag{2.11}$$

Finally, rotating around the z_2-axis through the angle θ yields the final, body embedded coordinate system, x, y, z. Rotating θ around the z_2-axis is shown in Fig. 2.4. The x, y, z frame is related to the x_2, y_2, z_2 frame by,

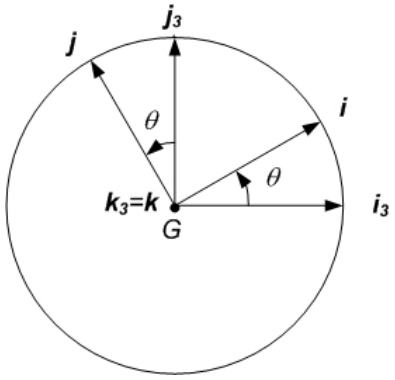

Figure 2.4: Rotating the body embedded coordinate frame through the angle θ about the body embedded z_2 coordinate gives the new body embbedded frame, x, y, z.

$$\boldsymbol{i} = \cos\psi \boldsymbol{i_2} + \sin\psi \boldsymbol{j_2}, \tag{2.12}$$

$$\boldsymbol{j} = -\sin\psi \boldsymbol{i_2} + \cos\psi \boldsymbol{j_2}, \tag{2.13}$$

$$\boldsymbol{k} = \boldsymbol{k_2}, \tag{2.14}$$

stated more compactly as

$$\boldsymbol{x} = R_{z,\theta} \boldsymbol{x_2}, \tag{2.15}$$

where

$$R_{z,\theta} = \begin{pmatrix} \cos\theta & \sin\theta & 0 \\ -\sin\theta & \cos\theta & 0 \\ 0 & 0 & 1 \end{pmatrix}. \tag{2.16}$$

The body and inertial frames are related using eqns 2.5, 2.10 and 2.15 by

$$\boldsymbol{x} = R_{z,\theta} R_{x,\psi} R_{y,\phi} \boldsymbol{X} = R_\theta R_\psi R_\phi \boldsymbol{X}. \tag{2.17}$$

2.1.3 Angular Velocity

After rotating through angles ϕ and ψ around the Y and x_1-axes respectively, the angular velocity in the body embedded frame is

$$\omega_c = \omega_1 + \omega_2, \tag{2.18}$$

where

$$\omega_1 = R_\psi \dot{\phi} \boldsymbol{j_1} = \dot{\phi}\cos\psi \boldsymbol{j_2} - \dot{\phi}\sin\psi \boldsymbol{k_2}, \tag{2.19}$$

and

$$\omega_2 = \dot{\psi} \boldsymbol{i_1} = \dot{\psi} \boldsymbol{i_2}. \tag{2.20}$$

After the final rotation through the angle, θ around the z_2 axis, the angular velocity in the body embedded frame is

$$\omega = \omega_c + \omega_3, \tag{2.21}$$

where

$$\omega_c = R_\theta \dot{\psi} \boldsymbol{i_2} + R_\theta \dot{\phi}\cos\psi \boldsymbol{j_2} - R_\theta \dot{\phi}\sin\psi \boldsymbol{k_2}, \tag{2.22}$$

and

$$\omega_3 = \dot{\theta}\boldsymbol{k}. \tag{2.23}$$

The angular velocity can be written in the body frame as

$$\boldsymbol{\Omega} = \Omega_1\boldsymbol{i} + \Omega_2\boldsymbol{j} + \Omega_3\boldsymbol{k}, \tag{2.24}$$

where

$$\Omega_1 = \dot{\psi}\cos\theta + \dot{\phi}\cos\psi\sin\theta,$$

$$\Omega_2 = \dot{\phi}\cos\psi\cos\theta - \dot{\psi}\sin\theta,$$

$$\Omega_3 = \dot{\theta} - \dot{\phi}\sin\psi.$$

2.1.4 Example

The last step in assembling Lagrange's equations is to derive the vector of generalized forces. This process is demonstrated through an example. The equations of motion for a rigid link are found using Lagrange's equation,

$$\frac{d}{dt}\frac{\partial L}{\partial \dot{q}} - \frac{\partial L}{\partial q} = Q. \tag{2.25}$$

The link has with one side attached to the origin of the inertial frame with a ball and socket joint. The z-axis of the body coordinates is coincident with the longitudinal axis of the link. The Lagrangian, L, is formed by taking the difference between the kinetic, K, and potential energies, V,

$$L = K - V. \tag{2.26}$$

The kinetic energy is given by,

$$K = \frac{1}{2} m \boldsymbol{v}_G \cdot \boldsymbol{v}_G + \frac{1}{2} \boldsymbol{\Omega}^T I_G \boldsymbol{\Omega}, \tag{2.27}$$

where the velocity is given in eqn 2.30 and the angular velocity is given in eqn 2.24. The potential energy is given by

$$V = mg\boldsymbol{r}_G \cdot \boldsymbol{K}. \tag{2.28}$$

Equation 2.17 can be used to find the position of the center COG. The axes of the body embedded frame are related to the inertial frame after rotations of ϕ, ψ, θ about the body frames Y, x_1, z_2 respectively by

$$\boldsymbol{r_G} = a \begin{pmatrix} \cos\psi \sin\phi & -\sin\psi & \cos\phi\cos\psi \end{pmatrix}^T. \tag{2.29}$$

The velocity of the center of mass is found by differentiating $\boldsymbol{r_G}$,

$$\boldsymbol{v}_G = a \begin{pmatrix} v_1 & v_2 & v_3 \end{pmatrix}^T, \tag{2.30}$$

with

$$v_1 = \dot{\phi}\cos\phi\cos\psi - \dot{\psi}\sin\phi\sin\psi,$$

$$v_2 = -\dot{\psi}\cos\psi,$$

$$v_3 = -\dot{\phi}\cos\psi\sin\phi - \dot{\psi}\cos\phi\sin\psi.$$

The mass moment of inertial, I_G, is conveniently expressed in body coordinates as a diagonal matrix

$$I_G = \begin{pmatrix} I_x & 0 & 0 \\ 0 & I_y & 0 \\ 0 & 0 & I_z \end{pmatrix} \tag{2.31}$$

because the body is symmetric about the body axes. The rigid link is subjected to a variable external couple, $\boldsymbol{M}$, about the body coordinate system. Following Langhaar [38], if the Cardan angles are given infinitesimal virtual increments, $\delta\psi, \delta\phi, \delta\theta$ about the body embedded coordinate system, x, y, z, the virtual work of the couple is

$$\delta W = Q_1\delta\psi + Q_2\delta\phi + Q_3\delta\theta \tag{2.32}$$

where Q_1, Q_2, Q_3 are the component of the generalized moments. Any infinitesimal angular displacement is a vector, $\delta\boldsymbol{\beta}$, and the components of the vector on the body embedded frame, x, y, z, are denoted by $\delta\beta_1, \delta\beta_2, \delta\beta_3$. If the angular velocity occurs over a time period, δt, then

$$\delta\boldsymbol{\beta} = \boldsymbol{\Omega}\delta t \tag{2.33}$$

and by egn 2.24

$$\delta\beta_1 = \cos\theta\delta\psi + \cos\psi\sin\theta\delta\phi, \tag{2.34}$$

$$\delta\beta_2 = \cos\psi\cos\theta\delta\phi - \sin\theta\delta\psi, \tag{2.35}$$

and

$$\delta\beta_3 = \delta\theta - \sin\psi\delta\phi. \tag{2.36}$$

The virtual work of the couple may be expressed as

$$\delta W = \boldsymbol{M}\cdot\delta\boldsymbol{\beta} = M_x\delta\beta_1 + M_y\delta\beta_2 + M_z\delta\beta_3, \tag{2.37}$$

Given eqn 2.32, the components of the generalized work due the external couple are

$$Q_1 = M_x\cos\theta - M_y\sin\theta, \tag{2.38}$$

$$Q_2 = M_x\cos\psi\sin\theta + M_y\cos\psi\cos\theta - M_z\sin\psi, \tag{2.39}$$

and

$$Q_3 = M_z. \tag{2.40}$$

2.2 Summary

For the models described in Chapter 3, for each link these quantities; the position of the center of mass, $\boldsymbol{r}_G$, the velocity of the center of mass, $\boldsymbol{v}_G$, the angular velocity, $\boldsymbol{\Omega}$, the mass-moment of inertial tensor, I_G, and the components of the vector of the generalized force, Q, are input into Mathematica which is used to derive the equations of motion symbolically (see Appendix C).

Chapter 3

Three-Dimensional Models

The aim of the thesis is to develop a framework for developing and evaluating crutches based on specific muscle weakness in modular way so that crutches can be custom assembled based on each individual patient's specific set of muscle weakness. Individuals with weak/paralyzed hip abductors exhibit compensatory motions that are thought to compensate for weak/paralyzed hip abductors, however weak/-paralyzed hip abductors are rarely if ever the only muscle disability exhibited by individuals with low-level spinal injuries. For example, individuals with low-level spina bifida have weak/parlyzed hip abductors and weak/paralyzed ankle plantar/-dorsi flexors. For this reason hip abductor weakness/paralysis is the focus of the analysis based on dynamic models.

Two dynamic models are developed, the first model assumes the kinetics are known, and the kinematics are solved for. The second model is used to calculate the time varying crutch load when a crutch is vertical and at an angle necessary to maintain "normal" gait kinematics (the kinematics are assumed known) whereas in the previous model the crutch loads are assumed to be a constant value.

Depending on whether the kinematics are assumed known or the kinetics are assumed known, the solution technique is called inverse or direct dynamics respectively. When the kinetics are assumed to be known (forward dynamics), the equa-

tions of motion are a system of ordinary differential equations. When the kinematics (inverse dynamics) are assumed known, the equations of motion are a system of algebraic equations. The inverse dynamics problem is the easier of the two to solve and as such it allows solution of more complicated systems. For this reason the inverse dynamics model has ten degrees of freedom (DOF) and the direct dynamics model has six DOF. The inputs used to derive the equations of motion of the 10 DOF dynamic model are presented first because the six DOF direct dynamics model is a simplified ten DOF model.

The models only consider the swing and stance phases of gait during steady walking. This excludes starting and stopping walking as well as the part of walking when both feet are on the ground. The angles of the joints, in the inverse dynamics model, are assumed known and fall within a normal range for non-disabled individuals. The range of motion of the joints is not constrained for the forward dynamics case. However, the range of motion the joints act through is within a normal range for the joint torques assumed. The joint torques could be changed to make a joint go through an angle that is not physically realistic. This is something that must be watched for.

A simplifying assumption used by the model is that the crutch force applied to the body is transferred perfectly through the arms to the shoulder. Any musculature that works to stabilize the crutch is not included in the model. Another assumption is that the joints are frictionless, i.e. damping is not included. Reasons to include damping would be so that a limit cycle might be found when solving the forward dynamics model. Another reason to include damping would be to model the energy

it takes to move against antagonistic muscles or inactive muscles.

3.1 Inverse Dynamics Model

The inverse dynamics model uses six rigid links with 10 degrees of freedom (Fig. 3.1). A trunk is included in the model as a rigid plate and a pelvis that can move in three-dimensions.

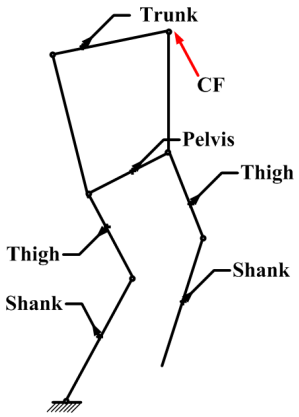

Figure 3.1: The three dimensional model has six rigid links, one link for each shank, thigh and one for the pelvis, and a plate for the trunk.

3.1.1 Configuration History of the Model

The position of the center of gravity (COG) of each link is determined in order to assemble Lagrange's equations. The COG of each link can be found recursively if the origin of the inertial frame is chosen as the point of contact between the ground and the stance foot. Then the position of the COG of each link is used to find the total potential energy and the total kinetic energy of the system which is then used

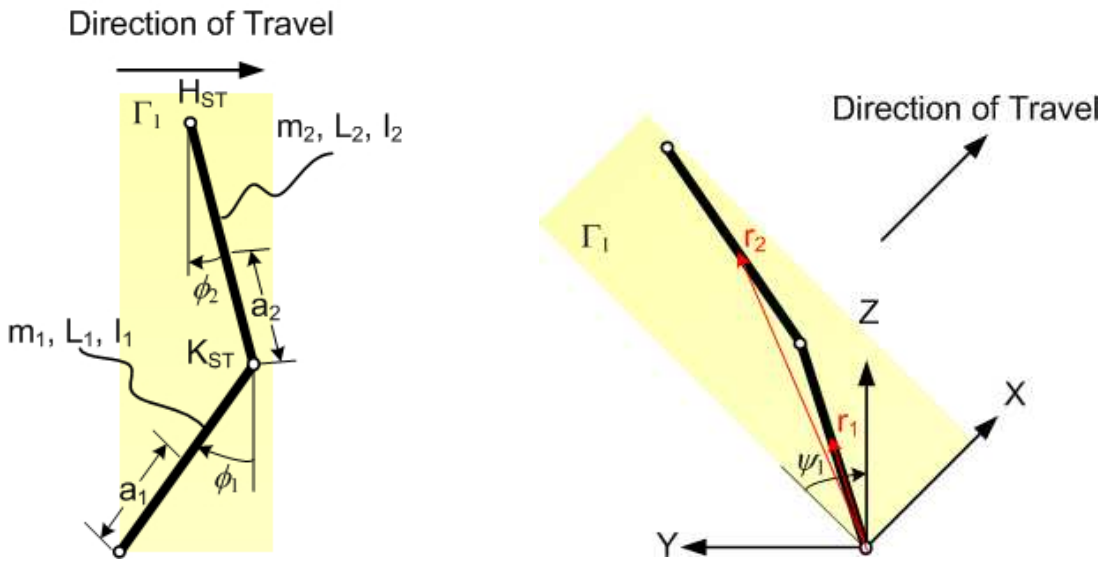

(a) (b)

Figure 3.2: (a) Side view of the stance leg in the Γ_1 plane. (b) Diagram of the stance leg in the inertial frame.

with Lagrange's equations to find the equations of motion of the system. Figure 3.1 is a rigid link model of human walking.

From here onward $\boldsymbol{i}, \boldsymbol{j}, \boldsymbol{k}$ are inertial unit vectors and $\boldsymbol{i'}, \boldsymbol{j'}, \boldsymbol{k'}$ are unit vectors in the body frame. Figure 3.2a shows the stance leg in the Γ_1 plane. The body frames of the shank and thigh are initially coincident with the inertial frame when the knee is not bent. Both the shank and thigh links rotate ϕ_1, ϕ_2 about the body y-axis of the shank and thigh respectively, which are both normal to the Γ_1 plane. The plane, Γ_1, is a rotation of the X-Z plane through an angle ψ_1 around the inertial X axis. The shank and thigh then both rotate an angle of ψ_1 around the body embedded x-axis (Fig. 3.2b). The center of gravity of the shank and the thigh are at a distance, a_1 and a_2 from the ankle and knee respectively (Fig. 3.2a).

The position, $\mathbf{r}_1$ of the center of gravity of link 1, the stance-side shank, is

$$\mathbf{r}_1 = a_1 \left(\cos\psi_1 \sin\phi_1 \boldsymbol{i} - sin\psi_1 \boldsymbol{j} + \cos\psi_1 \cos\phi_1 \boldsymbol{k}\right). \tag{3.1}$$

The position of the stance-side knee (K_{ST}) is

$$\mathbf{r}_{K_{ST}} = L_1 \left(\cos\psi_1 \sin\phi_1 \boldsymbol{i} - \sin\psi_1 \boldsymbol{j} + \cos\psi_1 \cos\phi_1 \boldsymbol{k}\right). \tag{3.2}$$

The position of the center of gravity of the thigh is,

$$\mathbf{r}_2 = \mathbf{r}_{K_{ST}} + a_2 \left(\cos\psi_1 \sin\phi_2 \boldsymbol{i} - \sin\psi_1 \boldsymbol{j} + \cos\psi_1 \cos\phi_2 \boldsymbol{k}\right), \tag{3.3}$$

and the position of the stance-side hip (H_{ST}) is

$$\mathbf{r}_{H_{ST}} = \mathbf{r}_{K_{ST}} + L_2 \left(\cos\psi_1 \sin\phi_2 \boldsymbol{i} - \sin\psi_1 \boldsymbol{j} + \cos\psi_1 \cos\phi_2 \boldsymbol{k}\right). \tag{3.4}$$

The pelvis is shown in Fig. 3.3. The position of the center of gravity of the pelvis is located a distance a_3 from the stance-side hip in the body embedded coordinate system, shown in Fig. 3.3. The axes of the body coordinates, x', y', z', are initially coincident with the inertial coordinates, X, Y, Z. The body coordinate system undergoes rotation, ψ_3, ϕ_3 then θ_3 around the y', x', z'-axes. After rotating ψ_3, ϕ_3, θ_3, the position of the center of gravity in the inertial coordinate system is given by

$$\boldsymbol{r}_3 = \boldsymbol{r}_{H_{ST}} + a_3 \left(r_{3x} \boldsymbol{i} + r_{3y} \boldsymbol{j} + r_{3z} \boldsymbol{k}\right) \tag{3.5}$$

where

$$r_{3x} = -\cos\phi_3 \sin\theta_3 + \cos\theta_3 \sin\phi_3 \sin\psi_3,$$

$$r_{3y} = \cos\theta_3 \cos\psi_3,$$

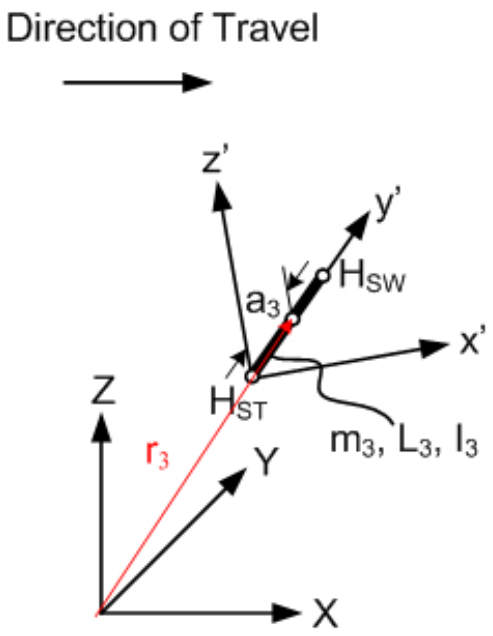

Figure 3.3: The pelvis has the coordinate system x', y', z' attached to it. The coordinate system is a distance $\mathbf{r}_{H_{ST}}$ from the origin of the inertial frame.

$$r_{3z} = \sin\theta_3 \sin\phi_3 + \cos\theta_3 \cos\phi_3 \sin\psi_3.$$

with ψ_3, ϕ_3 and θ_3 corresponding to pelvic obliquity, tilt and rotation [21]. The position of the swing side hip, $\boldsymbol{r}_{H_{SW}}$, in inertial coordinates is given by

$$\boldsymbol{r}_{H_{SW}} = \boldsymbol{r}_{H_{ST}} + L_3 \left(r_{3x}\boldsymbol{i} + r_{3y}\boldsymbol{j} + r_{3z}\boldsymbol{k}\right). \tag{3.6}$$

The swing-leg thigh and shank body coordinate systems are initially coincident with the inertial frame up to a translation. The body coordinate systems then rotate ϕ_4, ϕ_5 around their respective body y'-axes, the center of gravity of the links are at a distance of a_4 and a_5 from the knee and ankle, shown in Fig. 3.4a. The swing leg thigh and shank are then rotated ϕ_4 about their respective x'-axes in the Γ_2 plane, shown in Fig. 3.4b. The plane, Γ_2 is at an angle ψ_2 from the pelvis' body z'-axis.

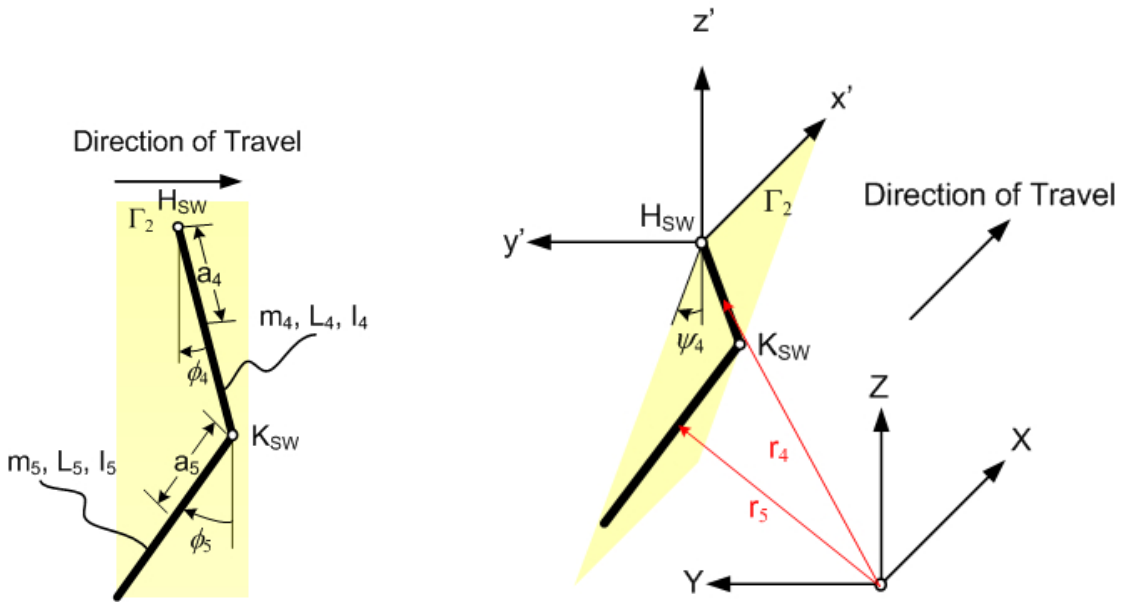

(a) (b)

Figure 3.4: (a) Side view of the swing leg in the Γ_2 plane. (b) Diagram of the swing leg in the inertial frame.

The position of the center of gravity of the swing-side thigh is

$$\mathbf{r}_4 = \mathbf{r}_{H_{SW}} + a_4 \left(-\cos\psi_4 \sin\phi_4 \boldsymbol{i} + \sin\psi_4 \boldsymbol{j} - \cos\psi_4 \cos\phi_4 \boldsymbol{k}\right), \tag{3.7}$$

the position of the swing-side knee (K_{SW}), is

$$\mathbf{r}_{K_{ST}} = \mathbf{r}_{H_{SW}} + L_4 \left(-\cos\psi_4 \sin\phi_4 \boldsymbol{i} + \sin\psi_4 \boldsymbol{j} - \cos\psi_4 \cos\phi_4 \boldsymbol{k}\right), \tag{3.8}$$

and the position of the center of gravity of the swing-side shank is

$$\mathbf{r}_5 = \mathbf{r}_{K_{SW}} + a_5 \left(-\cos\psi_4 \sin\phi_5 \boldsymbol{i} + \sin\psi_4 \boldsymbol{j} - \cos\psi_4 \cos\phi_5 \boldsymbol{k}\right). \tag{3.9}$$

The trunk, shown in Fig. 3.5, is a plate with a distributed mass, m_6. The plate has vertical length of L_6 and its mass is concentrated at a distance of a_6 from the trunk. The trunk is rotated about the pelvis, ϕ_6, from the vertical, measured counter-clockwise around the y'-axis. The position of the center of gravity of the trunk is

$$\mathbf{r}_6 = \mathbf{r}_3 + a_6 \left(\sin\phi_6 \cos\psi_6 \boldsymbol{i} - \sin\psi_6 \boldsymbol{j} + \cos\phi_6 \cos\psi_6 \boldsymbol{k}\right). \tag{3.10}$$

3.1.2 Angular Velocity

The angular velocity of the each link can be derived from eqn 2.24, the angular velocity of the stance-side shank and thigh are found by setting θ=0, assuming there is no internal/external rotation of either link, giving the angular velocity of the shank in body coordinates as

$$\omega_1 = \dot{\psi}_1 \boldsymbol{i'} + \dot{\phi}_1 \cos\psi_1 \boldsymbol{j'} - \dot{\phi}_1 \sin\psi_1 \boldsymbol{k'} \tag{3.11}$$

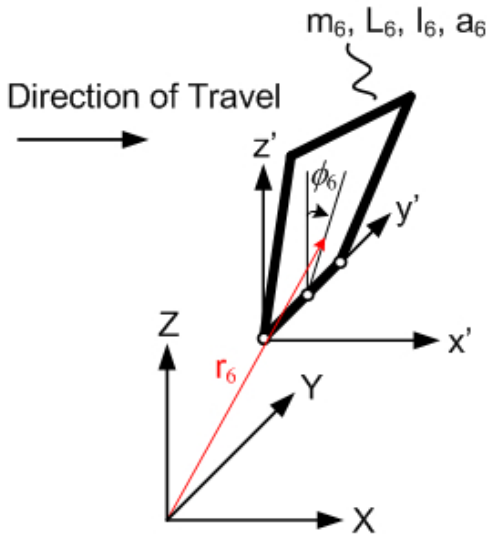

Figure 3.5: The trunk lies in the x', y', z' coordinate system at an angle, ϕ_6 from the z'-axis.

and the angular velocity of the thigh in the body embedded coordinate system

$$\omega_2 = \dot{\psi}_1 \boldsymbol{i'} + \dot{\phi}_2 \cos\psi_1 \boldsymbol{j'} - \dot{\phi}_2 \sin\psi_1 \boldsymbol{k'}. \tag{3.12}$$

The angular velocity of the pelvis is identical to eqn 2.24 and shown here only for convenience

$$\omega_3 = \omega_x \boldsymbol{i'} + \omega_y \boldsymbol{j'} + \omega_z \boldsymbol{k'}, \tag{3.13}$$

where

$$\omega_x = \dot{\psi}_3 \cos\theta_3 + \dot{\phi}_3 \cos\psi_3 \sin\theta_3,$$

$$\omega_y = \dot{\phi}_3 \cos\psi_3 \cos\theta_3 - \dot{\psi}_3 \sin\theta_3,$$

$$\omega_z = \dot{\theta}_3 - \dot{\phi}_3 \sin\psi_3.$$

Similarly the angular velocity of the swing side thigh and shank can be expressed in the body embedded coordinate system of each link respectively as

$$\omega_4 = \dot{\psi}_4 \boldsymbol{i'} + \dot{\phi}_4 \cos\psi_4 \boldsymbol{j'} - \dot{\phi}_4 \sin\psi_4 \boldsymbol{k'}, \tag{3.14}$$

$$\omega_5 = \dot{\psi}_4 \boldsymbol{i'} + \dot{\phi}_5 \cos\psi_4 \boldsymbol{j'} - \dot{\phi}_5 \sin\psi_4 \boldsymbol{k'}, \tag{3.15}$$

and finally the angular velocity of the torso can be expressed as

$$\omega_6 = \dot{\phi}_6 \boldsymbol{j'}. \tag{3.16}$$

3.1.3 Generalized Forces

The torques in the sagittal and frontal planes used in the model are shown in Fig. 3.6.

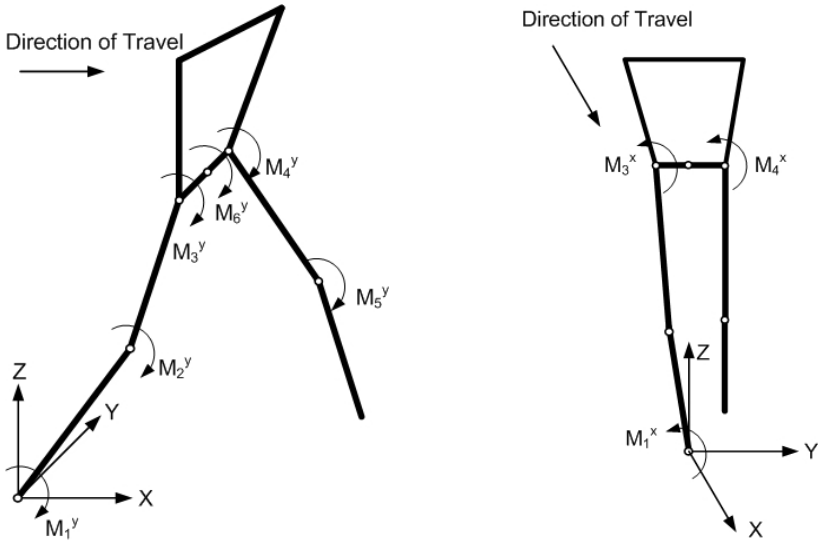

(a) (b)

Figure 3.6: The torques assumed in the model are shown in the sagittal plane (a) and frontal planes (b).

The components of the generalized work, Q_i, due to the couple of the ankle dorsi/plantar flexors (M_1^y), ankle everters/inverters (M_1^x), the knee flexors/extensors (M_2^y) and the hip abductors (M_3^x) are given by the following

$$Q_1^x = M_1^x, \tag{3.17}$$

and

$$Q_1^y = (M_1^y - M_2^y)\cos\psi_1, \tag{3.18}$$

following the example of section 2.1.4 with the subscript and superscript denoting the link number and the axis respectively. Similarly the components of the generalized work due to the external couples on the stance side thigh are given by

$$Q_2^x = M_3^x, \tag{3.19}$$

and

$$Q_2^y = (M_2^y - M_3^y)\cos\psi_1, \tag{3.20}$$

and the pelvis

$$Q_3^x = (M_3^x - M_4^x)\cos\theta_3 - (M_3^y - M_4^y - M_6^y)\sin\theta_3, \tag{3.21}$$

$$Q_3^y = (M_3^x - M_4^x)\cos\psi_3\sin\theta_3 + (M_3^y - M_4^y - M_6^y)\cos\psi_3\cos\theta_3 - (M_3^z - M_4^z)\sin\psi_3 \tag{3.22}$$

and

$$Q_3^z = M_3^z \tag{3.23}$$

where M_4^x, M_3^y, M_4^y, M_3^z and M_6^y are the stance side hip abduction, stance and swing side hip flexor/extensor, internal/external joint torque of the stance side pelvis and

the torso torques, respectively. The components of the generalized work for the swing side thigh are given by

$$Q_1^x = M_4^x, \tag{3.24}$$

$$Q_2^y = (M_4^y - M_5^y)\cos\psi_4, \tag{3.25}$$

the components of the generalized work for the swing side shank are

$$Q_2^y = M_5^y \cos\psi_4, \tag{3.26}$$

and finally the component of the generalized work for the torso is

$$Q_2^y = M_6^y \tag{3.27}$$

where M_5^y is the swing side knee torque. If a crutch force is applied to the model, the position of the application of the force is

$$\mathbf{r}_{crutch} = \mathbf{r}_{H_{SW}} + L_6\left(\sin\phi_6\cos\psi_6\boldsymbol{i} - \sin\psi_6\boldsymbol{j} + \cos\phi_6\cos\psi_6\boldsymbol{k}\right), \tag{3.28}$$

then the generalized force work due to the crutch is

$$Q_{crutch} = F_{crutch}\delta\mathbf{r}_{crutch} \tag{3.29}$$

where F_{crutch} is the force due to a contralateral crutch.

3.1.4 Summary

The Mathematica programs *ID_NoAbduct.nb* and *ID_angled_crutch.nb* (Appendix C) are used to derive the equations of motion of the six DOF model and solve for the joint torques and crutch force assuming that the body motions are known.

The program is also used to characterize the change in the torque developed by the hip abductors as a function of contralateral crutch use. The results are presented in the next chapter. The programs also calculates the work done per gait cycle.

3.2 Forward Dynamics Model

The inverse dynamics model assumes that the kinematics are known. This model is used to investigate how the forces change as a result of changing the assumed known input kinematics. Conversely, the forward dynamics model assumes that the kinetics are known and the model is used to characterize the change in body motions change as a result of varying the known kinetics.

Numerically speaking, compared to the same inverse dynamics problem, solving the forward dynamics problem is much more difficult. This is because in solving the equations of motion (EOM) using inverse dynamics, the kinematics are assumed to be known, which results in a system of algebraic equations. Solving the EOM using forward dynamics assumes that the kinetics are known and the resulting EOM are ordinary differential equations. In order to make the system of EOM easier to solve, some body motions, which have ranges of motion smaller than ten degrees are assumed to be constant. The stance and swing leg angles, ψ_1 and ψ_4, are held constant, pelvic tilt, ϕ_3, is assumed to be zero and the remaining pelvic angles, ψ_3 and θ_3, are assumed to be small to make the small angle approximation, $\sin\psi \sim \psi$.

3.2.1 Configuration History of the Model

Returning to the equations for the position of the center of mass from the previous section with the assumptions as outlined previously yields the following equations

$$\mathbf{r}_1 = a_1 \left(\cos\psi_1 \sin\phi_1 \boldsymbol{i} - \sin\psi_1 \boldsymbol{j} + \cos\psi_1 \cos\phi_1 \boldsymbol{k}\right), \tag{3.30}$$

$$\mathbf{r}_{K_{ST}} = L_1 \left(\cos\psi_1 \sin\phi_1 \boldsymbol{i} - \sin\psi_1 \boldsymbol{j} + \cos\psi_1 \cos\phi_1 \boldsymbol{k}\right), \tag{3.31}$$

$$\mathbf{r}_2 = \mathbf{r}_{K_{ST}} + a_2 \left(\cos\psi_1 \sin\phi_2 \boldsymbol{i} - \sin\psi_1 \boldsymbol{j} + \cos\psi_1 \cos\phi_2 \boldsymbol{k}\right), \tag{3.32}$$

$$\mathbf{r}_{H_{ST}} = \mathbf{r}_{K_{ST}} + L_2 \left(\cos\psi_1 \sin\phi_2 \boldsymbol{i} - \sin\psi_1 \boldsymbol{j} + \cos\psi_1 \cos\phi_2 \boldsymbol{k}\right), \tag{3.33}$$

$$\boldsymbol{r}_3 = \boldsymbol{r}_{H_{ST}} + a_3 \left(-\theta_3 \boldsymbol{i} + \boldsymbol{j} + \psi_3 \boldsymbol{k}\right), \tag{3.34}$$

$$\boldsymbol{r}_{H_{SW}} = \boldsymbol{r}_{H_{ST}} + L_3 \left(-\theta_3 \boldsymbol{i} + \boldsymbol{j} + \psi_3 \boldsymbol{k}\right), \tag{3.35}$$

$$\mathbf{r}_4 = \mathbf{r}_{H_{SW}} + a_4 \left(-\cos\psi_4 \sin\phi_4 \boldsymbol{i} + \sin\psi_4 \boldsymbol{j} - \cos\psi_4 \cos\phi_4 \boldsymbol{k}\right), \tag{3.36}$$

$$\mathbf{r}_{K_{ST}} = \mathbf{r}_{H_{SW}} + L_4 \left(-\cos\psi_4 \sin\phi_4 \boldsymbol{i} + \sin\psi_4 \boldsymbol{j} - \cos\psi_4 \cos\phi_4 \boldsymbol{k}\right), \tag{3.37}$$

$$\mathbf{r}_5 = \mathbf{r}_{K_{SW}} + a_5 \left(-\cos\psi_4 \sin\phi_5 \boldsymbol{i} + \sin\psi_4 \boldsymbol{j} - \cos\psi_4 \cos\phi_5 \boldsymbol{k}\right), \tag{3.38}$$

and

$$\mathbf{r}_6 = \mathbf{r}_3 + a_6 \left(\sin\phi_6 \cos\psi_6 \boldsymbol{i} - \sin\psi_6 \boldsymbol{j} + \cos\phi_6 \cos\psi_6 \boldsymbol{k}\right). \tag{3.39}$$

3.2.2 Angular Velocity

Following the same assumptions as the previous section, constant ψ_1, ψ_4, θ_3 and small pelvic angles, ψ_3 and ϕ_3, the angular velocities are found using eqn 2.24,

$$\omega_1 = \dot{\phi_1} \cos\psi_1 \boldsymbol{j'} - \dot{\phi_1} \sin\psi_1 \boldsymbol{k'}, \tag{3.40}$$

$$\omega_2 = \dot{\phi}_2 \cos\psi_1 \boldsymbol{j'} - \dot{\phi}_2 \sin\psi_1 \boldsymbol{k'}, \tag{3.41}$$

$$\omega_3 = \dot{\psi}_3 \cos\theta_3 \boldsymbol{i'} - \dot{\phi}_3 \sin\theta_3 \boldsymbol{j'} \dot{\theta}_3 \boldsymbol{k'}, \tag{3.42}$$

$$\omega_4 = \dot{\psi}_4 \boldsymbol{i'} + \dot{\phi}_4 \cos\psi_4 \boldsymbol{j'} - \dot{\phi}_4 \sin\psi_4 \boldsymbol{k'}, \tag{3.43}$$

$$\omega_5 = \dot{\psi}_4 \boldsymbol{i'} + \dot{\phi}_5 \cos\psi_4 \boldsymbol{j'} - \dot{\phi}_5 \sin\psi_4 \boldsymbol{k'}, \tag{3.44}$$

and

$$\omega_6 = \dot{\phi}_6 \boldsymbol{j'}. \tag{3.45}$$

3.2.3 Generalized Forces

Finally the components of the generalized work for each link are

$$Q_1 = 0, \tag{3.46}$$

$$Q_2 = (M_1^y - M_2^y)\cos\psi_1, \tag{3.47}$$

and

$$Q_3 = 0 \tag{3.48}$$

following the example of section 2.1.4. Similarly the components of the generalized work due to the external couples on the stance side thigh are given by

$$Q_1 = 0, \tag{3.49}$$

$$Q_2 = (M_2^y - M_3^y)\cos\psi_1, \tag{3.50}$$

and

$$Q_3 = 0 \tag{3.51}$$

and the pelvis

$$Q_1 = M_3^x, \tag{3.52}$$

$$Q_2 = 0, \tag{3.53}$$

and

$$Q_3 = M_3^z. \tag{3.54}$$

The components of the generalized work for the swing side thigh are given by

$$Q_1 = 0, \tag{3.55}$$

$$Q_2 = (M_4^y - M_5^y)\cos\psi_4, \tag{3.56}$$

$$Q_3 = 0, \tag{3.57}$$

the components of the generalized work for the swing side shank are

$$Q_1 = 0, \tag{3.58}$$

$$Q_2 = M_5^y \cos\psi_4, \tag{3.59}$$

$$Q_3 = 0. \tag{3.60}$$

3.3 Summary

The programs *FD_work_angled_crutch.nb* and *FD_work_angled_crutch_local_min.nb* in Appendix C derive the EOM for the ten DOF model and solve for the angle of each link during the swing and stance phases of gait. The program uses the position of the COG, the angular velocity and the generalized forces with assumed known joint torques to assemble Lagrange's equations. The programs also calculates the work done per gait cycle.

Chapter 4

Crutch Compensation of Hip Abductor Weakness and Paralysis

The two models of Chapter 3 are simulated to prove the hypothesis that an angled crutch compensates for the effect of paralyzed hip abductors on gait kinematics, the presence of other compensatory motions and/or lowers the work done. The first model shows how gait kinematics change as a result of hip abductor paralysis. Then the effect of the compensatory motions, torso tilting and hip hiking, are characterized in the model. The compensatory motions are presumed to be compensatory motions for weak or paralyzed hip abductors because they act in the same plane as the hip abductor muscles. If a crutch is to reduce the presence of compensatory motions, then the crutch must also reverse the effect of paralyzed hip abductors in the same way compensatory motions do.

The second model, which assumes that the kinematics are known, is used to calculate the time varying crutch load (and joint torques) needed for normal gait kinematics in the presence of paralyzed hip abductors. Finally, the crutch load is assumed to be various magnitude step functions, and the hip abductor moment needed for normal gait kinematics is calculated. The hypothesis is that the larger the body weight (BW) supported on a crutch, the lower the hip abductor moment the model predicts. This means a crutch reduces the need for hip abductors with the idea that the less the hip abductors are needed, the less compensatory motions

would be needed if the abductors were to be totally paralyzed.

4.1 Forward Dynamics Model

The forward dynamics model, as mentioned before, assumes that the joint torques are known. The assumed known joint kinetics or the torques are taken from the average measured in experiment for non-disabled individuals [48], [74]. Kinetic profiles for non-disabled individuals were used because of a lack of quantitative data for the specific disability chosen, weak or paralyzed hip abductors. Increasing hip abductor disability is idealized as a proportional decrease in the torque developed at the hip in the frontal plane. Another assumption is that the joints are frictionless. This assumption is a bit of a departure from reality because inactive or paralyzed muscles would tend to resist and dissipate movement somewhat. The assumed known joint torques are used to solve for the kinematics and compared to average normal kinematics. A detailed summary of the effect on each joint is presented in Appendix A and only the results that are related to the hypothesis are presented here.

4.1.1 Weak/Paralyzed Hip abductors

Body segment parameters are taken from de Leva [13] and used in the six degree of freedom (DOF) model of walking and walking with crutches and solved using forward dynamics. Average experimental joint kinematics (Neumann [48]) are curve fit with a five-term Fourier series. Winter [74] found that more than 99% of the

power is contained in frequencies below 6 Hz for body kinematics. The model only considers the swing and stance phases of steady gait. The model ignores the double support phase of gait as well as stopping and starting motions. For example, the knee kinematics are shown in Fig. 4.1, the stance phase is shown in the box on the left and the swing phase is shown in the box on the right. The kinematics or kinetics are substituted into the equations of motion to estimate the joint torques or joint angles respectively. The angular velocity and acceleration derived by differentiating the curve fit [69].

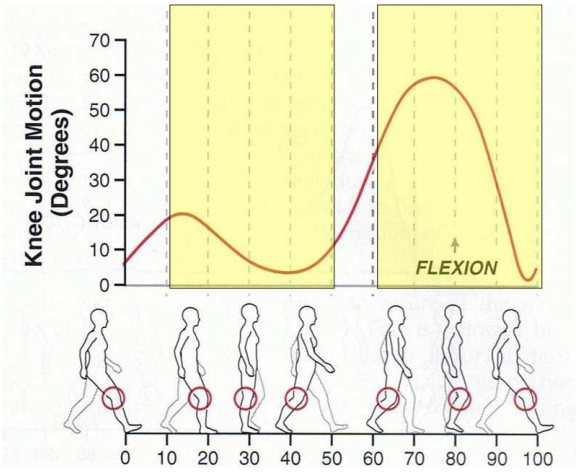

Figure 4.1: Angle of the knee joint during one cycle of non-disabled gait, adapted from Neumann [48]. The two regions that are not boxed, 0-10% and 50-50%, are the double support phase, a brief period when both feet are in contact with the ground. The x-axis is percent of the stride.

The six DOF model developed in section 3.2 is run with average joint torques of normal gait and then with the hip abductors 50% paralyzed and fully paralyzed. The average kinetics used as inputs to the model are derived from motion analysis

of live subjects. Pandy and Berme [54], [55], [57] were able to closely mimic average kinematics with assumed joint torques that are significantly different than average. This is indicative of differences between the model physics and those of a real person. The predicted kinematics are compared to average (from Neumann [48] and Winter [74]) in Fig. 4.2. The solid line represents average kinematics observed in experiment and the dashed, dot-dashed and dotted lines represent the model predicted kinematics for fully functional hip abductors, 50% paralyzed and fully paralyzed respectively.

Figure 4.2 shows the pelvic kinematics in the horizontal (Fig. 4.2a) and frontal (Fig. 4.2b) planes versus normalized time. The models predicts that the hip ab-

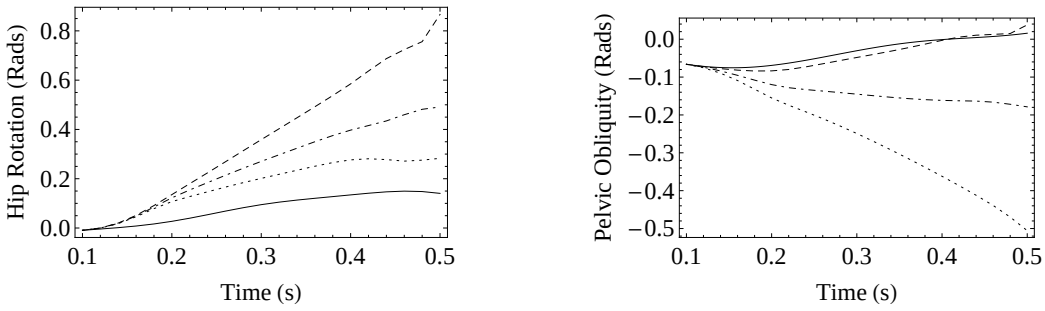

(a) Hip Rotation

(b) Pelvic Obliquity

Figure 4.2: The average frontal (a) and horizontal (b) plane kinematics for one gait cycle of non-disabled individuals are shown with a solid line. The three-dimensional model predicted kinematics with no crutch and fully-functional hip abductors are shown with a dashed line, 50% paralyzed hip abductors with a dot-dashed line and fully-paralyzed hip abductors with a dotted line. The model predicts a decrease in the range of pelvic obliquity and an increase in the range of pelvic rotation.

ductors play an important role in the kinematics of the pelvis in the frontal and

horizontal planes. The pelvic obliquity range of motion in the frontal plane (Fig. 4.2b) is increased nearly five times for paralyzed compared to fully functional hip abductors. This is expected because the hip abductors are the muscles that control the angle of the pelvis in the frontal plane, and in their absence the pelvis is depressed further and further throughout the gait cycle. The hip rotation in the horizontal plane, shown in Fig. 4.2a, reflects a change in the hip rotation kinematics brought on by the absence of hip abductors. The pelvis orientation in the frontal plane affects the kinematics in the horizontal plane by changing the mass moment of inertia.

Figure 4.3 is a plot of the work done by the model as a function of hip abductor strength. There are two important points in this figure. At zero on the x-axis, the

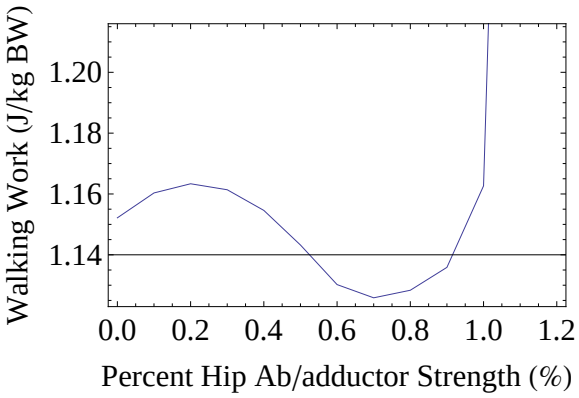

Figure 4.3: Model predicted work per half gait cycle as a function of the level of hip abductor paralysis. A local minima in the work done per step is found near 70%. The reason that the minima is not at 100% is likely due to physical differences between the model and reality.

hip abductors are paralyzed, and the work predicted by the model is more than the

lowest point at 0.7. This shows that the average hip abductor torque is not the optimal torque profile for the assumed model dimensions, in fact the hip abductor torque should be 70% of average for the model to have the most efficient stride with respect to work.

The effect of pelvic depression in the frontal and horizontal planes as a result of hip abductor weakness is shown in Fig. 4.4. The model assumes that the swing leg

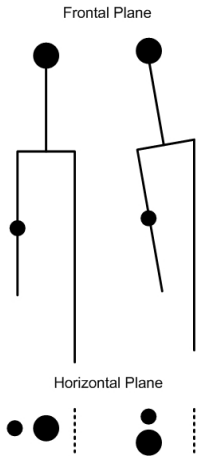

Figure 4.4: Drawing of the relative positions of the center of mass of the torso and swing leg in the frontal and horizontal planes. The left figure shows the approximate orientation of the pelvis for non-disabled walking. The right figure shows how the tendency of the pelvis to be depressed during a stride for individuals with weak or paralyzed hip abductors.

and torso are perpendicular to the pelvis at all times. The hip abductor weakness in this model shows that the more the pelvis is depressed in the frontal plane, the closer the swing leg gets to the stance leg and the further the torso gets from the stance leg. The stance leg can be assumed to be the axis of rotation for the pelvis in the frontal plane because of model assumptions. The torso accounts for approximately

50% of the body's mass, moving it further away from the axis of rotation increases the mass moment of inertia. For average hip abductor torque the pelvis rotates less when the torso is further from the rotation axis.

Despite the rapid pelvic depression, its presence is not reflected in the model's prediction of the height of the swing side toe during the stride, Fig. 4.5. However,

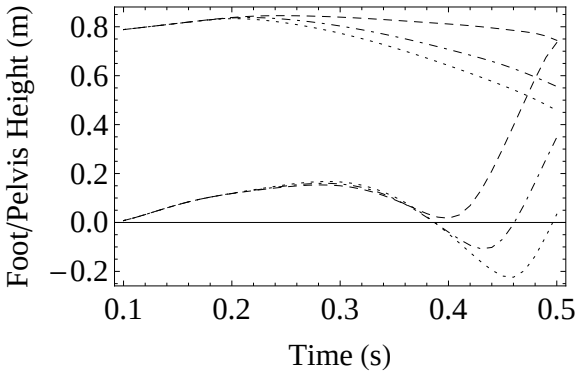

Figure 4.5: Height of the swing-side foot (lower curve) and the pelvis (upper curve). The model predicted trajectory of the pelvis and swing-toe with fully-functional hip abductors is shown with a dashed line, 50% paralyzed hip abductors with a dot-dashed line and fully-paralyzed with a dotted line. The model predicts that the hip abductors play a part in coordinating the height where the swing-side foot slows in preparation for heel-strike. The point where the swing-side foot slows down in preparation for heel-strike falls through the floor with hip abductors disability.

Fig. 4.5 shows that the zero vertical velocity point, the point where the swing-side toe begins to increase in height near 0.4 s, becomes lower as the hip abductors are more paralyzed. This means that the model predicts the hip abductors play a role in decelerating the swing-side toe in preparation for heel-contact.

There are several reasons that these so-called "normal" or average inputs pre-

dict a pathological gait or one that differs from "average". One reason is that the activation pattern and magnitudes of a person's joints vary widely and the pattern would have to be "tuned" for each specific person's anthropometry. Additionally, the model walks with a flat foot. This leads to exaggerated motions and coincides with a higher energy cost per unit distance than "normal" walking. The model predicts an energy cost of 2.19 J/kgBW-m for the first three-quarters of the gait cycle (until the swing-toe has zero vertical velocity) compared to an energy cost of 2.0 J/kgBW-m for "average" kinetics. The model also predicts a shorter step length of 0.53 m compared to an average step length of 0.6 m for an "average" individual which is consistent with this type of disability.

4.1.2 Torso Tilting

A gait pathology that is thought to be a compensation for the pathological effects associated with hip abductor weakness is lateral displacement of the trunk. This is idealized in the model as torso tilting. This motion places the body's center of gravity over the stance leg, reducing the demand on the hip abductors to stabilize the body in the frontal plane. The ability of torso tilting to compensate for the other pathological effects identified by the model is also examined.

The model idealizes the torso as rigidly attached to the pelvis. The effect of tilting the torso with respect to the pelvis in the frontal plane over the stance leg is characterized by simulating the model with the torso vertical, tilted 12 and 24 degrees over the stance leg in the frontal plane. Figure 4.6 shows the kinematics in

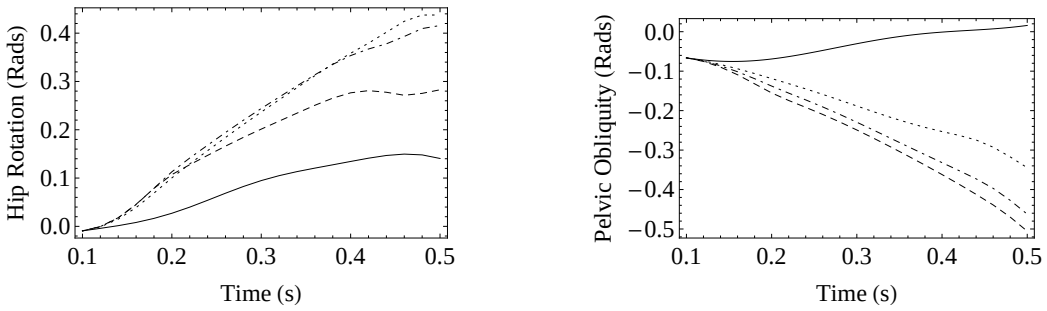

(a) Hip Rotation

(b) Pelvic Obliquity

Figure 4.6: The average horizontal (a) and frontal (b) plane kinematics for one gait cycle of non-disabled individuals is shown with a solid line. The three-dimensional model predicted kinematics with no crutch and the torso vertical, tilted 12 degrees and 24 degrees with a dashed, dot-dashed and dotted line respectively. The model predicts that gait kinematics return to more "normal" ranges (for the model) when the torso is tilted over the stance-leg in a gait with paralyzed hip abductors.

the frontal and horizontal planes versus normalized time. Figure 4.6b shows that torso tilting helps to reduce the range of the pelvic obliquity. Additionally torso tilting helps to increase the hip rotation, shown in Fig. 4.6a.

Figure 4.7 is the model predicted work for half a gait cycle, plotted as a function of the tilt angle of the torso. This graph shows that decreasing the range of pelvic obliquity and increasing the range of hip rotation decreases the work done to a certain point, after which it takes more work to complete a step. It is important to note that the model assumes no power is used to stabilize the torso in the frontal plane. This is why the model predicts it takes less work to walk with a tilted torso and paralyzed hip abductors than it does with fully functional hip abductors. The model also predicts an optimal torso tilt angle to minimize the work done during a

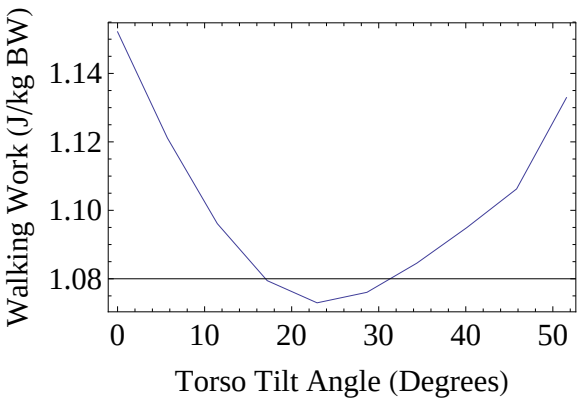

Figure 4.7: Model predicted work as a function of the tilt of the torso. A local minima is found at 22^0 where the center of mass of the torso is just a little past directly over top of the stance leg. The model predicts that the most energy efficient gait with paralyzed hip abductors is one where the torso and the swing-leg are balanced over the stance-leg.

stride. It will be demonstrated that the compensatory motions, torso tilting and hip hiking, as well as contralateral crutch reverse some pathological gait defects caused by paralyzed hip abductors, and there is a relationship between these compensatory motions, crutch use and the work done.

The increase in hip rotation can be explained by looking at how torso tilting alters the bodies configuration in the horizontal and frontal planes, Fig. 4.8. Tilting the torso over the stance leg places the center of mass of the torso over the stance leg, reducing the overall mass moment of inertia in the horizontal plane. This has the opposite effect from hip abductor weakness/paralysis as shown in Fig. 4.4. This difference is because the distance between the center of mass of the torso is closer to the axis of rotation. Hip rotation has been identified in literature as a motion that increases step length.

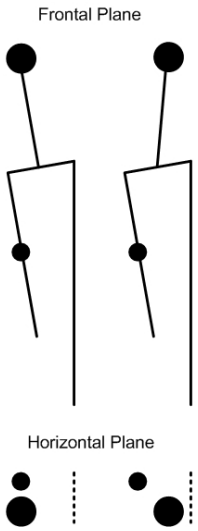

Figure 4.8: Drawing of the relative positions of the center of mass of the torso and swing leg in the frontal and horizontal planes with a drooping pelvis and with a drooping pelvis and the torso tilted. The left figure shows a snapshot of the characteristic orientation of the swing-leg, stance-leg and torso in a gait with paralyzed hip abductors. The right figure shows that same gait with torso tilted over the stance leg.

The tilt angle of the torso in the frontal plane has the opposite effect on the vertical swing-toe clearance as paralysis of the hip abductors, Fig. 4.9. The model predicts that tilting the torso over the stance leg decelerates the swing-side toe in the same way as the hip abductors do. This explains why individuals with weak/paralyzed hip abductors tilt their torso. Tilting the torso also helps control the height and deceleration of the swing-side foot in preparation for heel-contact as well as reduce the work done.

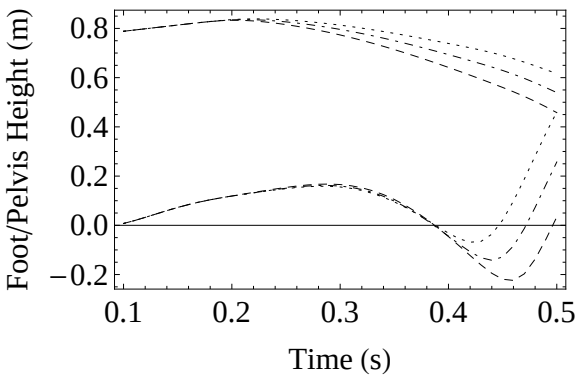

Figure 4.9: Height of the swing-side foot (lower curve) and the pelvis (upper curve), dashed line is with the torso vertical, dot-dashed with the torso at a 12 degree angle and dotted is with the torso at a 24 degree angle. The model predicts that tilting the torso over the stance-leg during gait with paralyzed hip abductors returns the height where the swing-side foot slows down in preparation for heel-strike to a more normal location.

4.1.3 Hip Hiking

Another gait pathology that is thought to be a compensation method for individuals with weak/paralyzed hip abductors is excessive hip hiking during gait. In gait with weak or paralyzed hip abductors, during double support, individuals raise the swing-side of the pelvis higher than normal. As a consequence, the swing-side pelvis begins the swing-phase higher than normal. Hip hiking is idealized in the model as an increase in the initial angle of the pelvis in the frontal plane. The sagittal plane kinematics are unchanged by the hip hiking and there is no predicted change in hip rotation. Figure 4.10 shows the model predicts a change in the range of the pelvic obliquity. Based on the argument given for the change in hip rotation brought on by weak/paralyzed hip abductor in Fig. 4.8 in section

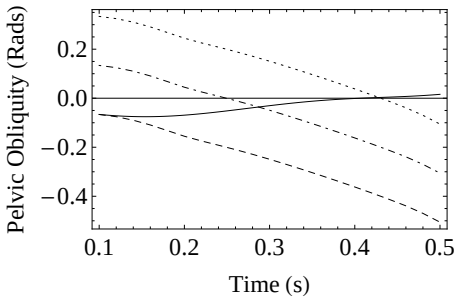

(a) Pelvic Obliquity

Figure 4.10: The average abduction kinematics for one gait cycle of non-disabled individuals is shown with a solid line. The three-dimensional model predicted kinematics with no crutch are shown with a dashed line. The dashed line shows the predicted kinematics with non-functional hip abductor muscles. The dot-dashed line shows the model predicted kinematics when the hip is hiked up 12 degrees at the beginning of the gait cycle and the dotted line, the hip is hiked up 24 degrees.

4.1.2, we would expect a similar change caused by torso tilting. However the model does not predict a change in hip rotation due to torso tilting. Alexander [1] claims that the explanatory power of a model is enhanced through simplicity. However, in this case, a simplified model only leads to confusion that could ultimately only be clarified through experimentation. The power or work that would have to be done to elevate the swing-side hip before the swing/stance phase of gait would be done during double support. The model does not consider the double support phase of gait, when both feet are on the ground so the model makes no prediction in that regard about the work required to hike the hip.

The model does predict that there is a slight increase in step length as the hip is hiked up (Fig. 4.11).

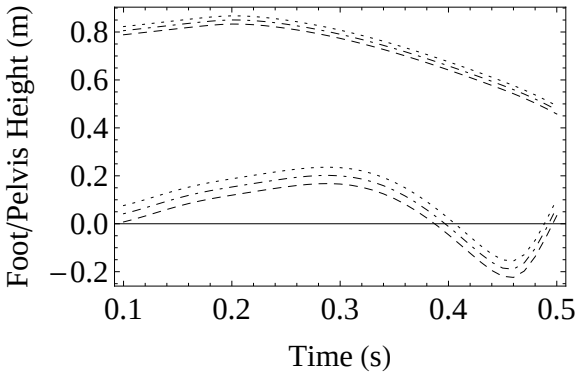

Figure 4.11: Model predicted height of the swing-side foot (lower curves) and the pelvis (upper curves). The dashed line represents a gait with paralyzed hip abductors and the dot-dashed and dotted lines are when the hip is hiked 12 and 24 degrees at the beginning of the gait cycle. The model assumes that hip hiking only changes the position that the pelvis tilts down from. Hiking the hip is predicted by the model to increase the ground clearance during a stride.

4.1.4 Crutch Compensation

Two main ways to compensate for weak or paralyzed hip abductors are by balancing the body over the stance-leg to reduce the need for hip abductors or by developing an equivalent moment. A method to develop an equivalent moment is use of a contralateral crutch. The crutch is idealized as perfectly transmitting the crutch force through the arm to the shoulder. This assumption neglects that the work that the arms must do to stabilize the crutch. The crutch is assumed to create an external vertical force on the swing-side shoulder, equivalent to 12.5% and 25% of body weight, the model predicted kinematics versus normalized time are shown in Fig. 4.12. The kinematics at the other joints change very little as a result of crutch

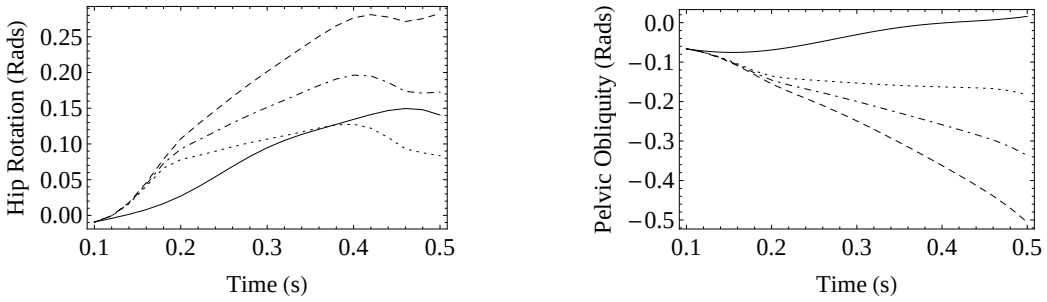

(a) Hip Rotation

(b) Pelvic Obliquity

Figure 4.12: The average horizontal (a) and frontal plane (b) kinematics for one gait cycle of non-disabled individuals is shown with a solid line. The three-dimensional model predicted kinematics with no crutch are shown with a dashed line. The dashed line shows the predicted kinematics with non-functional hip abductor muscles and the dot-dashed and dotted lines represent 12.5% and 25% BW supported on the crutch. The model predicts that contralateral crutch use decreases the range of hip rotation and pelvic obliquity, a greater reduction is achieved proportional to the body weight supported on the crutch.

use and are not discussed here. Figure 4.12b shows a return to more "normal" pelvic obliquity as a result of contralateral crutch use. Figure 4.12a shows the hip rotation as a result of crutch use. The model predicts that contralateral crutch use reduces the range of hip rotation. This may be viewed as an improvement because the range of motion is closer to "normal" but there is a decrease in the range of hip rotation. Figure 4.2a shows that, when the hip abductors are fully functional, the range of hip rotation is about 0.8 rads. When the abductors are fully paralyzed the range of hip rotation is 0.25 rads, which would result in a shortened step, although the model does not predict this. Contralateral crutch use does however improve the range of motion of pelvic obliquity by cutting the range in half when no crutch is

used versus supporting 25% BW on a contralateral crutch. This is shown in Fig. 4.12b with the dashed and dotted lines respectively.

Figure 4.13 is a plot of the model predicted work done as a function of the BW supported on a contralateral crutch. This figure shows that there is a slight

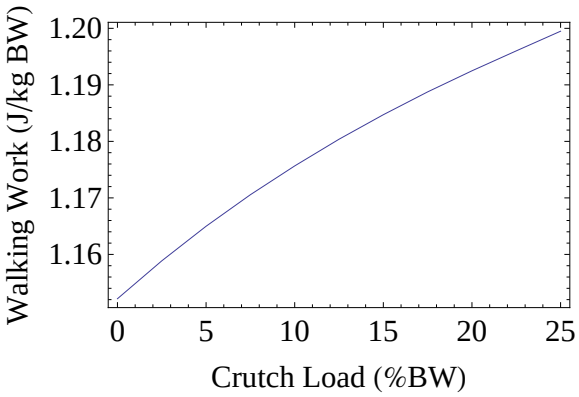

Figure 4.13: Model predicted work as a function of the body weight supported by a contralateral crutch. The model predicts a slight increase in the work per step as the load supported on a contralateral crutch increases.

increase in the work cost associated with improving the kinematics of the pelvis in the frontal plane through crutch use without altering the joint torques. This energetic cost may be worth it, though, because there are repetitive stress disorders associated with this kind of pelvic depression in the frontal plane.

4.1.4.1 Angled Crutch Use

Next, the effect of angling the crutch, which implies a horizontal force is applied to the user, is investigated. Again the crutch load is assumed to be transmitted through the arm to the shoulder where it is applied to the body. In the previous

section, it was found that a vertical contralateral crutch decreases the range of hip rotation. The model predicts that angling the crutch increases the range of motion of hip rotation (Fig. 4.14a). The increased range of motion is evidenced in the dot-dashed and dotted lines that represent using a 12 and 24 degree crutch angle respectively. The model predicts that contralateral crutch use returns the pelvic obliquity to a more "normal" trajectory, shown in Fig. 4.14b, which does not appear to depend on the crutch angle. Notice that the dashed and dotted lines are overlaid in Fig. 4.14b.

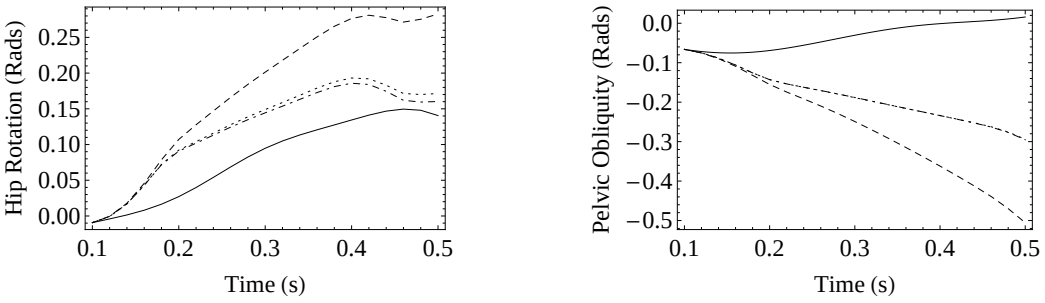

(a) Hip Rotation

(b) Pelvic Obliquity

Figure 4.14: The average horizontal (a) and frontal (b) plane kinematics for one gait cycle of non-disabled individuals are shown with a solid line. The three-dimensional model predicted kinematics and power with a crutch supporting 15% BW at an angle of 12 and 24 degrees are shown with a dot-dashed and dotted line. The model predicted kinematics and power with no crutch are shown with a dashed line for reference. The model predicts that angled crutch use increases the range of motion of hip rotation but does not have any other improved benefit on pelvic obliquity compared to vertical crutch use.

The previous energy plot, Fig. 4.13, predicted that the work done per half gait cycle increases as more load is supported vertically on a contralateral crutch.

The model predicts a decrease in work as the crutch angle is increased (Fig. 4.15). Loading of the underarm can lead to reduced repetitive stress damage, called crutch palsy, a disorder caused by excessively loading the axillary pad of a crutch with the underarm. Although, individuals are instructed not to support weight on the axillary support they frequently do. Load and duration are the risk factors associated with axillary nerve damage. Angling the crutch requires lower loads. If that load is inadvertently supported on the axillary support, the load is reduced.

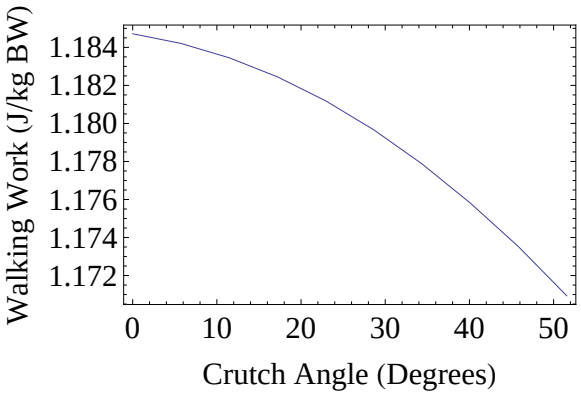

Figure 4.15: Work done per half gait cycle as a function of crutch angle with 15% BW supported on the crutch. The model predicts that it takes slightly less work per step as a wider crutch stance is employed.

A simple diagram, Fig. 4.16 shows how a horizontal force from a contralateral crutch creates an effective moment in the horizontal plane. As the pelvis rotates counterclockwise, the horizontal component of the crutch force helps to advance the hip rotation.

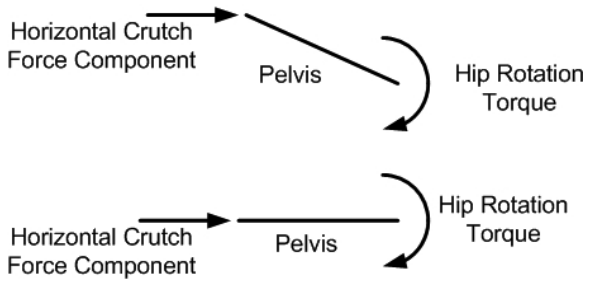

Figure 4.16: Free body diagram of the pelvis in the horizontal plane at time, t=0.1 (bottom) and at t=0.5 s (top). The horizontal component of a crutch force, angled in the frontal plane, constructively works with the hip rotator muscles.

4.1.5 Summary

In this section, three key pathological gait characteristics were identified as a consequence of weak or paralyzed hip abductors. They are excessive pelvic depression in the frontal plane, decreased hip rotation and a change in the coordination of slowing the swing-side foot for heel-contact, as well as a rise in the energy cost of walking. Two compensatory motions observed in individuals with weak hip abductor were investigated to see if they reduce or reverse the changes in gait kinematics caused by weak or paralyzed hip abductors. The compensatory motions, torso tilting and hip hiking were found to reduce excess pelvic obliquity, and hip hiking was found to increase the step length.

The compensatory motions, torso tilting and hip hiking, lead to repetitive stress pain in the lower back and knee. So, alternatives to these compensatory motions are preferable. Crutch use has been identified as another means of compensating for weak or paralyzed hip abductor in previous sections. The model

developed here predicts that crutch use improves pelvic obliquity kinematics, but there is a trade-off with respect to the work done and an increase in hip rotation. Conversely angled crutch use improves pelvic obliquity and hip rotation ranges of motion whereas vertical crutch use improve only pelvic obliquity kinematics. Additionally, angled crutch use is predicted to reduce the work done per stride, which makes it preferable to vertical crutch use.

The models predict that crutch use decreases the need for the compensatory motions hip hiking and lateral displacement of the torso but the work per step changes only a small amount. Both compensatory motions, torso tilting and hip hiking, cause strain on the lower back and knees [73], [46]. Avoiding these motions is desirable and may be so even if the energy cost of walking is increased slightly because walking is a healthier form of locomotion than wheelchair use.

Alleviating repetitive stress on the back and knee is likely a performance objective that is concurrent with lowering the energy cost of walking for individuals with weak or paralyzed hip abductors. Ren et al. [59] have suggested the existence of multiple performance objectives during walking and that they may change depending on the situation. Walking and running are an example differing performance objectives based on different situations. While walking the performance objective might be minimization of energy and while running the performance objective may be to maximize running speed. Competing performance objectives, which may lead to irregular walking motions, help explain why pathological gait increases the energy cost of walking.

4.2 Inverse Dynamics Model

The ten degree of freedom model is solved assuming that the kinematics of each joint are known at each point in time. The model predicts the torques at each joint and the force a contralateral crutch, used vertically and at a 12 degree angle, must develop in order for the model to have "average" kinematics. The work that must be done by the arms to support a load on the crutch is not calculated. Also the model is only valid for the swing and stance phases of gait during steady walking, not while starting or stopping. The model predicts that contralateral crutch use has little effect on the system kinetics except on the hip torque in the frontal plane (Fig. 4.17), which is plotted against normalized time. The remaining joint torques

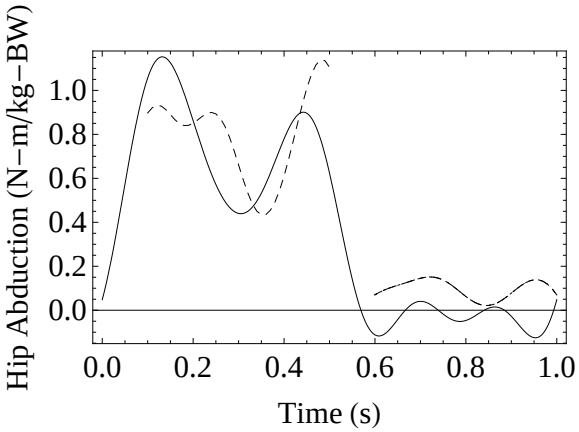

Figure 4.17: The average frontal plane torque for one gait cycle of non-disabled individuals are shown with a solid line. The three-dimensional model predicted in/eversion and abduction with no crutch is dashed. The model predicted torques are shown with a dashed line. Double support, which is not modeled is from 0.1-0.2 and 0.5-0.6 seconds.

are summarized in Appendix B. The two curves shown in Fig. 4.17 are the average

value found by Winter [74] (solid line) and the model predicted hip abductor torque (dashed line). The hip abductor torques predicted by the model are within the range of what is considered normal, which validates the model to some degree. Difficulty in experimentally measuring the mass moment of inertia of body segments, variability between subjects [9], and the assumed order of pelvic motions [21], all effect model predictions and inherent error associated with inverse dynamics [60].

When the model is solved to find the crutch force, the hip abductors are assumed to be paralyzed so no torque is developed or dissipated at that joint. In reality, a paralyzed joint may still dissipate power due to the elastic nature of the tissue that is still present. Figure 4.18 shows the time varying crutch load for a vertical crutch and one at a 12 degree angle that is needed to maintain normal joint kinematics with paralyzed hip abductors. The crutch loads are qualitatively identical to the stance-side hip abductor moment predicted by the model (see figs. 4.17 and 4.18). Quantitatively speaking, the load that must be developed by a crutch is 50% of the hip abductor moment that must be developed for normal gait kinematics when the crutch is vertical and 30% when the crutch is angled 12 degrees. The model shows that there is an angle at which a contralateral crutch compensates for hip abductor paralysis. moment is necessary. The static planar model of Neumann [48] is extended to allow the line of action of the assistive device to vary in the frontal plane, as allowed by the novel crutch designed by Haslach and Borrelli [32], [33]. The static planar model predicts a hip abductor torque that is comparable to the time-average hip abductor torque predicted by the 10-DOF model. The static planar model is presented next and the optimal crutch angle is

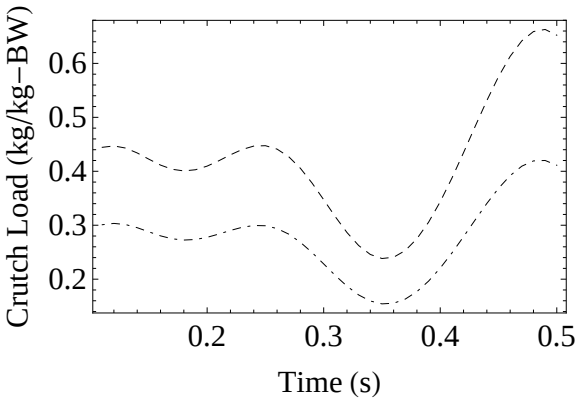

Figure 4.18: Plot of the model predicted time varying crutch load necessary to maintain "average" gait kinematics with fully paralyzed hip abductors. The dashed line is a vertical crutch and the dot-dashed line is with a crutch at a 12 degree angle. The model predicts that a normal gait is possible with paralyzed hip abductors if weight is supported on a contralateral crutch. Furthermore, less load can be supported on the contralateral crutch if the crutch is used at an angle.

calculated.

4.2.1 Trunk Model

The static model of Neumann [48] is extended [8] by assuming the joint reaction force (JRF), hip abductor force (HAF), the body weight (BW) and the crutch force (CF) act through a plate which represents the upper body. The reason for using a plate to model the upper body is that now the crutch force can act at an angle, β, in the frontal plane other than vertical. A free body diagram of the upper body in the frontal plane is shown in Fig. 4.19.

Assuming that all of the forces are known, the hip abductor force required for

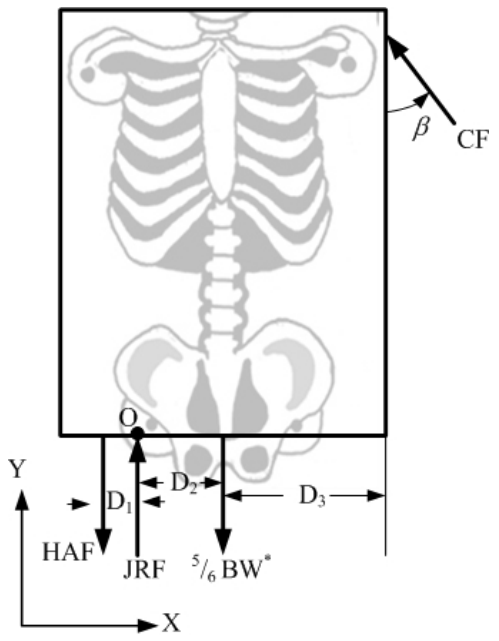

Figure 4.19: Free body diagram of the upper body. Five sixths body weight (5/6 BW) is the weight of the body minus the stance leg. Skeleton picture is from the web [29].

static equilibrium can be calculated by summing the moments about O,

$$\sum M_o = 0 : HAF \cdot D_1 - \frac{5}{6} BW \cdot D_2 + CF \cos\beta \cdot (D_2 + D_3) + CF \sin\beta \cdot D_4 = 0, \quad (4.1)$$

where β is the angle of the crutch force (CF) in the frontal plane. Neumann [48] gives values for D_1, D_2 and D_3. The distance from the HAF force to the JRF force, D_1, is 4.39 cm, the distance from the JRF to the center of gravity (COG), D_2, is 8.64 cm, the horizontal distance from the COG to the point of application of the CF, D_3 is 26.36 cm and the vertical distance from the pelvis to the point of application of the CF, $D_2 + D_3$, is 53.9 cm. Assume that the crutch force is equal to 10% of the total BW, and a BW of 77 kg.

The hip abductor moment necessary to stabilize the pelvis without a crutch, the solid line in Fig. 4.20, is 0.71 Nm/kg-BW. The dashed and dotted lines are the

hip abductor moment predicted by eqn 4.1 with 12.5% and 25% BW supported on a contralateral crutch. The average hip abductor moment predicted by the inverse dynamics model with 12.5% and 25% BW (not enough of a load to fully compensate for paralyzed hip abductors) and the planar static model predictions are shown in Fig. 4.20.

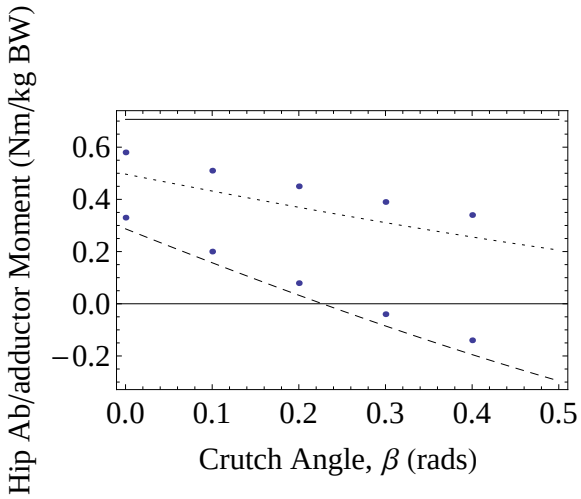

Figure 4.20: Plot comparing predictions from the static planar model and average values from the inverse dynamics model. The solid line is the hip abductor moment predicted by the static planar model for no crutch. The dashed line is the hip abductor moment predicted by the static planar model with a contralateral crutch supporting 12.5% BW and the dotted line is with 25% BW supported. The x-axis is the angle at which the crutch is used. The dots are the average hip abductor moment for the swing-side predicted by the three-dimensional ten degree of freedom model for various crutch loads and angles.

This model demonstrates that using a wide crutch stance, where the crutch is placed at a wider angle than normal, decreases the role of the hip abductors while standing still or reduces compensatory motions in individuals with weak or

paralyzed hip abductors. The hip abductor moment required for static equilibrium decreases as the crutch stance width increases. Assuming a coefficient of friction of 0.5, the value for a rubber type footpad on linoleum, a maximum angle of 0.46 radians (26.5^o) may be used before the device slips.

Both models, the static planar model and 10 degree of freedom three-dimensional model, predict a similar trend and similar hip abductor magnitudes. The dots are the average hip abductor moment for the swing-side predicted by the three-dimensional ten degree of freedom model for various crutch loads and angles. The solid lines are the hip abductor moment with no crutch (top line), with a contralateral crutch supporting 12.5% BW and 25% BW at various angles.

This simple diagram can facilitate crutch decisions affecting use and fitting by physical therapists. If compensatory motions are exhibited by a patient, a physical therapist can recommend that a wider crutch stance be used with the knowledge that the work done by the individual will increase slightly. The less the hip abductors are needed, the less compensatory motions are exhibited in the presence of paralyzed hip abductors.

4.2.2 Summary

The ten degree of freedom inverse dynamics model predicts a decreasing dependence on the hip abductor torque, necessary to maintain a "normal" gait, as more body weight is supported on a contralateral crutch. With the same load on a contralateral crutch, the hip abductor moment necessary decreases further as the

crutch is used with a wider base of support. Therefore the more weight supported on a contralateral crutch and/or the wider the crutch stance, the less work the hip abductors must do. The less work that is required by the hip abductors, the less need there is for compensatory motions needed in the presence of paralyzed hip abductors. The model predicts a slight, nearly negligible, increase in the total work done when the BW supported on a contralateral crutch is increased and/or the crutch angle is varied. The work that must be done by the arms to stabilize a crutch and support weight on the crutch is likely directly proportional to the BW supported. The model predicts that the same effect caused by using a vertical crutch on a gait with paralyzed hip abductors can be achieved by supporting less weight on a contralateral crutch if it is angled. It is likely that the work done by the arms is proportional to the weight supported on a contralateral crutch. So, this suggests that it would take less work if the crutch was used at an angle, if the work done by the arms was included, compared to if the crutch was used vertically.

Chapter 5

Summary and Future Work

Contralateral crutch use has been shown in the literature to reduce compensatory motions exhibited by individuals with gait pathologies including weak or paralyzed hip abductors. Individuals with weak/paralyzed hip abductors and various other gait pathologies have been observed by the author and others in patients using the *Strutter*© at an angle in the frontal plane as opposed to vertically. The Strutter is a crutch like orthosis which is similar to the new crutch discussed in this thesis. However, the Strutter is not designed to be used at an angle, and its structure deforms when the crutch is used in this way. Three models were used to evaluate the hypothesis behind the new crutch, that angling a contralateral crutch in the frontal plane compensates for weak or paralyzed hip abductors better than a vertical crutch.

The new crutch was designed using the Strutter as a frame, to which modular components can be added to based on specific muscle and gait pathologies. The muscle dealt with in this thesis is the hip abductor. Hip abductor weakness does not exist in isolation, meaning it is uncommon to find individuals with only weak or paralyzed hip abductors. For this reason human experiments are not feasible since a suitable cohort would be difficult to find. Therefore the disability is modeled.

The hypothesis is tested by assuming that the reasons people angle the crutch

are to improve gait kinematics, reduce compensatory motions and/or lower the work done during a step. Three models are used to identify the effect of the disability hip abductor weakness/paralysis on gait kinematics, the effect of compensatory motions on weak/paralyzed hip abductor gait and how the work done varies as a function of these changes. The effect of the two compensatory motions, torso tilting and hip hiking, on weak/paralyzed hip abductor gait are characterized. In order to verify that a crutch reduces compensatory motions, it must be shown to produce the same effect on gait as compensatory motions. The effect of crutch use and angled crutch use on weak/paralyzed hip abductor gait is also characterized.

First a static planar model of standing is developed. The model shows that while standing still, tilting the torso over the stance leg and hiking the hip move the body center of gravity over the stance leg. These motion reduce the moment required by the hip abductor muscles for static equilibrium. There is even a point where the body is balanced over the stance leg and so no hip abductor moment is needed for static equilibrium. The model is used to show that static equilibrium can be achieved with a contralateral crutch and no hip abductor moment but without compensatory motions. Also, angling the crutch reduces the load that must be supported on the crutch because angling the crutch increases the moment arm the crutch acts through.

The second model is a six degree of freedom three-dimensional dynamic model solved using forward dynamics. This assumes the torque at each joint is known for all time. The simulation using the model first characterizes the effect of hip abductor paralysis on gait. The model predicts that all the gait kinematics are

changed, but the biggest change is in the range of motion of the pelvic obliquity and hip rotation. The pelvic obliquity range of motion increases and alters the height where the swing-side foot slows down in preparation for heel-contact. The hip rotation range of motion decreases, which would cause a decrease in step length, although this is not predicted by the model. Lastly, the total work done per stride is calculated. The model predicts it requires more work to walk without hip abductors than with them.

The simulation by the six degree of freedom model characterizes the effect of torso tilting and hip hiking. Torso tilting improves the range of pelvic obliquity and worsens the range of hip rotation. Torso tilting also helps to return the height where the swing-side foot slows to down to a more normal level. Hip hiking is predicted to increase step length. A local minimum is found with respect to torso tilt angle for the total work done per step. The work done for hip hiking is not modeled. The model shows that the compensatory motions each contribute some improvement to the pathological gait and may each have an optimal coordination with respect to the total work required.

Next the model shows that crutch use improves range of pelvic obliquity (decreased range) and restricts the range of hip rotation (decreased range). Crutch use was also shown to improve swing-side foot coordination. The model also predicts it takes more work per step, as more weight is supported on a contralateral crutch. The most important prediction of the model is that angling the crutch improves the range of motion of both pelvic obliquity (decreased range) and hip rotation (increased range) as well as the coordination of the swing-side foot. Angled crutch use

is also predicted to decrease the total work done as the crutch angle increases.

The third model is a ten degree of freedom three-dimensional dynamic model solved using inverse dynamics. The hip abductor moment is assumed to be zero, and the load that must be supported on a vertical contralateral crutch necessary to maintain normal gait kinematic is calculated. The model predicts that an average of 40% body weight supported on a contralateral crutch completely compensates for paralyzed hip abductors. However if the crutch is angled 12 degree, the average body body weight that must be supported is 30%.

The inverse dynamics model is also used to calculate how the hip abductor moment changes when a constant load is supported on a vertical contralateral crutch. As more load is supported on a vertical contralateral crutch, the model predicts that the hip abductor moment required for normal gait decreases. The required hip abductor moment decreases further still if the crutch is angled. The time-average hip abductor moment predicted by the inverse dynamics model is compared to that predicted by the static planar model as a function of crutch load and angle. Both models predict the same trend. The more load supported on a vertical contralateral crutch, the less need there is for the hip abductors to stabilize the body in the frontal plane. Angling the crutch further reduces the need for the hip abductors. So it follows that an individual with weak or paralyzed hip abductors should use crutches at as wide a stance as they can tolerate, until the point at which the crutch slips or constrained by space to walk.

A relationship between hip abductor weakness, compensatory motions and crutch use has been suggested in literature from experimental observation. This

thesis provides an explanation for the observed link. Torso tilting and hip hiking reverse pathological gait kinematics in the same way as a contralateral crutch. The models in this thesis suggest that angling a contralateral crutch decreases pathological gait kinematics more than a vertical crutch. Upright ambulation is preferable to wheelchair use because the longer a person maintains upright ambulation, the better the general health of the person [61]. For this reason individuals with weak or paralyzed hip abductors should try using a wide crutch stance before upright ambulation is abandoned. The models presented here suggest that the new crutch reduces compensatory motions when used at an angle further than a vertical crutch and provides relief from repetitive stress on the knees and back caused by torso tilting and hip hiking.

Future Work

Individuals with weak or paralyzed hip abductors frequently have accompanying muscle disabilities such as weak or paralyzed ankle dorsi/plantarflexors, knee flexors/extensors and/or hip flexors/extensors. This study models the individual muscle disability hip abductor weakness or paralysis to identify how gait kinematics are affected and how compensatory motions or crutch use corrects these irregularities. The models developed here could also be used to better understand the effect of other muscle disabilities, such as ankle dorsi/plantarflexor, knee flexor/extensor or hip flexor/extensor disability, and associated compensatory motions on gait. This information can be used to identify best practice for crutch use for these particular

disabilities and aid in the understanding of how different disabilities interact and change a non-disabled gait.

The work here makes two predictions that lead to questions that could be answered through further study. The first is the prediction of the six degree of freedom model of an increase in hip rotation and a decrease in the work done per step when using an angled crutch compared to vertical. The second is that local minimums in the required work were found with respect to hip abductor paralysis level and torso tilt angle.

Without a human study, angled crutch use should only be employed, following a physical therapist's recommendation, if an individual is planning to abandon crutch walking in favor of a wheelchair because of knee and/or back pain. Based on the six degree of freedom model predictions, the results of a human experiment study can be expected to show a decrease in energy expenditure and an increase in step length for individuals with weak hip abductors when using an angled crutch as opposed to a vertical one. The models, in general, predict a small decrease in work and, although the model does not predict an increase in step length, it is likely to occur. The six degree of freedom model does not predict an increase in step length because it predicts an increase in knee and hip extension. It is unlikely that individuals with hip abductor weakness will exhibit excessive hip and knee extension, in fact the opposite is true. Individuals with weak hip abductors exhibit excessive knee flexion.

Many other studies indicate that gait is chosen to minimize the energy cost. The required work curves presented in this thesis provide further evidence that

walking is an energy optimization process because local minima were found. The local minima indicate that one gait takes less energy than another. The solution techniques used were inverse and forward dynamics. These solution techniques are heavily dependent on the assumed known quantities, the kinematics and kinetics respectively. Assuming that a gait cycle minimizes the work done and solving as an optimization problem reduces the number of input parameters needed. Reducing the dependence on input parameters allows both the kinematics and kinetics to vary, which is likely more realistic than assuming the kinetics or kinematics stay the same, as done in this thesis. A dynamics walking model solved using optimization would be more useful for physical therapists considering individual orthosis usage. An optimization model could theoretically reduce the inputs to measuring step length or stride time from a complete kinematic (3-D motion analysis) or kinetic (body mounted goniometers) description.

All of the so-called perturbations to each model are, in effect, a sensitivity analysis. The physical orientation of the body was perturbed in the form of varying the initial pelvic angle in the frontal plane or varying the angle of the torso in the frontal plane. The magnitude of the torque at the hip in the frontal plane was also varied. Lastly, the effect on gait of varying magnitude and direction of an external force, acting on the model's "shoulder", in the frontal plane was characterized. The predictions of these simulations indicate the models are highly sensitive to perturbations. This is indicative of a system with a small basin of attraction.

This raises the question of the stability of the models presented here. The inverse dynamics model is implicitly stable because it is constrained to go through

a stable gait motion. The forward dynamics model does not necessarily go through a stable motion. The gait predicted by the models must be checked to determine whether it is realistic or not. For example the inverse dynamics model may predict joint torques that are unrealistic or the forward dynamics model may pick a motion that is impossible, excessive knee flexion for example. Solving the models using optimization is a way to incorporate a stability criterion and/or impose limits on the range of motion of some or all of the joints in the model.

The current models do not include the double support phase of gait and are only valid for steady walking, one that is a limit cycle. Double support as well as the energy lost from heel contact and due to joint dissipation must be included to model an entire gait cycle and/or starting or stopping walking. Including the double support phase of gait in the model introduces new constraints and makes the system harder to solve. Modeling walking as a system with non-continuous constraints allows for the inclusion of double support and walking at a non-steady speed.

Appendix A

Forward Dynamics Results

The model predicted ankle angle is shown in Fig. A.1a. The angle shown with a solid line is the negative of the ankle plantar flexion recorded by Winter [74] and Neumann [48]. Since the model lacks a foot, the "ankle angle" cannot be directly compared to ankle flexion. This is because during the stance phase, the foot is only flat on the ground for a short period of time in the middle of a stride. This leads to the initial difference between the experimental ankle angle and the model predicted angle. Experiment and the model show positive work being done by the ankle or rather, power is developed at the ankle for the duration of the gait cycle. The model predicted ankle power reaches the same maximum observed in experiment if only the first three-quarters of the gait cycle are considered, Fig. A.1b, resulting in a shorter step.

Figure A.1c is the model predicted knee flexion/extension (flexion is shown as positive and extension is shown negative) and experimental observations. The model solves for the right knee motion during the stance phase and left knee motion during the swing phase. Symmetry is assumed, meaning that when the right knee is in the swing phase, it follows the same trajectory as the left knee during its stance phase. Joint kinematics in the stance phase are plotted from 0.1 to 0.5 second and joint kinematics in the swing phase are plotted from 0.6 to 1 second.

By symmetry, it is assumed that the kinematics are for the right side of the body. It is also assumed that double support occurs between 0 and 0.1 seconds and 0.5 to 0.6 second. During the stance phase of gait, the stance knee extends prematurely and excessively. The swing leg knee follows a somewhat normal trajectory until approximately three-quarters of the gait cycle until it extends excessively. The hip also extends excessively, shown in Fig. A.1e.

The power curves are the product of the angular velocity at a joint and the torque. Positive power means that the joint is generating power and negative power means that the joint is absorbing power. Simply put, this means that when a joint is developing power, it is accelerating the body and when a joint is absorbing power, it is decelerating the body. The power developed at the knees, Fig. A.1d, follows a similar pattern as observed in experiment. However, the model predicts that stance-side knee develops and absorbs more power than what is observed in experiment. The model predicted swing-side knee develops/absorbs nearly no power at all until after three-quarters of the gait cycle. After three-quarters of the gait cycle, the swing-side knee absorbs about 5 times more power than any other joint. The power absorbed by the swing-side knee is developed at the hip, both stance and swing-sides, just after three-quarters of the gait cycle, Fig. A.1f.

The model predicts a hip rotation trajectory that is also excessive, Fig. A.2a but the pelvic obliquity predicted by the model is in good agreement with experiment, figure A.2c. However, some of the the power developed at the hip is also absorbed by the hip rotators, Fig. A.2b after three-quarters of the gait cycle. Some power is also generated by the pelvis in the frontal plane after three-quarters of the

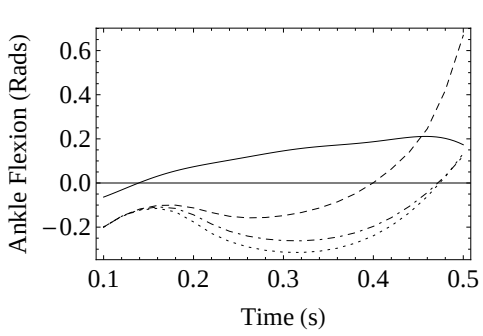

(a) Ankle dorsi/plantar flexion

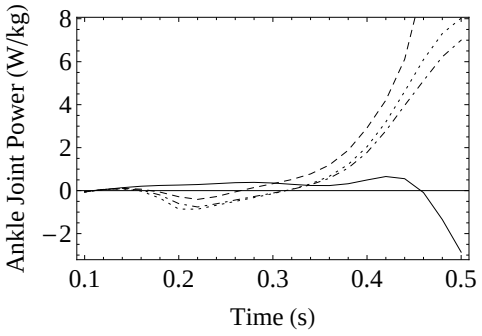

(b) Ankle Joint Power

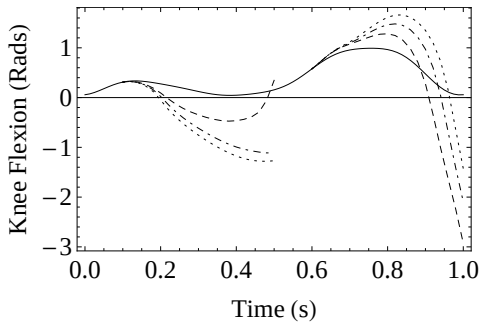

(c) Knee flexion/extension

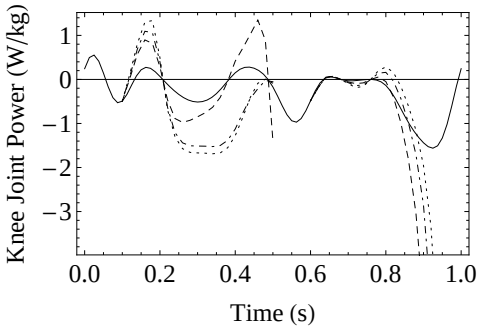

(d) Knee Joint Power

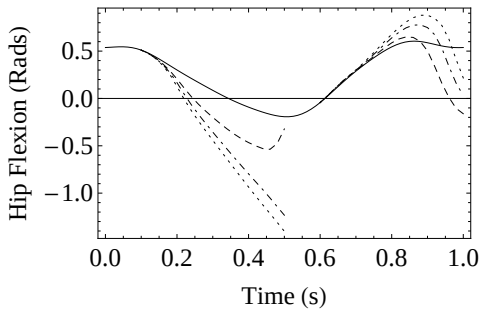

(e) Hip flexion/extension

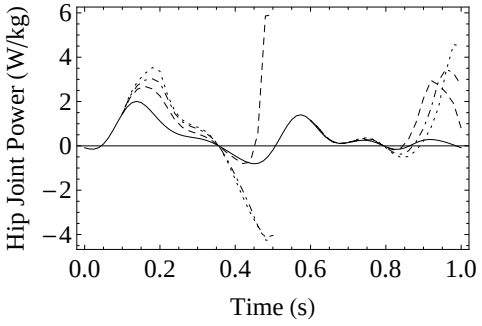

(f) Hip Joint Power

Figure A.1: The average flexion/extension and power profiles in the sagittal plane for one gait cycle of non-disabled individuals are shown in black. The three-dimensional model predicted kinematics with no crutch and fully-functional hip abductors are shown with a dashed line, 50% paralyzed hip abductors with a dot-dashed line and fully-paralyzed hip abductors with a dotted line.

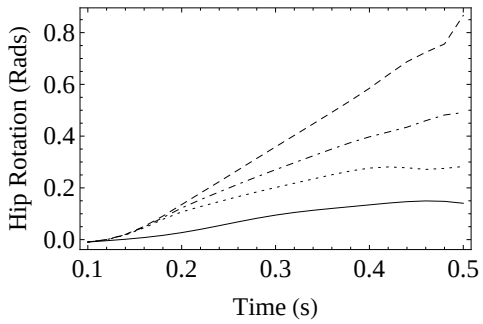

(a) Hip Rotation

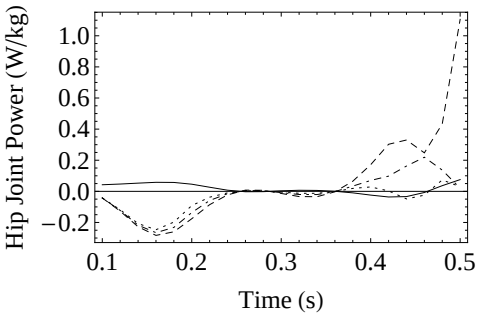

(b) Hip Joint Power

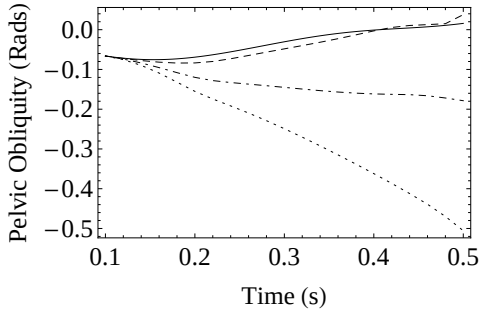

(c) Pelvic Obliquity

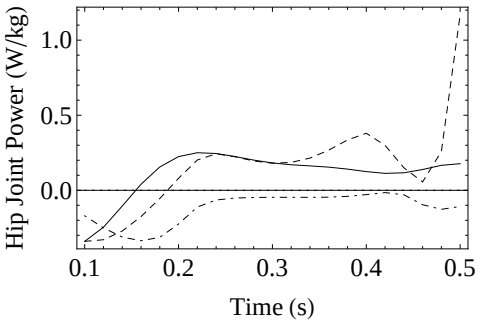

(d) Hip Joint Power

Figure A.2: The average frontal (4.2a) and horizontal (4.2b) plane kinematics and power profiles for one gait cycle of non-disabled individuals are shown in black. The three-dimensional model predicted kinematics with no crutch and fully-functional hip abductors are shown with a dashed line, 50% paralyzed hip abductors with a dot-dashed line and fully-paralyzed hip abductors with a dotted line.

gait cycle. This suggests that there are significant drawbacks to not following the average joint kinematics. As a result of the difference, the rest of the joints absorb significant more power generated by the hip abductors and flexors than normal. The effect of weak/paralyzed hip abductor torques are shown in the following figures; figs. A.1, A.2 and A.3. The model is run with normal hip abductor torques and then with decreasing magnitude torques, in 50% increments, until the effect of the hip

abductor torques are absent. Dashed lines indicate fully functional hip abductor, dot-dashed lines represent 50% paralyzation and dotted lines show fully paralyzed hip abductors. Figure A.2c shows how profound an effect the hip abductors have on the obliquity of the pelvis. As the hip abductor effect decreases, the pelvis depresses towards the ground 30 degrees more, which would certainly shorten a person's step length. However, the model predicts that as the level of paralysis of the hip abductor muscles increases, knee and hip extension increases, shown in figs. A.1c and A.1e, which raises the height of the swing-side toe enough to offset the pelvic depression.

The level of hip abductor paralysis modeled had a profound effect on the other joint powers as well. When the hip abductor are completely paralyzed, the model predicts that the stance-side hip, Fig. A.1e, absorbs power after three-quarters of the gait cycle and the stance-side knee also absorbs power, Fig. A.1c. More power is also absorbed in the frontal plane by the hip, Fig. A.2d.

Figure 4.5 shows the pelvis and swing-side toe clearance or height above the ground. After three-quarters of the gait cycle, the swing side hip and knee extend excessively. This motion could be described as a high-kick. The model is only realistically valid until just before the "high-kick". The point when the swing-side toe-clearance reaches a minimum, where the velocity in the vertical direction is zero. This point is constructively considered toe-contact.

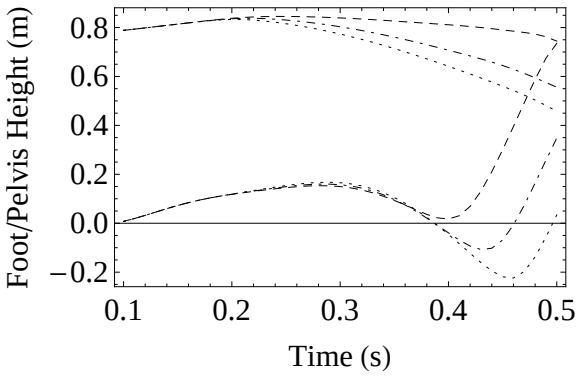

Figure A.3: Height of the swing-side foot (lower curves) and pelvis (upper curves). The model predicted trajectory of the pelvis and swing-toe with fully-functional hip abductors is shown with a dashed line, 50% paralyzed hip abductors with a dot-dashed line and fully-paralyzed with a dotted line.

Appendix B

Inverse Dynamics Results

The ten degree of freedom model is solved assuming that the kinematics of each joint are known at each point in time. The model predicts the torques at each joint which are compared to values found by Neumann [48]. The model predicted torques for no-crutch and for a contralateral crutch supporting 12.5% and 25% body weight (BW) are shown in Fig. B.1. The model predicts that contralateral crutch use has little effect on the sagittal plane kinetics but the difference between the model predictions and what is in literature is significant. The inverse dynamics model predicts torques that are significantly different from what is in literature for the no-crutch case. There are several things that are likely causing this difference, the absence of a foot, the variation exhibited from one person to the next and the fact that the error associated with inverse dynamics is known to be as high as 200%.

With this in mind, it is more instructive to examine the power curves at each joint. In normal walking, power is developed on the swing-side at the ankle, knee and hip, from 0.1 to 0.2 seconds, then the knee absorbs power and then develops power again. The hip absorbs power from 0.4 seconds until the end of the stance phase. The model predicts excessive power is developed at the swing-side ankle, knee and hip, then absorbs excessive power for the rest of the cycle except for the ankle and hip, begin to develop power again at the end of the swing phase from 0.4

to 0.5 seconds. It is like a bad controller, oscillating excessively about the desired power. The hip abductor and ankle in/everter moment predicted is shown in Fig. B.3, and the hip rotator torque is shown in Fig. B.3a. The crutch also has no effect on the predicted hip rotation torque in the horizontal plane. The model predicted work at the ankle is twenty times greater than what is in the literature. This could be because the moment at the ankle acts like a ground reaction moment, Fig. B.2b. The hip abductor moment predicted by the model could be considered normal, which make the predicted power developed at the hip normal as well, figs. B.2c and B.2d. The model predicts minor changes in the kinetics and power as a result of contralateral crutch use. However the model predicts a significant change in the hip abductor moment required. As the crutch load increases, the hip abductor moment predicted decreases. A reduction in the hip abductor moment necessary reduces the need for compensatory motions in the presence of paralyzed hip abductors. The excessive torques predicted by the model will inevitably lead to an increase in the work predicted by the model. Work is the sum of the time integral of all the power curves. The model predicts the work is three times the work in the literature. When using a contralateral crutch with 12.5% and 25% BW supported, the work predicted is 2.99 times and 2.96 times larger.

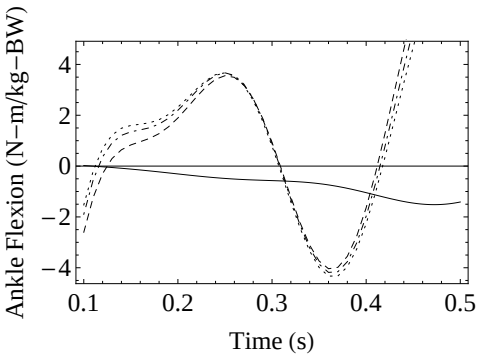

(a) Ankle dorsi/plantar flexion

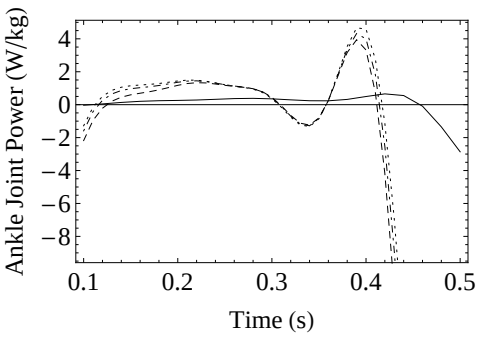

(b) Ankle dorsi/plantar flexion

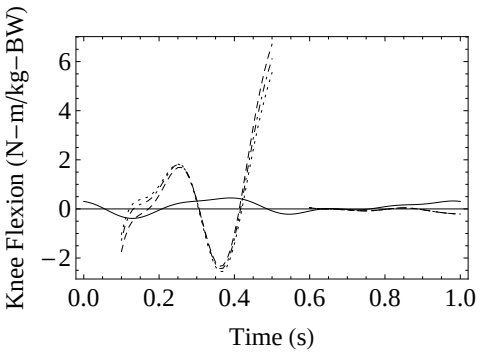

(c) Knee flexion/extension

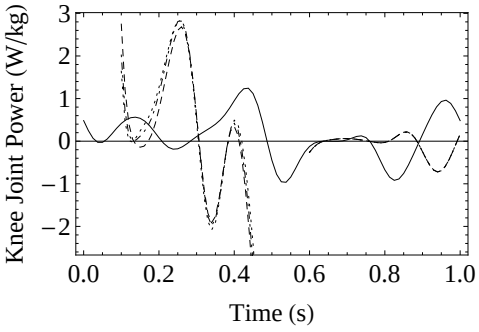

(d) Knee flexion/extension

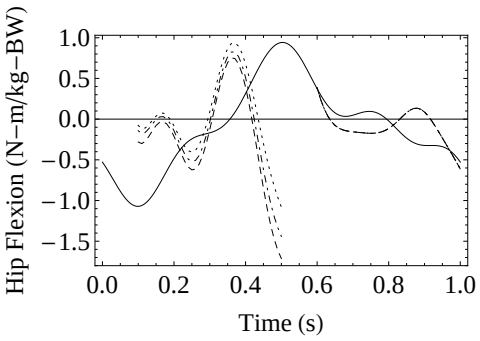

(e) Hip flexion/extension

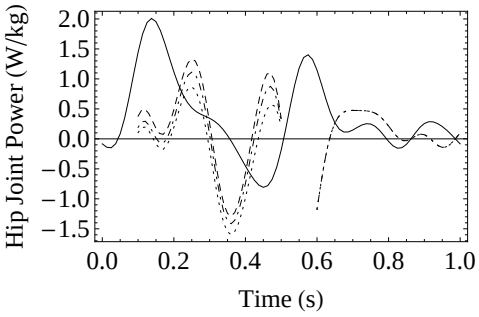

(f) Hip flexion/extension

Figure B.1: The average sagittal plane torque and power profiles for one gait cycle of non-disabled individuals are shown with a solid line. The three-dimensional model predicted flexion/extension torque and power curves with no crutch are shown with a dashed line and with a contralateral crutch supporting 12.5% BW and 25% BW with a dotted and dot-dashed line.

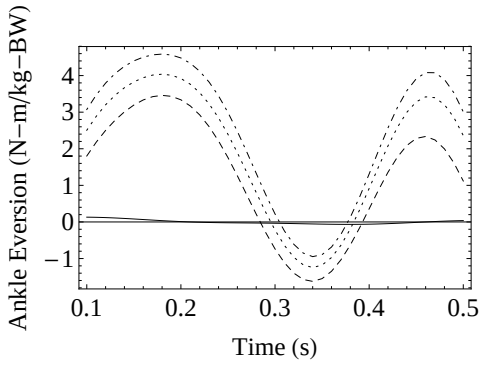

(a) Ankle eversion/inversion

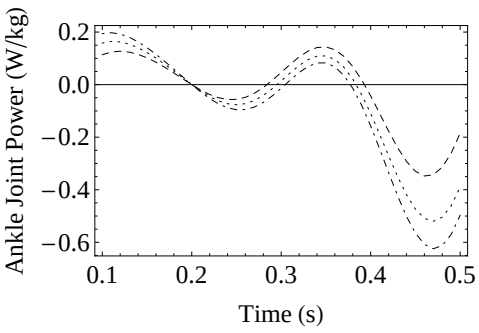

(b) Ankle eversion/inversion

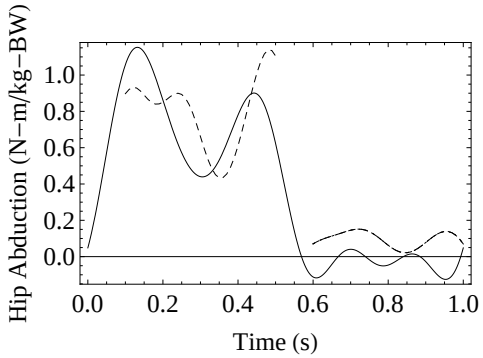

(c) Hip abbduction/adduction

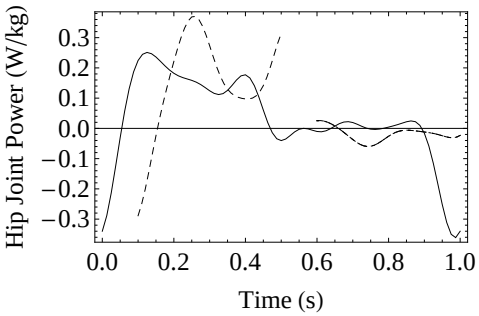

(d) Hip abbduction/adduction

Figure B.2: The average frontal plane torque and power profiles for one gait cycle of non-disabled individuals are shown with a solid line. The three-dimensional model predicted in/eversion and abduction with no crutch is dashed. The model predicted torques and power with a contralateral crutch supporting 12.5% BW and 25% BW are shown with a dotted and dot-dashed line.

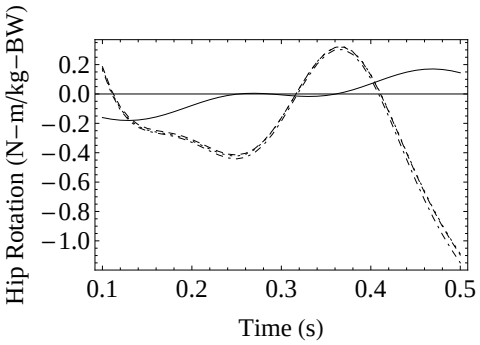

(a) Hip Rotation

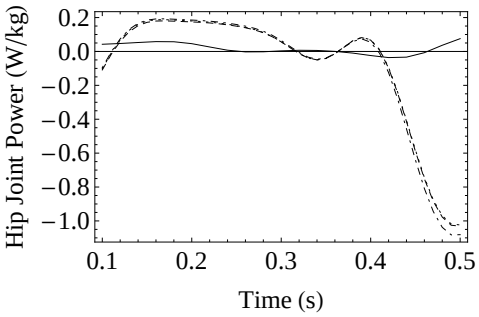

(b) Hip Rotation

Figure B.3: The average horizontal plane torque and power profiles for one gait cycle of non-disabled individuals are shown with solid line. The three-dimensional model predictions with no crutch are shown with dashed, dotted and dot-dashed lines which represent the model predictions with 12.5% BW and 25% BW supported on a contralateral crutch respectively.

Appendix C

Mathematica Code

The position of the center of mass, $\boldsymbol{r}_G$, the velocity of the center of mass, $\boldsymbol{v}_G$, the angular velocity, $\boldsymbol{\Omega}$, the mass-moment of inertial tensor, I_G, and the components of the vector of the generalized force, Q derived in chapter 3 are input into the Mathematica codes that follow. The equations of motion are derived symbolically and can be stated generally as

$$\frac{d}{dt}\frac{\partial L}{\partial \dot{q}} - \frac{\partial L}{\partial q} = Q. \tag{C.1}$$

In the programs *FD_work_angled_crutch.nb* and *FD_work_angled_crutch_local_min.nb* the generalized forces, Q, are assumed to be known and generalized coordinates are solved for as a function of time using the Mathematica package NDSolve. *FD_work_angled_crutch_local_min.nb* calculates the total work done for different gait cycles

In programs *ID_NoAbduct.nb* and *ID_angled_crutch.nb*, the left hand side of eqn C.1 is assumed to be known and the resulting equations are algebraic. The output of *ID_NoAbduct.nb* and *ID_angled_crutch.nb* are the generalized forces, Q, of eqn. C.1.

```
BW = 71.953;
beta1 = 0.1;
beta2 = 0.2;
beta3 = 0.3;
beta4 = 0.4;
Inertia1 = {{0.0369, 0, 0}, {0, 0.0387, 0}, {0, 0, 0.0063}};
Inertia2 = {{0.199, 0, 0}, {0, 0.199, 0}, {0, 0, 0.0409}};
Inertia3 = {{0, 0, 0}, {0, 0, 0}, {0, 0, 0}};
Inertia4 = {{0.199, 0, 0}, {0, 0.199, 0}, {0, 0, 0.0409}};
Inertia5 = {{0.0369, 0, 0}, {0, 0.0387, 0}, {0, 0, 0.0063}};
Inertia6 = {{1.567, 0, 0}, {0, 1.801, 0}, {0, 0, 0.475}};

ΩShankST = {0, ϕ1'[t] Cos[ψ1[t]], - ϕ1'[t] Sin[ψ1[t]]};
ΩThighST = {0, ϕ2'[t] Cos[ψ1[t]], - ϕ2'[t] Sin[ψ1[t]]};
ΩPelvis = { ψ3'[t] Cos[θ3[t]], -ψ3'[t] Sin[θ3[t]] , θ3'[t]};
ΩThighSW = {0, ϕ4'[t] Cos[ψ4[t]], - ϕ4'[t] Sin[ψ4[t]]};
ΩShankSW = {0, ϕ5'[t] Cos[ψ4[t]], - ϕ5'[t] Sin[ψ4[t]]};
ΩTorso = {Cos[θ3[t]] (ψ3)'[t], Sin[ψ6[t]] (θ3)'[t] - Cos[ψ6[t]] Sin[θ3[t]] (ψ3)'[t],
   Cos[ψ6[t]] (θ3)'[t] + Sin[θ3[t]] Sin[ψ6[t]] (ψ3)'[t]};
CurveParams = {1, Sin[2 t π], Sin[4 t π], Sin[6 t π], Sin[8 t π],
   Sin[10 t π], Cos[2 t π], Cos[4 t π], Cos[6 t π], Cos[8 t π], Cos[10 t π]};
AF = Fit[Import["AnkleFlexion.csv"], CurveParams, t];
HA = Fit[Import["HipAbduction.csv"], CurveParams, t];
HF = Fit[Import["HipFlexion.csv"], CurveParams, t];
HR = Fit[Import["HipRotation.csv"], CurveParams, t];
KF = Fit[Import["KneeFlexion.csv"], CurveParams, t];
PO = Fit[Import["PelvicObliquity.csv"], CurveParams, t];
PT = Fit[Import["PelvicTilt.csv"], CurveParams, t];
TF = Fit[Import["Torso_Flexion.csv"], CurveParams, t];
AE = Fit[Import["AnkleEversion.csv"], CurveParams, t];

AEST = -AE /. t → t + 0.1;
AFST = AF /. t → t + 0.1;
HAST = HA /. t → t + 0.1;
HASW = HA /. t → t + 0.6;
HFST = -HF /. t → t + 0.1;
HFSW = -HF /. t → t + 0.6;
HRST = -HR /. t → t + 0.1;
HRSW = -HR /. t → t + 0.6;
KFST = Simplify[KF - HF] /. t → t + 0.1;
KFSW = Simplify[KF - HF] /. t → t + 0.6;
POST = PO /. t → t + 0.1;
```

```
POSW = PO /. t → t + 0.6;
PTST = PT /. t → t + 0.1;
PTSW = PT /. t → t + 0.6;
TFST = TF /. t → t + 0.1;
InitialConditions[1] =
  {ϕ1[0] == KFST, ϕ1'[0] == D[KFST, t], ϕ2[0] == HFST, ϕ2'[0] == D[HFST, t],
    θ3[0] == HRST, θ3'[0] == D[HRST, t], ϕ4[0] == HFSW, ϕ4'[0] == D[HFSW, t],
    ϕ5[0] == KFSW, ϕ5'[0] == D[KFSW, t], ψ3[0] == POST, ψ3'[0] == D[POST, t]} /. t → 0;
InitialConditions[2] = {ϕ1[0] == KFST, ϕ1'[0] == D[KFST, t], ϕ2[0] == HFST, ϕ2'[0] ==
     D[HFST, t], θ3[0] == HRST, θ3'[0] == D[HRST, t], ϕ4[0] == HFSW, ϕ4'[0] == D[HFSW, t],
    ϕ5[0] == KFSW, ϕ5'[0] == D[KFSW, t], ψ3[0] == POST, ψ3'[0] == D[POST, t]} /. t → 0;
InitialConditions[3] = {ϕ1[0] == KFST, ϕ1'[0] == D[KFST, t], ϕ2[0] == HFST, ϕ2'[0] ==
     D[HFST, t], θ3[0] == HRST, θ3'[0] == D[HRST, t], ϕ4[0] == HFSW, ϕ4'[0] == D[HFSW, t],
    ϕ5[0] == KFSW, ϕ5'[0] == D[KFSW, t], ψ3[0] == POST, ψ3'[0] == D[POST, t]} /. t → 0;
InitialConditions[4] = {ϕ1[0] == KFST, ϕ1'[0] == D[KFST, t], ϕ2[0] == HFST, ϕ2'[0] ==
     D[HFST, t], θ3[0] == HRST, θ3'[0] == D[HRST, t], ϕ4[0] == HFSW, ϕ4'[0] == D[HFSW, t],
    ϕ5[0] == KFSW, ϕ5'[0] == D[KFSW, t], ψ3[0] == POST, ψ3'[0] == D[POST, t]} /. t → 0;
InitialConditions[5] = {ϕ1[0] == KFST, ϕ1'[0] == D[KFST, t], ϕ2[0] == HFST, ϕ2'[0] ==
     D[HFST, t], θ3[0] == HRST, θ3'[0] == D[HRST, t], ϕ4[0] == HFSW, ϕ4'[0] == D[HFSW, t],
    ϕ5[0] == KFSW, ϕ5'[0] == D[KFSW, t], ψ3[0] == POST, ψ3'[0] == D[POST, t]} /. t → 0;
StaticVel = {ψ1'[t] -> 0, ψ4'[t] -> 0, ψ6'[t] -> 0, ψ1''[t] -> 0, ψ4''[t] -> 0, ψ6''[t] -> 0};
StaticAngs[1] = {ψ1[t] -> 0, ψ4[t] -> 0, ψ6[t] → 0};
StaticAngs[2] = {ψ1[t] -> 0, ψ4[t] -> 0, ψ6[t] → 0};
StaticAngs[3] = {ψ1[t] -> 0, ψ4[t] -> 0, ψ6[t] → 0};
StaticAngs[4] = {ψ1[t] -> 0, ψ4[t] -> 0, ψ6[t] → 0};
StaticAngs[5] = {ψ1[t] → 0, ψ4[t] → 0, ψ6[t] → 0};



Parameters = {m1 → 3.16, m2 → 10.34, m3 → 5, m4 → 10.34, m5 → 3.16, m6 → 39.953,
   L1 → 0.4344, L2 → 0.4222, L3 → 0.171, L4 → 0.4222, L5 → 0.4344, L6 → .5319,
   a1 → 0.5541 * 0.4344, a2 → 0.5905 * 0.4222, a3 → 0.171 / 2,
   a4 → 0.4095 * 0.4222, a5 → 0.4459 * 0.4344, a6 → 0.5534 * 0.5319,
   g → 9.81};


r1 = a1 {Cos[ψ1[t]] Sin[ϕ1[t]], -Sin[ψ1[t]], Cos[ϕ1[t]] Cos[ψ1[t]]};
rKST = L1 {Cos[ψ1[t]] Sin[ϕ1[t]], -Sin[ψ1[t]], Cos[ϕ1[t]] Cos[ψ1[t]]};
r2 = Simplify[rKST + a2 {Cos[ψ1[t]] Sin[ϕ2[t]], -Sin[ψ1[t]], Cos[ϕ2[t]] Cos[ψ1[t]]}];
rHST = Simplify[rKST + L2 {Cos[ψ1[t]] Sin[ϕ2[t]], -Sin[ψ1[t]], Cos[ϕ2[t]] Cos[ψ1[t]]}];

Rotation1 = {{1, 0, 0}, {0, 1, ψ3[t]}, {0, -ψ3[t], 1}};
Rotation3 = {{1, θ3[t], 0}, {-θ3[t], 1, 0}, {0, 0, 1}};
```

```
C1 = Transpose[Rotation3.Rotation1];

r3 = Simplify[rHST + C1.{0, a3, 0}];
rHSW = Simplify[rHST + C1.{0, L3, 0}];

r4 = Simplify[rHSW + a4 {-Cos[ψ4[t]] Sin[ϕ4[t]], Sin[ψ4[t]], -Cos[ϕ4[t]] Cos[ψ4[t]]}];
rKSW
  = Simplify[rHSW + L4 {-Cos[ψ4[t]] Sin[ϕ4[t]], Sin[ψ4[t]], -Cos[ϕ4[t]] Cos[ψ4[t]]}];
r5 = Simplify[rKSW + a5 {-Cos[ψ4[t]] Sin[ϕ5[t]], Sin[ψ4[t]], -Cos[ϕ5[t]] Cos[ψ4[t]]}];
rtoe = Simplify[rKSW + L5 {-Cos[ψ4[t]] Sin[ϕ5[t]], Sin[ψ4[t]], -Cos[ϕ5[t]] Cos[ψ4[t]]}];

Rotationt1 = {{1, 0, 0}, {0, Cos[ψ6[t]], Sin[ψ6[t]]}, {0, -Sin[ψ6[t]], Cos[ψ6[t]]}};
C2 = Transpose[Rotationt1];
r6 = Simplify[r3 + C2.C1.{0, 0, a6}];
rcrutch = Simplify[r3 + C2.C1.{0, a3, L6}];
v1 = D[r1, t];
v2 = D[r2, t];
v3 = D[r3, t];
v4 = D[r4, t];
v5 = D[r5, t];
v6 = D[r6, t];
Kinetic = 1 / 2 m1 v1.v1 + 1 / 2 m2 v2.v2 + 1 / 2 m3 v3.v3 + 1 / 2 m4 v4.v4 + 1 / 2 m5 v5.v5 + 1 / 2 m6 v6.v6 +
    1 / 2 Simplify[ΩShankST . Inertia1.ΩShankST] + 1 / 2 Simplify[ΩThighST . Inertia2.ΩThighST] +
    1 / 2 Simplify[ΩPelvis . Inertia3.ΩPelvis] + 1 / 2 Simplify[ΩThighSW . Inertia4.ΩThighSW] +
    1 / 2 Simplify[ΩShankSW . Inertia5.ΩShankSW] + 1 / 2 Simplify[ΩTorso . Inertia6.ΩTorso];
Potential = m1 g Part[r1, 3] + m2 g Part[r2, 3] + m3 g Part[r3, 3] +
    m4 g Part[r4, 3] + m5 g Part[r5, 3] + m6 g Part[r6, 3];
Lagrange = Kinetic - Potential;


Eqn1 = D[D[Lagrange, ϕ1'[t], NonConstants → ϕ1'[t]], t] -
    D[Lagrange, ϕ1[t], NonConstants → ϕ1[t]] - Fcrutch . D[rcrutch, ϕ1[t]];
Eqn2 = D[D[Lagrange, ϕ2'[t], NonConstants → ϕ2'[t]], t] -
    D[Lagrange, ϕ2[t], NonConstants → ϕ2[t]] - Fcrutch . D[rcrutch, ϕ2[t]];
Eqn4 = D[D[Lagrange, Θ3'[t], NonConstants → Θ3'[t]], t] -
    D[Lagrange, Θ3[t], NonConstants → Θ3[t]] - Fcrutch . D[rcrutch, Θ3[t]];
Eqn5 = D[D[Lagrange, ψ3'[t], NonConstants → ψ3'[t]], t] -
    D[Lagrange, ψ3[t], NonConstants → ψ3[t]] - Fcrutch . D[rcrutch, ψ3[t]];
Eqn6 = D[D[Lagrange, ϕ4'[t], NonConstants → ϕ4'[t]], t] -
    D[Lagrange, ϕ4[t], NonConstants → ϕ4[t]] - Fcrutch . D[rcrutch, ϕ4[t]];
Eqn7 = D[D[Lagrange, ϕ5'[t], NonConstants → ϕ5'[t]], t] -
    D[Lagrange, ϕ5[t], NonConstants → ϕ5[t]] - Fcrutch . D[rcrutch, ϕ5[t]];
```

```
TorqueAnkleFlexion = Fit[Import["Torque_Ankle_Flexion.xls"], CurveParams, t];
TorqueKneeFlexion = Fit[Import["Torque_Knee_Flexion.csv"], CurveParams, t];
TorqueHF = Fit[Import["Torque_Hip_Flexion.csv"], CurveParams, t];
TorqueAnkleAbduction = Fit[Import["Torque_Ankle_Eversion.xls"], CurveParams, t];
TorqueHipAbduction = Fit[Import["Torque_Hip_Abduction.xls"], CurveParams, t];
TorqueHipRotation = Fit[Import["Torque_Hip_Rotation.csv"], CurveParams, t];

TorqueHRST = TorqueHipRotation /. t → t + 0.1;

TorqueHAST = TorqueHipAbduction /. t → t + 0.1;
TorqueHASW = TorqueHipAbduction /. t → t + 0.6;

TorqueAAST = TorqueAnkleAbduction /. t → t + 0.1;
TorqueAFST = TorqueAnkleFlexion /. t → t + 0.1;

TorqueKFST = TorqueKneeFlexion /. t → t + 0.1;
TorqueKFSW = TorqueKneeFlexion /. t → t + 0.6;

TorqueHFST = TorqueHF /. t → t + 0.1;
TorqueHFSW = TorqueHF /. t → t + 0.6;
Forces[1] = {M1y[t] → -BW TorqueAFST, M2y[t] → -BW TorqueKFST,
    M3y[t] → BW TorqueHFST, M3x[t] → 0, M3z[t] -> BW TorqueHRST,
    M4y[t] → -BW TorqueHFSW, M5y[t] → -BW TorqueKFSW, F_crutch -> {0, 0, 0}};
Forces[2] = {M1y[t] → -BW TorqueAFST, M2y[t] → -BW TorqueKFST, M3y[t] → BW TorqueHFST,
    M3x[t] → 0, M3z[t] -> BW TorqueHRST, M4y[t] → -BW TorqueHFSW,
    M5y[t] → -BW TorqueKFSW, F_crutch -> {0, - 20 Sin[beta1], 20 BW Cos[beta1]}};
Forces[3] = {M1y[t] → -BW TorqueAFST, M2y[t] → -BW TorqueKFST, M3y[t] → BW TorqueHFST,
    M3x[t] → 0, M3z[t] -> BW TorqueHRST, M4y[t] → -BW TorqueHFSW,
    M5y[t] → -BW TorqueKFSW, F_crutch -> {0, - 1.5 BW Sin[beta2], 1.5 BW Cos[beta2]}};
Forces[4] = {M1y[t] → -BW TorqueAFST, M2y[t] → -BW TorqueKFST, M3y[t] → BW TorqueHFST,
    M3x[t] → 0, M3z[t] -> BW TorqueHRST, M4y[t] → -BW TorqueHFSW,
    M5y[t] → -BW TorqueKFSW, F_crutch -> {0, -20 BW Sin[beta3], 20 BW Cos[beta3]}};
Forces[5] = {M1y[t] → -BW TorqueAFST, M2y[t] → -BW TorqueKFST, M3y[t] → BW TorqueHFST,
    M3x[t] → 0, M3z[t] -> BW TorqueHRST, M4y[t] → -BW TorqueHFSW,
    M5y[t] → -BW TorqueKFSW, F_crutch -> {0, -1.5 BW Sin[beta4], 1.5 BW Cos[beta4]}};
Do[EOM[i] = {Eqn1 == (M1y[t] - M2y[t]) Cos[ψ1[t]], Eqn2 == (M2y[t] - M3y[t]) Cos[ψ1[t]],
        Eqn4 == M3z[t], Eqn5 == M3x[t], Eqn6 == (M4y[t] - M5y[t]) Cos[ψ4[t]], Eqn7 == M5y[t]} /.
      StaticVel /. StaticAngs[i] /. Parameters /. Forces[i];
 ggg[i] = Join[EOM[i], InitialConditions[i]];
 output[i] = NDSolve[ggg[i], {ϕ1, ϕ2, Θ3, ψ3, ϕ4, ϕ5}, {t, 0, 0.4}], {i, 1, 5}]
KneeTraj = Table[{1 n / 80, KF /. t → n / 80}, {n, 0, 80}];
```

```
HipTraj = Table[{1 n / 80, HF /. t → n / 80}, {n, 0, 80}];
RotTraj = Table[{0.1 + 0.4 n / 20, -HRST /. t → 0.4 n / 20}, {n, 0, 20}];
AbductionTraj = Table[{0.1 + 0.4 n / 80, PO /. t → 0.1 + 0.4 n / 80}, {n, 0, 80}];
AnkleTraj = Table[{0.1 + 0.4 n / 80, AF /. t → 0.1 + 0.4 n / 80}, {n, 0, 80}];

linestype = {{Black}, {Black, Dashed}, {Black, DotDashed},
    {Black, Dotted}, {Black, Dashed}, {Black, DotDashed}, {Black, Dotted}};

Do[KneeFlexionST[i] =
    Table[{0.1 + 0.4 n / 20, First[ϕ1[t] - ϕ2[t] /. output[i] /. t → 0.4 n / 20]}, {n, 0, 20}];
  KneeFlexionSW[i] = Table[{0.6 + 0.4 n / 20, First[ϕ5[t] - ϕ4[t] /. output[i] /. t → 0.4 n / 20]},
    {n, 0, 20}];
  HipFlexionST[i] = Table[{0.1 + 0.4 n / 20, First[-ϕ2[t] /. output[i] /. t → 0.4 n / 20]},
    {n, 0, 20}];
  HipFlexionSW[i] = Table[{0.6 + 0.4 n / 20, First[-ϕ4[t] /. output[i] /. t → 0.4 n / 20]},
    {n, 0, 20}];
  HipRotationST[i] = Table[{0.1 + 0.4 n / 20, First[-θ3[t] /. output[i] /. t → 0.4 n / 20]},
    {n, 0, 20}];
  HipAbductionST[i] = Table[{0.1 + 0.4 n / 20, First[ψ3[t] /. output[i] /. t → 0.4 n / 20]},
    {n, 0, 20}];
  AnkleFlexion[i] = Table[{0.1 + 0.4 n / 20, First[ϕ1[t] /. output[i] /. t → 0.4 n / 20]},
    {n, 0, 20}], {i, 1, 5}];
KneeFD = ListPlot[{KneeTraj, KneeFlexionST[1], KneeFlexionST[3], KneeFlexionST[5],
    KneeFlexionSW[1], KneeFlexionSW[3], KneeFlexionSW[5]}, Frame → True,
  FrameLabel → {"Time (s)", "Knee Flexion (Rads)"}, PlotRange → All,
  TextStyle → {FontSize → 16}, PlotStyle → linestype, Joined → True]

HipFD = ListPlot[{HipTraj, HipFlexionST[1], HipFlexionST[3],
    HipFlexionST[5], HipFlexionSW[1], HipFlexionSW[3], HipFlexionSW[5]},
  Frame → True, FrameLabel → {"Time (s)", "Hip Flexion (Rads)"}, PlotRange → All,
  TextStyle → {FontSize → 16}, PlotStyle → linestype, Joined → True]

RotFD = ListPlot[{RotTraj, HipRotationST[1], HipRotationST[3], HipRotationST[5]},
  Frame → True, FrameLabel → {"Time (s)", "Hip Rotation (Rads)"}, PlotRange → All,
  TextStyle → {FontSize → 16}, PlotStyle → linestype, Joined → True]

AbductFD =
 ListPlot[{AbductionTraj, HipAbductionST[1], HipAbductionST[3], HipAbductionST[5]},
  Frame → True, FrameLabel → {"Time (s)", "Pelvic Obliquity (Rads)"}, PlotRange → All,
  TextStyle → {FontSize → 16}, PlotStyle → linestype, PlotRange → All, Joined → True]

AnkleFD = ListPlot[{AnkleTraj, AnkleFlexion[1], AnkleFlexion[3], AnkleFlexion[5]},
  Frame → True, FrameLabel → {"Time (s)", "Ankle Flexion (Rads)"}, PlotRange → All,
```

```
  TextStyle → {FontSize → 16}, PlotStyle → linestype, Joined → True]

Do[PelvisHeight[i] =
  Table[{0.1 + 0.4 n / 40, First[Part[r3, 3] /. Parameters /. output[i] /. StaticAngs[i] /.
      StaticVel /. t → 0.4 n / 40]}, {n, 0, 40}]; FootFall[i] =
  Table[{0.1 + 0.4 n / 40, First[Part[rtoe, 3] /. Parameters /. output[i] /. StaticAngs[i] /.
      StaticVel /. t → 0.4 n / 40]}, {n, 0, 40}];
 StepDist[i] = Table[{0.1 + 0.4 n / 40, First[Part[rtoe, 1] /. Parameters /. output[i] /.
      StaticAngs[i] /. StaticVel /. t → 0.4 n / 40]}, {n, 0, 40}], {i, 1, 5}]

ClearanceFD =
 ListPlot[{PelvisHeight[1], PelvisHeight[3], PelvisHeight[5], FootFall[1], FootFall[3],
   FootFall[5]}, PlotStyle → {{Black, Dashed}, {Black, DotDashed}, {Black, Dotted}},
  Frame → True, FrameLabel → {"Time (s)", "Step Height/Distance (m)"},
  PlotRange → All, TextStyle → {FontSize → 16}, Joined → True]

Do[pKneeFlexionST[i] = Table[{0.1 + 0.4 n / 20,
    First[TorqueKFST (ϕ1'[t] - ϕ2'[t]) /. output[i] /. t → 0.4 n / 20]}, {n, 0, 20}];
  pKneeFlexionSW[i] = Table[{0.6 + 0.4 n / 20,
    First[TorqueKFSW (ϕ5'[t] - ϕ4'[t]) /. output[i] /. t → 0.4 n / 20]}, {n, 0, 20}];
  pHipFlexionST[i] = Table[{0.1 + 0.4 n / 20,
    First[-TorqueHFST (ϕ2'[t]) /. output[i] /. t → 0.4 n / 20]}, {n, 0, 20}];
  pHipFlexionSW[i] = Table[{0.6 + 0.4 n / 20,
    First[-TorqueHFSW (ϕ4'[t]) /. output[i] /. t → 0.4 n / 20]}, {n, 0, 20}];
  pHipRotationST[i] = Table[{0.1 + 0.4 n / 20,
    First[-θ3'[t] TorqueHRST /. output[i] /. t → 0.4 n / 20]}, {n, 0, 20}];
  pHipAbductionST[i] = Table[{0.1 + 0.4 n / 20, 0}, {n, 0, 20}];
  pAnkleFlexion[i] = Table[{0.1 + 0.4 n / 20,
    First[-ϕ1'[t] TorqueAFST /. output[i] /. t → 0.4 n / 20]}, {n, 0, 20}], {i, 1, 5}];
ActpKneeFlexion = Table[{ n / 80, TorqueKneeFlexion D[KF, t] /. t → n / 80}, {n, 0, 80}];
ActpHipFlexion = Table[{ n / 80, TorqueHF (D[HF, t]) /. t → n / 80}, {n, 0, 80}];
ActpHipRotationST =
  Table[{0.1 + 0.4 n / 20, D[HRST, t] TorqueHRST /. t → 0.4 n / 20}, {n, 0, 20}];
ActpHipAbductionST = Table[{0.1 + 0.4 n / 20, D[POST, t] TorqueHAST /. t → 0.4 n / 20},
   {n, 0, 20}];
ActpAnkleFlexion = Table[{0.1 + 0.4 n / 20, -D[AFST, t] TorqueAFST /. t → 0.4 n / 20}, {n, 0, 20}];

pKneeFD = ListPlot[{ActpKneeFlexion, pKneeFlexionST[1], pKneeFlexionST[3],
   pKneeFlexionST[5], pKneeFlexionSW[1], pKneeFlexionSW[3], pKneeFlexionSW[5]},
  Frame → True, FrameLabel → {"Time (s)", "Knee Joint Power (W/kg)"},
  TextStyle → {FontSize → 16}, PlotStyle → linestype, Joined → True]

pHipFD = ListPlot[{ActpHipFlexion, pHipFlexionST[1], pHipFlexionST[3],
```

```
   pHipFlexionST[5], pHipFlexionSW[1], pHipFlexionSW[3], pHipFlexionSW[5]},
  Frame → True, FrameLabel → {"Time (s)", "Hip Joint Power (W/kg)"},
  TextStyle → {FontSize → 16}, PlotStyle → linestype, Joined → True]

pRotFD =
 ListPlot[{ActpHipRotationST, pHipRotationST[1], pHipRotationST[3], pHipRotationST[5]},
  Frame → True, FrameLabel → {"Time (s)", "Hip Joint Power (W/kg)"},
  PlotRange → All, TextStyle → {FontSize → 16}, PlotStyle → linestype, Joined → True]

pAbductFD =
 ListPlot[{ActpHipAbductionST, pHipAbductionST[1], pHipAbductionST[3], pHipAbductionST[5]},
  Frame → True, FrameLabel → {"Time (s)", "Hip Joint Power (W/kg)"}, PlotRange → All,
  TextStyle → {FontSize → 16}, PlotStyle → linestype, PlotRange → All, Joined → True]

pAnkleFD =
 ListPlot[{ActpAnkleFlexion, pAnkleFlexion[1], pAnkleFlexion[3], pAnkleFlexion[5]},
  Frame → True, FrameLabel → {"Time (s)", "Ankle Joint Power (W/kg)"},
  TextStyle → {FontSize → 16}, PlotStyle → linestype, Joined → True]

steps = 100;
time = 0.3;
CalcWork =
 72 (Sum[{Abs[TorqueKFST (D[KFST, t] + D[HFST, t]) time / steps /. t → time n / steps]}, {n,
       0, steps}] +
    Sum[{Abs[TorqueKFSW (D[KFSW, t] + D[HFSW, t]) time / steps /. t → time n / steps]},
     {n, 0, steps}] +
    Sum[{Abs[TorqueHFST (D[HFST, t]) time / steps /. t → time n / steps]}, {n, 0, steps}] +
    Sum[{Abs[TorqueHFSW (D[HFSW, t]) time / steps /. t → time n / steps]}, {n, 0, steps}] +
    Sum[{Abs[D[HRST, t] TorqueHRST time / steps /. t → time n / steps]}, {n, 0, steps}] +
    Sum[{Abs[D[POST, t] TorqueHAST time / steps /. t → time n / steps]}, {n, 0, steps}] +
    Sum[{Abs[D[AFST, t] TorqueAFST time / steps /. t → time n / steps]}, {n, 0, steps}])

Do[{ModelWork[i] =
   72 (Sum[{Abs[time TorqueKFST (ϕ1'[t] - ϕ2'[t]) / steps /. output[i] /. t → time n / steps]},
       {n, 0, steps}] + Sum[{ Abs[time TorqueKFSW (ϕ5'[t] - ϕ4'[t]) / steps /. output[i] /.
          t → time n / steps]}, {n, 0, steps}] +
      Sum[{Abs[-time ϕ4'[t] TorqueHFST / steps /. output[i] /. t → time n / steps]},
       {n, 0, steps}] + Sum[{Abs[-time TorqueHFSW ϕ4'[t] / steps /. output[i] /.
          t → time n / steps]}, {n, 0, steps}] + Sum[
       {Abs[time θ3'[t] TorqueHRST / steps /. output[i] /. t → time n / steps]}, {n, 0, steps}] +
      Sum[{Abs[time ψ3'[t] TorqueHAST / steps /. output[i] /. t → time n / steps]},
       {n, 0, steps}] + Sum[{Abs[ time ϕ1'[t] TorqueAFST / steps /. output[i] /.
          t → time n / steps]}, {n, 0, steps}])}, {i, 1, 5}]
ModelWork[1]
ModelWork[2]
ModelWork[3]
ModelWork[4]
ModelWork[5]
```

```
BW = 71.953;
loops = 10;
beta1 = 0; beta2 = 0.1; beta3 = 0.2; beta4 = 0.3; beta5 = 0.4; beta6 = 0.5;
beta7 = 0.6; beta8 = 0.7; beta9 = 0.8; beta10 = 0.9; beta11 = 1;
Inertia1 = {{0.0369, 0, 0}, {0, 0.0387, 0}, {0, 0, 0.0063}};
Inertia2 = {{0.199, 0, 0}, {0, 0.199, 0}, {0, 0, 0.0409}};
Inertia3 = {{0, 0, 0}, {0, 0, 0}, {0, 0, 0}};
Inertia4 = {{0.199, 0, 0}, {0, 0.199, 0}, {0, 0, 0.0409}};
Inertia5 = {{0.0369, 0, 0}, {0, 0.0387, 0}, {0, 0, 0.0063}};
Inertia6 = {{1.567, 0, 0}, {0, 1.801, 0}, {0, 0, 0.475}};

ΩShankST = {0, ϕ1'[t] Cos[ψ1[t]], - ϕ1'[t] Sin[ψ1[t]]};
ΩThighST = {0, ϕ2'[t] Cos[ψ1[t]], - ϕ2'[t] Sin[ψ1[t]]};
ΩPelvis = { ψ3'[t] Cos[θ3[t]], -ψ3'[t] Sin[θ3[t]] , θ3'[t]};
ΩThighSW = {0, ϕ4'[t] Cos[ψ4[t]], - ϕ4'[t] Sin[ψ4[t]]};
ΩShankSW = {0, ϕ5'[t] Cos[ψ4[t]], - ϕ5'[t] Sin[ψ4[t]]};
ΩTorso = {Cos[θ3[t]] (ψ3)'[t], Sin[ψ6[t]] (θ3)'[t] - Cos[ψ6[t]] Sin[θ3[t]] (ψ3)'[t],
   Cos[ψ6[t]] (θ3)'[t] + Sin[θ3[t]] Sin[ψ6[t]] (ψ3)'[t]};
CurveParams = {1, Sin[2 t π], Sin[4 t π], Sin[6 t π], Sin[8 t π],
   Sin[10 t π], Cos[2 t π], Cos[4 t π], Cos[6 t π], Cos[8 t π], Cos[10 t π]};
AF = Fit[Import["AnkleFlexion.csv"], CurveParams, t];
HA = Fit[Import["HipAbduction.csv"], CurveParams, t];
HF = Fit[Import["HipFlexion.csv"], CurveParams, t];
HR = Fit[Import["HipRotation.csv"], CurveParams, t];
KF = Fit[Import["KneeFlexion.csv"], CurveParams, t];
PO = Fit[Import["PelvicObliquity.csv"], CurveParams, t];
PT = Fit[Import["PelvicTilt.csv"], CurveParams, t];
TF = Fit[Import["Torso_Flexion.csv"], CurveParams, t];
AE = Fit[Import["AnkleEversion.csv"], CurveParams, t];

AEST = -AE /. t → t + 0.1;
AFST = AF /. t → t + 0.1;
HAST = HA /. t → t + 0.1;
HASW = HA /. t → t + 0.6;
HFST = -HF /. t → t + 0.1;
HFSW = -HF /. t → t + 0.6;
HRST = -HR /. t → t + 0.1;
HRSW = -HR /. t → t + 0.6;
KFST = Simplify[KF - HF] /. t → t + 0.1;
KFSW = Simplify[KF - HF] /. t → t + 0.6;
POST = PO /. t → t + 0.1;
POSW = PO /. t → t + 0.6;
```

```
PTST = PT /. t → t + 0.1;
PTSW = PT /. t → t + 0.6;
TFST = TF /. t → t + 0.1;

InitialConditions = {ϕ1[0] == KFST, ϕ1'[0] == D[KFST, t], ϕ2[0] == HFST, ϕ2'[0] == D[HFST, t],
    Θ3[0] == HRST, Θ3'[0] == D[HRST, t], ϕ4[0] == HFSW, ϕ4'[0] == D[HFSW, t],
    ϕ5[0] == KFSW, ϕ5'[0] == D[KFSW, t], ψ3[0] == POST, ψ3'[0] == D[POST, t]} /. t → 0;
StaticVel = {ψ1'[t] -> 0, ψ4'[t] -> 0, ψ6'[t] -> 0, ψ1''[t] -> 0, ψ4''[t] -> 0, ψ6''[t] -> 0};
StaticAngs = {ψ1[t] -> 0, ψ4[t] -> 0, ψ6[t] → 0};

Parameters = {m1 → 3.16, m2 → 10.34, m3 → 5, m4 → 10.34, m5 → 3.16, m6 → 39.953,
   L1 → 0.4344, L2 → 0.4222, L3 → 0.171, L4 → 0.4222, L5 → 0.4344, L6 → .5319,
   a1 → 0.5541 * 0.4344, a2 → 0.5905 * 0.4222, a3 → 0.171 / 2,
   a4 → 0.4095 * 0.4222, a5 → 0.4459 * 0.4344, a6 → 0.5534 * 0.5319,
   g → 9.81};

r1 = a1 {Cos[ψ1[t]] Sin[ϕ1[t]], -Sin[ψ1[t]], Cos[ϕ1[t]] Cos[ψ1[t]]};
rKST = L1 {Cos[ψ1[t]] Sin[ϕ1[t]], -Sin[ψ1[t]], Cos[ϕ1[t]] Cos[ψ1[t]]};
r2 = Simplify[rKST + a2 {Cos[ψ1[t]] Sin[ϕ2[t]], -Sin[ψ1[t]], Cos[ϕ2[t]] Cos[ψ1[t]]}];
rHST = Simplify[rKST + L2 {Cos[ψ1[t]] Sin[ϕ2[t]], -Sin[ψ1[t]], Cos[ϕ2[t]] Cos[ψ1[t]]}];

Rotation1 = {{1, 0, 0}, {0, 1, ψ3[t]}, {0, -ψ3[t], 1}};
Rotation3 = {{1, Θ3[t], 0}, {-Θ3[t], 1, 0}, {0, 0, 1}};
C1 = Transpose[Rotation3.Rotation1];

r3 = Simplify[rHST + C1.{0, a3, 0}];
rHSW = Simplify[rHST + C1.{0, L3, 0}];

r4 = Simplify[rHSW + a4 {-Cos[ψ4[t]] Sin[ϕ4[t]], Sin[ψ4[t]], -Cos[ϕ4[t]] Cos[ψ4[t]]}];
rKSW
  = Simplify[rHSW + L4 {-Cos[ψ4[t]] Sin[ϕ4[t]], Sin[ψ4[t]], -Cos[ϕ4[t]] Cos[ψ4[t]]}];
r5 = Simplify[rKSW + a5 {-Cos[ψ4[t]] Sin[ϕ5[t]], Sin[ψ4[t]], -Cos[ϕ5[t]] Cos[ψ4[t]]}];
rtoe = Simplify[rKSW + L5 {-Cos[ψ4[t]] Sin[ϕ5[t]], Sin[ψ4[t]], -Cos[ϕ5[t]] Cos[ψ4[t]]}];

Rotationt1 = {{1, 0, 0}, {0, Cos[ψ6[t]], Sin[ψ6[t]]}, {0, -Sin[ψ6[t]], Cos[ψ6[t]]}};
C2 = Transpose[Rotationt1];
r6 = Simplify[r3 + C2.C1.{0, 0, a6}];
rcrutch = Simplify[r3 + C2.C1.{0, a3, L6}];
v1 = D[r1, t];
v2 = D[r2, t];
v3 = D[r3, t];
v4 = D[r4, t];
```

```
v5 = D[r5, t];
v6 = D[r6, t];
Kinetic = 1 / 2 m1 v1.v1 + 1 / 2 m2 v2.v2 + 1 / 2 m3 v3.v3 + 1 / 2 m4 v4.v4 + 1 / 2 m5 v5.v5 + 1 / 2 m6 v6.v6 +
    1 / 2 Simplify[ΩShankST . Inertia1.ΩShankST] + 1 / 2 Simplify[ΩThighST . Inertia2.ΩThighST] +
    1 / 2 Simplify[ΩPelvis . Inertia3.ΩPelvis] + 1 / 2 Simplify[ΩThighSW . Inertia4.ΩThighSW] +
    1 / 2 Simplify[ΩShankSW . Inertia5.ΩShankSW] + 1 / 2 Simplify[ΩTorso . Inertia6.ΩTorso];
Potential = m1 g Part[r1, 3] + m2 g Part[r2, 3] + m3 g Part[r3, 3] +
    m4 g Part[r4, 3] + m5 g Part[r5, 3] + m6 g Part[r6, 3];
Lagrange = Kinetic - Potential;


Eqn1 = D[D[Lagrange, ϕ1'[t], NonConstants → ϕ1'[t]], t] -
    D[Lagrange, ϕ1[t], NonConstants → ϕ1[t]] - Fcrutch . D[rcrutch, ϕ1[t]];
Eqn2 = D[D[Lagrange, ϕ2'[t], NonConstants → ϕ2'[t]], t] -
    D[Lagrange, ϕ2[t], NonConstants → ϕ2[t]] - Fcrutch . D[rcrutch, ϕ2[t]];
Eqn4 = D[D[Lagrange, θ3'[t], NonConstants → θ3'[t]], t] -
    D[Lagrange, θ3[t], NonConstants → θ3[t]] - Fcrutch . D[rcrutch, θ3[t]];
Eqn5 = D[D[Lagrange, ψ3'[t], NonConstants → ψ3'[t]], t] -
    D[Lagrange, ψ3[t], NonConstants → ψ3[t]] - Fcrutch . D[rcrutch, ψ3[t]];
Eqn6 = D[D[Lagrange, ϕ4'[t], NonConstants → ϕ4'[t]], t] -
    D[Lagrange, ϕ4[t], NonConstants → ϕ4[t]] - Fcrutch . D[rcrutch, ϕ4[t]];
Eqn7 = D[D[Lagrange, ϕ5'[t], NonConstants → ϕ5'[t]], t] -
    D[Lagrange, ϕ5[t], NonConstants → ϕ5[t]] - Fcrutch . D[rcrutch, ϕ5[t]];
TorqueAnkleFlexion = Fit[Import["Torque_Ankle_Flexion.xls"], CurveParams, t];
TorqueKneeFlexion = Fit[Import["Torque_Knee_Flexion.csv"], CurveParams, t];
TorqueHF = Fit[Import["Torque_Hip_Flexion.csv"], CurveParams, t];
TorqueAnkleAbduction = Fit[Import["Torque_Ankle_Eversion.xls"], CurveParams, t];
TorqueHipAbduction = Fit[Import["Torque_Hip_Abduction.xls"], CurveParams, t];
TorqueHipRotation = Fit[Import["Torque_Hip_Rotation.csv"], CurveParams, t];

TorqueHRST = TorqueHipRotation /. t → t + 0.1;

TorqueHAST = TorqueHipAbduction /. t → t + 0.1;
TorqueHASW = TorqueHipAbduction /. t → t + 0.6;

TorqueAAST = TorqueAnkleAbduction /. t → t + 0.1;
TorqueAFST = TorqueAnkleFlexion /. t → t + 0.1;

TorqueKFST = TorqueKneeFlexion /. t → t + 0.1;
TorqueKFSW = TorqueKneeFlexion /. t → t + 0.6;

TorqueHFST = TorqueHF /. t → t + 0.1;
```

```
TorqueHFSW = TorqueHF /. t → t + 0.6;
ConstForces = {M1y[t] → -BW TorqueAFST, M2y[t] → -BW TorqueKFST, M3y[t] → BW TorqueHFST,
    M3x[t] → 0, M3z[t] -> BW TorqueHRST, M4y[t] → -BW TorqueHFSW, M5y[t] → -BW TorqueKFSW};
Coeff = 1.5;
Forces[1] = {F_crutch -> {0, -Coeff BW Sin[beta1], Coeff BW Cos[beta1]}};
Forces[2] = {F_crutch -> {0, -Coeff BW Sin[beta2], Coeff BW Cos[beta2]}};
Forces[3] = {F_crutch -> {0, - Coeff BW Sin[beta3], Coeff BW Cos[beta3]}};
Forces[4] = {F_crutch -> {0, - Coeff BW Sin[beta4], Coeff BW Cos[beta4]}};
Forces[5] = {F_crutch -> {0, -Coeff BW Sin[beta5], Coeff BW Cos[beta5]}};
Forces[6] = {F_crutch -> {0, -Coeff BW Sin[beta6], Coeff BW Cos[beta6]}};
Forces[7] = {F_crutch -> {0, -Coeff BW Sin[beta7], Coeff BW Cos[beta7]}};
Forces[8] = {F_crutch -> {0, -Coeff BW Sin[beta8], Coeff BW Cos[beta8]}};
Forces[9] = {F_crutch -> {0, -Coeff BW Sin[beta9], Coeff BW Cos[beta9]}};
Forces[10] = {F_crutch -> {0, -Coeff BW Sin[beta10], Coeff BW Cos[beta10]}};


Do[EOM[i] =
   {Eqn1 == (M1y[t] - M2y[t]) Cos[ψ1[t]], Eqn2 == (M2y[t] - M3y[t]) Cos[ψ1[t]], Eqn4 == M3z[t],
         Eqn5 == M3x[t], Eqn6 == (M4y[t] - M5y[t]) Cos[ψ4[t]], Eqn7 == M5y[t]} /. StaticVel /.
       StaticAngs /. Parameters /. ConstForces /. Forces[i];
 ggg[i] = Join[EOM[i], InitialConditions];
 output[i] = NDSolve[ggg[i], {ϕ1, ϕ2, Θ3, ψ3, ϕ4, ϕ5}, {t, 0, 0.4}], {i, 1, loops}]
```

```
nBW = 71.953;
beta1 = 0;
beta2 = 0;
beta3 = 0.2;
F_crutch1 = {0, 0, 0};
F_crutch2 = {0, -CF1 Sin[beta2], CF1 Cos[beta2]};
F_crutch3 = {0, -CF2 Sin[beta3] , CF2 Cos[beta3]};

RHSeqn1 = (M1y[t] - M2y[t]) Cos[ψ1[t]];
RHSeqn2 = M1x[t] - M3x[t];
RHSeqn3 = (M2y[t] - M3y[t]) Cos[ψ1[t]];
RHSeqn4 = M3z[t];
RHSeqn5 = (M3x[t] - M4x[t]) Cos[ψ3[t]] Sin[θ3[t]] +
    (M3y[t] - M4y[t] - M6y[t]) Cos[ψ3[t]] Cos[θ3[t]] - M3z[t] Sin[ψ3[t]];
RHSeqn6 = (M3x[t] - M4x[t]) Cos[θ3[t]] - (M3y[t] - M4y[t]) Sin[θ3[t]];
RHSeqn7 = (M4y[t] - M5y[t]) Cos[ψ4[t]];
RHSeqn8 = M4x[t];
RHSeqn9 = M5y[t] Cos[ψ4[t]];
RHSeqn10 = M6y[t];

Inertia1 = {{0.0369, 0, 0}, {0, 0.0387, 0}, {0, 0, 0.0063}};
Inertia2 = {{0.199, 0, 0}, {0, 0.199, 0}, {0, 0, 0.0409}};
Inertia3 = {{0, 0, 0}, {0, 0, 0}, {0, 0, 0}};
Inertia4 = {{0.199, 0, 0}, {0, 0.199, 0}, {0, 0, 0.0409}};
Inertia5 = {{0.0369, 0, 0}, {0, 0.0387, 0}, {0, 0, 0.0063}};
Inertia6 = {{1.567, 0, 0}, {0, 1.801, 0}, {0, 0, 0.475}};

Parameters = {m1 → 3.16, m2 → 10.34, m3 → 5, m4 → 10.34, m5 → 3.16, m6 → 39.953,
    L1 → 0.4344, L2 → 0.4222, L3 → 0.171, L4 → 0.4222, L5 → 0.4344, L6 → .5319,
    a1 → 0.5541 * 0.4344, a2 → 0.5905 * 0.4222, a3 → 0.171 / 2,
    a4 → 0.4095 * 0.4222, a5 → 0.4459 * 0.4344, a6 → 0.5534 * 0.5319,
    g → 9.81};

r1 =  a1 {Cos[ψ1[t]] Sin[φ1[t]], -Sin[ψ1[t]], Cos[φ1[t]] Cos[ψ1[t]]};
r_KST = L1 {Cos[ψ1[t]] Sin[φ1[t]], -Sin[ψ1[t]], Cos[φ1[t]] Cos[ψ1[t]]};
r2 = Simplify[r_KST + a2 {Cos[ψ1[t]] Sin[φ2[t]], -Sin[ψ1[t]], Cos[φ2[t]] Cos[ψ1[t]]}];
r_HST =  Simplify[r_KST + L2 {Cos[ψ1[t]] Sin[φ2[t]], -Sin[ψ1[t]], Cos[φ2[t]] Cos[ψ1[t]]}];

Rotation1 = {{1, 0, 0}, {0, Cos[ψ3[t]], Sin[ψ3[t]]}, {0, -Sin[ψ3[t]], Cos[ψ3[t]]}};
Rotation2 = {{Cos[φ3[t]], 0, -Sin[φ3[t]]}, {0, 1, 0}, {Sin[φ3[t]], 0, Cos[φ3[t]]}};
Rotation3 = {{Cos[θ3[t]], Sin[θ3[t]], 0}, {-Sin[θ3[t]], Cos[θ3[t]], 0}, {0, 0, 1}};
C1 = Transpose[Rotation3.Rotation1.Rotation2];
```

```
r3 = Simplify[rHST + C1.{0, a3, 0}];
rHSW = Simplify[rHST + C1.{0, L3, 0}];

r4 = Simplify[rHSW + a4 {-Cos[ψ4[t]] Sin[ϕ4[t]], Sin[ψ4[t]], -Cos[ϕ4[t]] Cos[ψ4[t]]}];
rKSW
  = Simplify[rHSW + L4 {-Cos[ψ4[t]] Sin[ϕ4[t]], Sin[ψ4[t]], -Cos[ϕ4[t]] Cos[ψ4[t]]}];
r5 = Simplify[rKSW + a5 {-Cos[ψ4[t]] Sin[ϕ5[t]], Sin[ψ4[t]], -Cos[ϕ5[t]] Cos[ψ4[t]]}];
rtoe = Simplify[rKSW + L5 {-Cos[ψ4[t]] Sin[ϕ4[t]], Sin[ψ4[t]], -Cos[ϕ5[t]] Cos[ψ4[t]]}];
r6 = Simplify[r3 + {a6 Sin[ϕ6[t]], 0, a6 Cos[ϕ6[t]]}];
rcrutch = Simplify[rHSW + C1.{L6 Sin[ϕ6[t]], 0, L6 Cos[ϕ6[t]]}];

v1 = D[r1, t]; v2 = D[r2, t]; v3 = D[r3, t]; v4 = D[r4, t]; v5 = D[r5, t]; v6 = D[r6, t];
ΩShankST = {ψ1'[t] , ϕ1'[t] Cos[ψ1[t]], -ϕ1'[t] Sin[ψ1[t]]};
ΩThighST = {ψ1'[t] , ϕ2'[t] Cos[ψ1[t]], -ϕ2'[t] Sin[ψ1[t]]};
ΩPelvis = {ψ3'[t] Cos[θ3[t]] + ϕ3'[t] Cos[ψ3[t]] Sin[θ3[t]],
    ϕ3'[t] Cos[ψ3[t]] Cos[θ3[t]] - ψ3'[t] Sin[θ3[t]], θ3'[t] - ϕ3'[t] Sin[ψ3[t]]};
ΩThighSW = {ψ4'[t] , ϕ4'[t] Cos[ψ4[t]], -ϕ4'[t] Sin[ψ4[t]]};
ΩShankSW = {ψ4'[t] , ϕ5'[t] Cos[ψ4[t]], -ϕ5'[t] Sin[ψ4[t]]};
ΩTorso = {0, ϕ6'[t], 0};
Kinetic = 1 / 2 m1 v1.v1 + 1 / 2 m2 v2.v2 + 1 / 2 m3 v3.v3 + 1 / 2 m4 v4.v4 + 1 / 2 m5 v5.v5 + 1 / 2 m6 v6.v6 +
    1 / 2 Simplify[ΩShankST . Inertia1.ΩShankST] + 1 / 2 Simplify[ΩThighST . Inertia2.ΩThighST] +
    1 / 2 Simplify[ΩPelvis . Inertia3.ΩPelvis] + 1 / 2 Simplify[ΩThighSW . Inertia4.ΩThighSW] +
    1 / 2 Simplify[ΩShankSW . Inertia5.ΩShankSW] + 1 / 2 Simplify[ΩTorso . Inertia6.ΩTorso];
Potential = m1 g Part[r1, 3] + m2 g Part[r2, 3] + m3 g Part[r3, 3] +
    m4 g Part[r4, 3] + m5 g Part[r5, 3] + m6 g Part[r6, 3];
Lagrange = Kinetic - Potential;
E1 =
  D[D[Lagrange, ϕ1'[t], NonConstants → ϕ1'[t]], t] - D[Lagrange, ϕ1[t], NonConstants → ϕ1[t]];
E2 = D[D[Lagrange, ψ1'[t], NonConstants → ψ1'[t]], t] -
    D[Lagrange, ψ1[t], NonConstants → ψ1[t]];
E3 = D[D[Lagrange, ϕ2'[t], NonConstants → ϕ2'[t]], t] -
    D[Lagrange, ϕ2[t], NonConstants → ϕ2[t]];
E4 = D[D[Lagrange, θ3'[t], NonConstants → θ3'[t]], t] -
    D[Lagrange, θ3[t], NonConstants → θ3[t]];
E5 = D[D[Lagrange, ϕ3'[t], NonConstants → ϕ3'[t]], t] -
    D[Lagrange, ϕ3[t], NonConstants → ϕ3[t]];
E6 = D[D[Lagrange, ψ3'[t], NonConstants → ψ3'[t]], t] -
    D[Lagrange, ψ3[t], NonConstants → ψ3[t]];
E7 = D[D[Lagrange, ϕ4'[t], NonConstants → ϕ4'[t]], t] -
    D[Lagrange, ϕ4[t], NonConstants → ϕ4[t]];
E8 = D[D[Lagrange, ψ4'[t], NonConstants → ψ4'[t]], t] -
```

```
    D[Lagrange, ψ4[t], NonConstants → ψ4[t]];
E9 = D[D[Lagrange, ϕ5'[t], NonConstants → ϕ5'[t]], t] -
    D[Lagrange, ϕ5[t], NonConstants → ϕ5[t]];
E10 = D[D[Lagrange, ϕ6'[t], NonConstants → ϕ6'[t]], t] -
    D[Lagrange, ϕ6[t], NonConstants → ϕ6[t]];
Eqn1 = E1 - Fcrutch1 . D[rcrutch, ϕ1[t]];
Eqn2 = E2 - Fcrutch1 .D[rcrutch, ψ1[t]];
Eqn3 = E3 - Fcrutch1 .D[rcrutch, ϕ2[t]];
Eqn4 = E4 - Fcrutch1 .D[rcrutch, Θ3[t]];
Eqn5 =  E5 - Fcrutch1 .D[rcrutch, ϕ3[t]];
Eqn6 =  E6 - Fcrutch1 .D[rcrutch, ψ3[t]];
Eqn7 =  E7 - Fcrutch1 .D[rcrutch, ϕ4[t]];
Eqn8 =  E8 - Fcrutch1 .D[rcrutch, ψ4[t]];
Eqn9 =  E9 - Fcrutch1 .D[rcrutch, ϕ5[t]];
Eqn10 =  E10 - Fcrutch1 .D[rcrutch, ϕ6[t]];

Eqn1b = E1 - Fcrutch2 . D[rcrutch, ϕ1[t]];
Eqn2b = E2 - Fcrutch2 .D[rcrutch, ψ1[t]];
Eqn3b = E3 - Fcrutch2 .D[rcrutch, ϕ2[t]];
Eqn4b = E4 - Fcrutch2 .D[rcrutch, Θ3[t]];
Eqn5b = E5 - Fcrutch2 .D[rcrutch, ϕ3[t]];
Eqn6b = E6 - Fcrutch2 .D[rcrutch, ψ3[t]];
Eqn7b = E7 - Fcrutch2 .D[rcrutch, ϕ4[t]];
Eqn8b = E8 - Fcrutch2 .D[rcrutch, ψ4[t]];
Eqn9b = E9 - Fcrutch2 .D[rcrutch, ϕ5[t]];
Eqn10b = E10 - Fcrutch2 .D[rcrutch, ϕ6[t]];

Eqn1c = E1 - Fcrutch3 . D[rcrutch, ϕ1[t]];
Eqn2c = E2 - Fcrutch3 .D[rcrutch, ψ1[t]];
Eqn3c = E3 - Fcrutch3 .D[rcrutch, ϕ2[t]];
Eqn4c = E4 - Fcrutch3 .D[rcrutch, Θ3[t]];
Eqn5c = E5 - Fcrutch3 .D[rcrutch, ϕ3[t]];
Eqn6c = E6 - Fcrutch3 .D[rcrutch, ψ3[t]];
Eqn7c = E7 - Fcrutch3 .D[rcrutch, ϕ4[t]];
Eqn8c = E8 - Fcrutch3 .D[rcrutch, ψ4[t]];
Eqn9c = E9 - Fcrutch3 .D[rcrutch, ϕ5[t]];
Eqn10c = E10 - Fcrutch3 .D[rcrutch, ϕ6[t]];

CurveParams = {1, Sin[2 t π], Sin[4 t π], Sin[6 t π],  Sin[8 t π],
    Sin[10 t π], Cos[2 t π], Cos[4 t π], Cos[6 t π], Cos[8 t π], Cos[10 t π]};
AF = Fit[Import["AnkleFlexion.csv"], CurveParams, t];
HA = Fit[Import["HipAbduction.csv"], CurveParams, t];
HF = Fit[Import["HipFlexion.csv"], CurveParams, t];
```

```
HR = Fit[Import["HipRotation.csv"], CurveParams, t];
KF = Fit[Import["KneeFlexion.csv"], CurveParams, t];
PO = Fit[Import["PelvicObliquity.csv"], CurveParams, t];
PT = Fit[Import["PelvicTilt.csv"], CurveParams, t];
TF = Fit[Import["Torso_Flexion.csv"], CurveParams, t];
AE = Fit[Import["AnkleEversion.csv"], CurveParams, t];

TorqueAnkleFlexion = Fit[Import["Torque_Ankle_Flexion.xls"], CurveParams, t];
TorqueKneeFlexion = Fit[Import["Torque_Knee_Flexion.csv"], CurveParams, t];
TorqueHF = Fit[Import["Torque_Hip_Flexion.csv"], CurveParams, t];
TorqueAnkleAbduction = Fit[Import["Torque_Ankle_Eversion.xls"], CurveParams, t];
TorqueHipAbduction = Fit[Import["Torque_Hip_Abduction.xls"], CurveParams, t];
TorqueHipRotation = Fit[Import["Torque_Hip_Rotation.csv"], CurveParams, t];

TorqueHRST = TorqueHipRotation /. t → t + 0.1;
TorqueHAST = TorqueHipAbduction /. t → t + 0.1;
TorqueHASW = TorqueHipAbduction /. t → t + 0.6;
TorqueAAST = TorqueAnkleAbduction /. t → t + 0.1;
TorqueAFST = TorqueAnkleFlexion /. t → t + 0.1;
TorqueKFST = TorqueKneeFlexion /. t → t + 0.1;
TorqueKFSW = TorqueKneeFlexion /. t → t + 0.6;
TorqueHFST = TorqueHF /. t → t + 0.1;
TorqueHFSW = TorqueHF /. t → t + 0.6;
Iter = 40;

AEST = 0.065 Cos[2 Pi (t - 0.2) / 2];
AFST = AF /. t → t + 0.1;
HAST = HA /. t → t + 0.1;
HASW = HA /. t → t + 0.6;
HFST = -HF /. t → t + 0.1;
HFSW = -HF /. t → t + 0.6;
HRST = -HR /. t → t + 0.1;
HRSW = -HR /. t → t + 0.6;
KFST = Simplify[KF - HF] /. t → t + 0.1;
KFSW = Simplify[KF - HF] /. t → t + 0.6;
POST = PO /. t → t + 0.1;
POSW = PO /. t → t + 0.6;
PTST = PT /. t → t + 0.1;
PTSW = PT /. t → t + 0.6;
TFST = TF /. t → t + 0.1;

Kinematics =
```

```
  {ϕ1[t] → KFST, ϕ1'[t] → D[KFST, t], ϕ1''[t] → D[D[KFST, t], t],
   ψ1[t] → -HAST, ψ1'[t] → D[-HAST, t], ψ1''[t] → D[D[-HAST, t], t],
   ϕ2[t] → HFST, ϕ2'[t] → D[HFST, t], ϕ2''[t] → D[D[HFST, t], t],
   ϕ3[t] → PTST, ϕ3'[t] → D[PTST, t], ϕ3''[t] → D[D[PTST, t], t],
   ψ3[t] → POST, ψ3'[t] → D[POST, t], ψ3''[t] → D[D[POST, t], t],
   Θ3[t] → HRST, Θ3'[t] → D[HRST, t], Θ3''[t] → D[D[HRST, t], t],
   ϕ4[t] → HFSW, ϕ4'[t] → D[HFSW, t], ϕ4''[t] → D[D[HFSW, t], t],
   ψ4[t] → HASW, ψ4'[t] → D[HASW, t], ψ4''[t] → D[D[HASW, t], t], ϕ5[t] → KFSW, ϕ5'[t] → D[KFSW, t],
   ϕ5''[t] → D[D[KFSW, t], t], ϕ6[t] → TFST, ϕ6'[t] → D[TFST, t], ϕ6''[t] → D[D[TFST, t], t]};

EOM = {Eqn1 == RHSeqn1, Eqn2 == RHSeqn2, Eqn3 == RHSeqn3, Eqn4 == RHSeqn4,
       Eqn5 == RHSeqn5, Eqn6 == RHSeqn6, Eqn7 == RHSeqn7, Eqn8 == RHSeqn8,
       Eqn9 == RHSeqn9, Eqn10 == RHSeqn10} /. Parameters /. Kinematics /.
    {M1y[t] -> M1y, M2y[t] -> M2y, M1x[t] -> M1x, M3x[t] -> M3x, M3y[t] -> M3y,
     M3z[t] -> M3z, M4y[t] -> M4y, M4x[t] -> M4x, M5y[t] -> M5y, M6y[t] -> M6y};
EOM2 = {Eqn1b == RHSeqn1, Eqn2b == RHSeqn2, Eqn3b == RHSeqn3, Eqn4b == RHSeqn4,
       Eqn5b == RHSeqn5, Eqn6b == RHSeqn6, Eqn7b == RHSeqn7, Eqn8b == RHSeqn8,
       Eqn9b == RHSeqn9, Eqn10b == RHSeqn10} /. Parameters /. Kinematics /.
    {M1y[t] -> M1yb, M2y[t] -> M2yb, M1x[t] -> M1xb, M3x[t] → 0, M3y[t] -> M3yb,
     M3z[t] -> M3zb, M4y[t] -> M4yb, M4x[t] -> M4xb, M5y[t] -> M5yb, M6y[t] -> M6yb};
EOM3 = {Eqn1c == RHSeqn1, Eqn2c == RHSeqn2, Eqn3c == RHSeqn3, Eqn4c == RHSeqn4,
       Eqn5c == RHSeqn5, Eqn6c == RHSeqn6, Eqn7c == RHSeqn7, Eqn8c == RHSeqn8,
       Eqn9c == RHSeqn9, Eqn10c == RHSeqn10} /. Parameters /. Kinematics /.
    {M1y[t] -> M1yc, M2y[t] -> M2yc, M1x[t] -> M1xc, M3x[t] → 0, M3y[t] -> M3yc,
     M3z[t] -> M3zc, M4y[t] -> M4yc, M4x[t] -> M4xc, M5y[t] -> M5yc, M6y[t] -> M6yc};
Do[output[n] = NSolve[EOM /. t → (0.4 n / Iter),
    {M1y, M2y, M1x, M3x, M3y, M3z, M4y, M4x, M5y, M6y}];
 outputb[n] = NSolve[EOM2 /. t → (0.4 n / Iter),
    {M1yb, M2yb, M1xb, CF1, M3yb, M3zb, M4yb, M4xb, M5yb, M6yb}];
 outputc[n] = NSolve[EOM3 /. t → (0.4 n / Iter),
    {M1yc, M2yc, M1xc, CF2, M3yc, M3zc, M4yc, M4xc, M5yc, M6yc}], {n, 0, Iter}]
```

```
nBW = 71.953;
beta1 = 0;
beta2 = 0.2;
beta3 = 0.4;
F_crutch1 = {0, -1.5 nBW Sin[beta1], 1.5 nBW Cos[beta1]}
F_crutch2 = {0, -1.5 nBW Sin[beta2], 1.5 nBW Cos[beta2]}
F_crutch3 = {0, -1.5 nBW Sin[beta3] , 1.5 nBW Cos[beta3]}

RHSeqn1 = (M1y[t] - M2y[t]) Cos[ψ1[t]];
RHSeqn2 = M1x[t] - M3x[t];
RHSeqn3 = (M2y[t] - M3y[t]) Cos[ψ1[t]];
RHSeqn4 = M3z[t];
RHSeqn5 = (M3x[t] - M4x[t]) Cos[ψ3[t]] Sin[θ3[t]] +
    (M3y[t] - M4y[t] - M6y[t]) Cos[ψ3[t]] Cos[θ3[t]] - M3z[t] Sin[ψ3[t]];
RHSeqn6 = (M3x[t] - M4x[t]) Cos[θ3[t]] - (M3y[t] - M4y[t]) Sin[θ3[t]];
RHSeqn7 = (M4y[t] - M5y[t]) Cos[ψ4[t]];
RHSeqn8 = M4x[t];
RHSeqn9 = M5y[t] Cos[ψ4[t]];
RHSeqn10 = M6y[t];

Inertia1 = {{0.0369, 0, 0}, {0, 0.0387, 0}, {0, 0, 0.0063}};
Inertia2 = {{0.199, 0, 0}, {0, 0.199, 0}, {0, 0, 0.0409}};
Inertia3 = {{0, 0, 0}, {0, 0, 0}, {0, 0, 0}};
Inertia4 = {{0.199, 0, 0}, {0, 0.199, 0}, {0, 0, 0.0409}};
Inertia5 = {{0.0369, 0, 0}, {0, 0.0387, 0}, {0, 0, 0.0063}};
Inertia6 = {{1.567, 0, 0}, {0, 1.801, 0}, {0, 0, 0.475}};

Parameters = {m1 → 3.16, m2 → 10.34, m3 → 5, m4 → 10.34, m5 → 3.16, m6 → 39.953,
    L1 → 0.4344, L2 → 0.4222, L3 → 0.171, L4 → 0.4222, L5 → 0.4344, L6 → .5319,
    a1 → 0.5541 * 0.4344, a2 → 0.5905 * 0.4222, a3 → 0.171 / 2,
    a4 → 0.4095 * 0.4222, a5 → 0.4459 * 0.4344, a6 → 0.5534 * 0.5319,
    g → 9.81};

r1 =  a1 {Cos[ψ1[t]] Sin[φ1[t]], -Sin[ψ1[t]], Cos[φ1[t]] Cos[ψ1[t]]};
r_KST = L1 {Cos[ψ1[t]] Sin[φ1[t]], -Sin[ψ1[t]], Cos[φ1[t]] Cos[ψ1[t]]};
r2 = Simplify[r_KST + a2 {Cos[ψ1[t]] Sin[φ2[t]], -Sin[ψ1[t]], Cos[φ2[t]] Cos[ψ1[t]]}];
r_HST =  Simplify[r_KST + L2 {Cos[ψ1[t]] Sin[φ2[t]], -Sin[ψ1[t]], Cos[φ2[t]] Cos[ψ1[t]]}];

Rotation1 = {{1, 0, 0}, {0, Cos[ψ3[t]], Sin[ψ3[t]]}, {0, -Sin[ψ3[t]], Cos[ψ3[t]]}};
Rotation2 = {{Cos[φ3[t]], 0, -Sin[φ3[t]]}, {0, 1, 0}, {Sin[φ3[t]], 0, Cos[φ3[t]]}};
Rotation3 = {{Cos[θ3[t]], Sin[θ3[t]], 0}, {-Sin[θ3[t]], Cos[θ3[t]], 0}, {0, 0, 1}};
C1 = Transpose[Rotation3.Rotation1.Rotation2];
```

```
r3 = Simplify[rHST + C1.{0, a3, 0}];
rHSW = Simplify[rHST + C1.{0, L3, 0}];

r4 = Simplify[rHSW + a4 {-Cos[ψ4[t]] Sin[ϕ4[t]], Sin[ψ4[t]], -Cos[ϕ4[t]] Cos[ψ4[t]]}];
rKSW
  = Simplify[rHSW + L4 {-Cos[ψ4[t]] Sin[ϕ4[t]], Sin[ψ4[t]], -Cos[ϕ4[t]] Cos[ψ4[t]]}];
r5 = Simplify[rKSW + a5 {-Cos[ψ4[t]] Sin[ϕ5[t]], Sin[ψ4[t]], -Cos[ϕ5[t]] Cos[ψ4[t]]}];
rtoe = Simplify[rKSW + L5 {-Cos[ψ4[t]] Sin[ϕ4[t]], Sin[ψ4[t]], -Cos[ϕ5[t]] Cos[ψ4[t]]}];
r6 = Simplify[r3 + {a6 Sin[ϕ6[t]], 0, a6 Cos[ϕ6[t]]}];
rcrutch = Simplify[rHSW + C1.{L6 Sin[ϕ6[t]], 0, L6 Cos[ϕ6[t]]}];

v1 = D[r1, t]; v2 = D[r2, t]; v3 = D[r3, t]; v4 = D[r4, t]; v5 = D[r5, t]; v6 = D[r6, t];
ΩShankST = {ψ1'[t] , ϕ1'[t] Cos[ψ1[t]], -ϕ1'[t] Sin[ψ1[t]]};
ΩThighST = {ψ1'[t] , ϕ2'[t] Cos[ψ1[t]], -ϕ2'[t] Sin[ψ1[t]]};
ΩPelvis = {ψ3'[t] Cos[θ3[t]] + ϕ3'[t] Cos[ψ3[t]] Sin[θ3[t]],
    ϕ3'[t] Cos[ψ3[t]] Cos[θ3[t]] - ψ3'[t] Sin[θ3[t]], θ3'[t] - ϕ3'[t] Sin[ψ3[t]]};
ΩThighSW = {ψ4'[t] , ϕ4'[t] Cos[ψ4[t]], -ϕ4'[t] Sin[ψ4[t]]};
ΩShankSW = {ψ4'[t] , ϕ5'[t] Cos[ψ4[t]], -ϕ5'[t] Sin[ψ4[t]]};
ΩTorso = {0, ϕ6'[t], 0};
Kinetic = 1 / 2 m1 v1.v1 + 1 / 2 m2 v2.v2 + 1 / 2 m3 v3.v3 + 1 / 2 m4 v4.v4 + 1 / 2 m5 v5.v5 + 1 / 2 m6 v6.v6 +
    1 / 2 Simplify[ΩShankST . Inertia1.ΩShankST] + 1 / 2 Simplify[ΩThighST . Inertia2.ΩThighST] +
    1 / 2 Simplify[ΩPelvis . Inertia3.ΩPelvis] + 1 / 2 Simplify[ΩThighSW . Inertia4.ΩThighSW] +
    1 / 2 Simplify[ΩShankSW . Inertia5.ΩShankSW] + 1 / 2 Simplify[ΩTorso . Inertia6.ΩTorso];
Potential = m1 g Part[r1, 3] + m2 g Part[r2, 3] + m3 g Part[r3, 3] +
    m4 g Part[r4, 3] + m5 g Part[r5, 3] + m6 g Part[r6, 3];
Lagrange = Kinetic - Potential;
E1 =
  D[D[Lagrange, ϕ1'[t], NonConstants → ϕ1'[t]], t] - D[Lagrange, ϕ1[t], NonConstants → ϕ1[t]];
E2 = D[D[Lagrange, ψ1'[t], NonConstants → ψ1'[t]], t] -
    D[Lagrange, ψ1[t], NonConstants → ψ1[t]];
E3 = D[D[Lagrange, ϕ2'[t], NonConstants → ϕ2'[t]], t] -
    D[Lagrange, ϕ2[t], NonConstants → ϕ2[t]];
E4 = D[D[Lagrange, θ3'[t], NonConstants → θ3'[t]], t] -
    D[Lagrange, θ3[t], NonConstants → θ3[t]];
E5 = D[D[Lagrange, ϕ3'[t], NonConstants → ϕ3'[t]], t] -
    D[Lagrange, ϕ3[t], NonConstants → ϕ3[t]];
E6 = D[D[Lagrange, ψ3'[t], NonConstants → ψ3'[t]], t] -
    D[Lagrange, ψ3[t], NonConstants → ψ3[t]];
E7 = D[D[Lagrange, ϕ4'[t], NonConstants → ϕ4'[t]], t] -
    D[Lagrange, ϕ4[t], NonConstants → ϕ4[t]];
E8 = D[D[Lagrange, ψ4'[t], NonConstants → ψ4'[t]], t] -
```

```
    D[Lagrange, ψ4[t], NonConstants → ψ4[t]];
E9 = D[D[Lagrange, ϕ5'[t], NonConstants → ϕ5'[t]], t] -
    D[Lagrange, ϕ5[t], NonConstants → ϕ5[t]];
E10 = D[D[Lagrange, ϕ6'[t], NonConstants → ϕ6'[t]], t] -
    D[Lagrange, ϕ6[t], NonConstants → ϕ6[t]];
Eqn1 = E1 - Fcrutch1 . D[rcrutch, ϕ1[t]];
Eqn2 = E2 - Fcrutch1 .D[rcrutch, ψ1[t]];
Eqn3 = E3 - Fcrutch1 .D[rcrutch, ϕ2[t]];
Eqn4 = E4 - Fcrutch1 .D[rcrutch, Θ3[t]];
Eqn5 =  E5 - Fcrutch1 .D[rcrutch, ϕ3[t]];
Eqn6 =  E6 - Fcrutch1 .D[rcrutch, ψ3[t]];
Eqn7 =  E7 - Fcrutch1 .D[rcrutch, ϕ4[t]];
Eqn8 =  E8 - Fcrutch1 .D[rcrutch, ψ4[t]];
Eqn9 =  E9 - Fcrutch1 .D[rcrutch, ϕ5[t]];
Eqn10 =  E10 - Fcrutch1 .D[rcrutch, ϕ6[t]];

Eqn1b = E1 - Fcrutch2 . D[rcrutch, ϕ1[t]];
Eqn2b = E2 - Fcrutch2 .D[rcrutch, ψ1[t]];
Eqn3b = E3 - Fcrutch2 .D[rcrutch, ϕ2[t]];
Eqn4b = E4 - Fcrutch2 .D[rcrutch, Θ3[t]];
Eqn5b = E5 - Fcrutch2 .D[rcrutch, ϕ3[t]];
Eqn6b = E6 - Fcrutch2 .D[rcrutch, ψ3[t]];
Eqn7b = E7 - Fcrutch2 .D[rcrutch, ϕ4[t]];
Eqn8b = E8 - Fcrutch2 .D[rcrutch, ψ4[t]];
Eqn9b = E9 - Fcrutch2 .D[rcrutch, ϕ5[t]];
Eqn10b = E10 - Fcrutch2 .D[rcrutch, ϕ6[t]];

Eqn1c = E1 - Fcrutch3 . D[rcrutch, ϕ1[t]];
Eqn2c = E2 - Fcrutch3 .D[rcrutch, ψ1[t]];
Eqn3c = E3 - Fcrutch3 .D[rcrutch, ϕ2[t]];
Eqn4c = E4 - Fcrutch3 .D[rcrutch, Θ3[t]];
Eqn5c = E5 - Fcrutch3 .D[rcrutch, ϕ3[t]];
Eqn6c = E6 - Fcrutch3 .D[rcrutch, ψ3[t]];
Eqn7c = E7 - Fcrutch3 .D[rcrutch, ϕ4[t]];
Eqn8c = E8 - Fcrutch3 .D[rcrutch, ψ4[t]];
Eqn9c = E9 - Fcrutch3 .D[rcrutch, ϕ5[t]];
Eqn10c = E10 - Fcrutch3 .D[rcrutch, ϕ6[t]];

CurveParams = {1, Sin[2 t π], Sin[4 t π], Sin[6 t π], Sin[8 t π],
    Sin[10 t π], Cos[2 t π], Cos[4 t π], Cos[6 t π], Cos[8 t π], Cos[10 t π]};
AF = Fit[Import["AnkleFlexion.csv"], CurveParams, t];
HA = Fit[Import["HipAbduction.csv"], CurveParams, t];
HF = Fit[Import["HipFlexion.csv"], CurveParams, t];
```

```
HR = Fit[Import["HipRotation.csv"], CurveParams, t];
KF = Fit[Import["KneeFlexion.csv"], CurveParams, t];
PO = Fit[Import["PelvicObliquity.csv"], CurveParams, t];
PT = Fit[Import["PelvicTilt.csv"], CurveParams, t];
TF = Fit[Import["Torso_Flexion.csv"], CurveParams, t];
AE = Fit[Import["AnkleEversion.csv"], CurveParams, t];

TorqueAnkleFlexion = Fit[Import["Torque_Ankle_Flexion.xls"], CurveParams, t];
TorqueKneeFlexion = Fit[Import["Torque_Knee_Flexion.csv"], CurveParams, t];
TorqueHF = Fit[Import["Torque_Hip_Flexion.csv"], CurveParams, t];
TorqueAnkleAbduction = Fit[Import["Torque_Ankle_Eversion.xls"], CurveParams, t];
TorqueHipAbduction = Fit[Import["Torque_Hip_Abduction.xls"], CurveParams, t];
TorqueHipRotation = Fit[Import["Torque_Hip_Rotation.csv"], CurveParams, t];

TorqueHRST = TorqueHipRotation /. t → t + 0.1;
TorqueHAST = TorqueHipAbduction /. t → t + 0.1;
TorqueHASW = TorqueHipAbduction /. t → t + 0.6;
TorqueAAST = TorqueAnkleAbduction /. t → t + 0.1;
TorqueAFST = TorqueAnkleFlexion /. t → t + 0.1;
TorqueKFST = TorqueKneeFlexion /. t → t + 0.1;
TorqueKFSW = TorqueKneeFlexion /. t → t + 0.6;
TorqueHFST = TorqueHF /. t → t + 0.1;
TorqueHFSW = TorqueHF /. t → t + 0.6;
Iter = 40;

AEST = 0.065 Cos[2 Pi (t - 0.2) / 2];
AFST = AF /. t → t + 0.1;
HAST = HA /. t → t + 0.1;
HASW = HA /. t → t + 0.6;
HFST = -HF /. t → t + 0.1;
HFSW = -HF /. t → t + 0.6;
HRST = -HR /. t → t + 0.1;
HRSW = -HR /. t → t + 0.6;
KFST = Simplify[KF - HF] /. t → t + 0.1;
KFSW = Simplify[KF - HF] /. t → t + 0.6;
POST = PO /. t → t + 0.1;
POSW = PO /. t → t + 0.6;
PTST = PT /. t → t + 0.1;
PTSW = PT /. t → t + 0.6;
TFST = TF /. t → t + 0.1;

Kinematics =
```

```
  {ϕ1[t] → KFST, ϕ1'[t] → D[KFST, t], ϕ1''[t] → D[D[KFST, t], t],
   ψ1[t] → -HAST, ψ1'[t] → D[-HAST, t], ψ1''[t] → D[D[-HAST, t], t],
   ϕ2[t] → HFST, ϕ2'[t] → D[HFST, t], ϕ2''[t] → D[D[HFST, t], t],
   ϕ3[t] → PTST, ϕ3'[t] → D[PTST, t], ϕ3''[t] → D[D[PTST, t], t],
   ψ3[t] → POST, ψ3'[t] → D[POST, t], ψ3''[t] → D[D[POST, t], t],
   Θ3[t] → HRST, Θ3'[t] → D[HRST, t], Θ3''[t] → D[D[HRST, t], t],
   ϕ4[t] → HFSW, ϕ4'[t] → D[HFSW, t], ϕ4''[t] → D[D[HFSW, t], t],
   ψ4[t] → HASW, ψ4'[t] → D[HASW, t], ψ4''[t] → D[D[HASW, t], t], ϕ5[t] → KFSW, ϕ5'[t] → D[KFSW, t],
   ϕ5''[t] → D[D[KFSW, t], t], ϕ6[t] → TFST, ϕ6'[t] → D[TFST, t], ϕ6''[t] → D[D[TFST, t], t]};

EOM = {Eqn1 == RHSeqn1, Eqn2 == RHSeqn2, Eqn3 == RHSeqn3, Eqn4 == RHSeqn4,
       Eqn5 == RHSeqn5, Eqn6 == RHSeqn6, Eqn7 == RHSeqn7, Eqn8 == RHSeqn8,
       Eqn9 == RHSeqn9, Eqn10 == RHSeqn10} /. Parameters /. Kinematics /.
    {M1y[t] -> M1y, M2y[t] -> M2y, M1x[t] -> M1x, M3x[t] -> M3x, M3y[t] -> M3y,
     M3z[t] -> M3z, M4y[t] -> M4y, M4x[t] -> M4x, M5y[t] -> M5y, M6y[t] -> M6y};
EOM2 = {Eqn1b == RHSeqn1, Eqn2b == RHSeqn2, Eqn3b == RHSeqn3, Eqn4b == RHSeqn4,
       Eqn5b == RHSeqn5, Eqn6b == RHSeqn6, Eqn7b == RHSeqn7, Eqn8b == RHSeqn8,
       Eqn9b == RHSeqn9, Eqn10b == RHSeqn10} /. Parameters /. Kinematics /.
    {M1y[t] -> M1yb, M2y[t] -> M2yb, M1x[t] -> M1xb, M3x[t] -> M3xb, M3y[t] -> M3yb,
     M3z[t] -> M3zb, M4y[t] -> M4yb, M4x[t] -> M4xb, M5y[t] -> M5yb, M6y[t] -> M6yb};
EOM3 = {Eqn1c == RHSeqn1, Eqn2c == RHSeqn2, Eqn3c == RHSeqn3, Eqn4c == RHSeqn4,
       Eqn5c == RHSeqn5, Eqn6c == RHSeqn6, Eqn7c == RHSeqn7, Eqn8c == RHSeqn8,
       Eqn9c == RHSeqn9, Eqn10c == RHSeqn10} /. Parameters /. Kinematics /.
    {M1y[t] -> M1yc, M2y[t] -> M2yc, M1x[t] -> M1xc, M3x[t] -> M3xc, M3y[t] -> M3yc,
     M3z[t] -> M3zc, M4y[t] -> M4yc, M4x[t] -> M4xc, M5y[t] -> M5yc, M6y[t] -> M6yc};
Do[output[n] = NSolve[EOM /. t → (0.4 n / Iter),
    {M1y, M2y, M1x, M3x, M3y, M3z, M4y, M4x, M5y, M6y}];
 outputb[n] = NSolve[EOM2 /. t → (0.4 n / Iter),
    {M1yb, M2yb, M1xb, M3xb, M3yb, M3zb, M4yb, M4xb, M5yb, M6yb}];
 outputc[n] = NSolve[EOM3 /. t → (0.4 n / Iter),
    {M1yc, M2yc, M1xc, M3xc, M3yc, M3zc, M4yc, M4xc, M5yc, M6yc}], {n, 0, Iter}]
```

```
steps = 40;
time = 0.4;
CalcWork = 72
   (Sum[{Abs[TorqueAnkleAbduction D[AEST, t] time / steps /. t → time n / steps]}, {n, 0, steps}] +
     Sum[{Abs[D[AFST, t] TorqueAFST time / steps /. t → time n / steps]}, {n, 0, steps}] +
     Sum[{Abs[TorqueKFST (D[KFST, t] + D[HFST, t]) time / steps /. t → time n / steps]},
      {n, 0, steps}] + Sum[{Abs[
        TorqueKFSW (D[KFSW, t] + D[HFSW, t]) time / steps /. t → time n / steps]}, {n, 0, steps}] +
     Sum[{Abs[TorqueHFST (D[HFST, t]) time / steps /. t → time n / steps]}, {n, 0, steps}] +
     Sum[{Abs[TorqueHFSW (D[HFSW, t]) time / steps /. t → time n / steps]}, {n, 0, steps}] +
     Sum[{Abs[D[HRST, t] TorqueHRST time / steps /. t → time n / steps]}, {n, 0, steps}] +
     Sum[{Abs[D[POST, t] TorqueHAST time / steps /. t → time n / steps]}, {n, 0, steps}] +
     Sum[{Abs[D[POSW, t] TorqueHASW time / steps /. t → time n / steps]}, {n, 0, steps}])

ModelWork =
  (Sum[{Abs[M2y (D[KFST, t] + D[HFST, t]) time / steps /. output[n] /. t → time n / steps]},
     {n, 0, steps}] +
    Sum[{Abs[M3y (D[HFST, t]) time / steps /. output[n] /. t → time n / steps]}, {n, 0, steps}] +
    Sum[{Abs[M1x D[AEST, t] time / steps /. output[n] /. t → time n / steps]}, {n, 0, steps}] +
    Sum[{Abs[D[AFST, t] M1y time / steps /. output[n] /. t → time n / steps]}, {n, 0, steps}] +
    Sum[{Abs[M5y (D[KFSW, t] + D[HFSW, t]) time / steps /. output[n] /. t → time n / steps]},
     {n, 0, steps}] +
    Sum[{Abs[M4y (D[HFSW, t]) time / steps /. output[n] /. t → time n / steps]}, {n, 0, steps}] +
    Sum[{Abs[D[HRST, t] M3z time / steps /. output[n] /. t → time n / steps]}, {n, 0, steps}] +
    Sum[{Abs[D[POST, t] M3x time / steps /. output[n] /. t → time n / steps]}, {n, 0, steps}] +
    Sum[{Abs[D[POSW, t] M4x time / steps /. output[n] /. t → time n / steps]}, {n, 0, steps}])

ModelWork2 =
  (Sum[{Abs[M2yb (D[KFST, t] + D[HFST, t]) time / steps /. outputb[n] /. t → time n / steps]},
     {n, 0, steps}] +
    Sum[{Abs[M3yb (D[HFST, t]) time / steps /. outputb[n] /. t → time n / steps]}, {n, 0, steps}] +
    Sum[{Abs[M1xb D[AEST, t] time / steps /. outputb[n] /. t → time n / steps]}, {n, 0, steps}] +
    Sum[{Abs[D[AFST, t] M1yb time / steps /. outputb[n] /. t → time n / steps]}, {n, 0, steps}] +
    Sum[{Abs[M5yb (D[KFSW, t] + D[HFSW, t]) time / steps /. outputb[n] /. t → time n / steps]},
     {n, 0, steps}] +
    Sum[{Abs[M4yb (D[HFSW, t]) time / steps /. outputb[n] /. t → time n / steps]}, {n, 0, steps}] +
    Sum[{Abs[D[HRST, t] M3zb time / steps /. outputb[n] /. t → time n / steps]}, {n, 0, steps}] +
    Sum[{Abs[D[POST, t] M3xb time / steps /. outputb[n] /. t → time n / steps]}, {n, 0, steps}] +
    Sum[{Abs[D[POSW, t] M4xb time / steps /. outputb[n] /. t → time n / steps]}, {n, 0, steps}])

ModelWork3 =
  (Sum[{Abs[M2yc (D[KFST, t] + D[HFST, t]) time / steps /. outputc[n] /. t → time n / steps]},
     {n, 0, steps}] +
    Sum[{Abs[M3yc (D[HFST, t]) time / steps /. outputc[n] /. t → time n / steps]}, {n, 0, steps}] +
    Sum[{Abs[M1xc D[AEST, t] time / steps /. outputc[n] /. t → time n / steps]}, {n, 0, steps}] +
    Sum[{Abs[D[AFST, t] M1yc time / steps /. outputc[n] /. t → time n / steps]}, {n, 0, steps}] +
    Sum[{Abs[M5yc (D[KFSW, t] + D[HFSW, t]) time / steps /. outputc[n] /. t → time n / steps]},
     {n, 0, steps}] +
    Sum[{Abs[M4yc (D[HFSW, t]) time / steps /. outputc[n] /. t → time n / steps]}, {n, 0, steps}] +
    Sum[{Abs[D[HRST, t] M3zc time / steps /. outputc[n] /. t → time n / steps]}, {n, 0, steps}] +
    Sum[{Abs[D[POST, t] M3xc time / steps /. outputc[n] /. t → time n / steps]}, {n, 0, steps}] +
    Sum[{Abs[D[POSW, t] M4xc time / steps /. outputc[n] /. t → time n / steps]}, {n, 0, steps}])
```

Bibliography

[1] R.M. Alexander. Simple models of human movement. *Applied Mechanics Review*, 28:461–469, 1995.

[2] P. Allard, R. Lachance, R. Aissaoui, H. Sadeghi, and M. Duhaime. *Three-dimensional analysis of human locomotion*, chapter Able-bodied gait in men and women, pages 307–334. Wiley, England, 1997.

[3] F.C. Anderson and M.G. Pandy. Dynamic optimization of human walking. *Journal of Biomechanical Engineering*, 123:381–390, 2001.

[4] J.G. Andrews. *Three-dimensional analysis of human movement*, chapter Euler's and Lagrange's Equations for Linked Rigid-Body Models of Three-Dimensional Human Movement, pages 145–175. Human Kinetics, Champagne, IL, 1995.

[5] J. Apkarian, S. Naumann, and B. Cairns. A three-dimensional kinematics and dynamics model of the lower limb. *Journal of Biomechanics*, 22:143–155, 1989.

[6] H. Baruh. *Analytical Dynamics*. McGraw-Hill, Boston, USA, 1999.

[7] J.R. Borrelli. Comparison of assistive mobility devices with axillary supports. Master's thesis, University of Maryland at College Park, 2006.

[8] J.R. Borrelli and H.W. Haslach. Compensation for weak hip abductors in gait assisted by a novel crutch-like device. pages 122–126, College Park, MD, April 2010. 26th Southern Biomedical Engineering Conference.

[9] B. Bresler and J.P. Frankel. The forces and moments in the leg during level walking. *Transactions of the American Society of Mechanical Engineers*, 27:27–36, 1950.

[10] D.S. Childress and S.A. Gard. *Human Walking 3rd edition*, chapter Commentary on the six determinants of gait, pages 19–21. Lippincott Williams & Wilkins, Philadelphia, 2006.

[11] C.K. Chow and D.H. Jacobson. Studies of human locomotion via optimal programming. *Mathematical Biosciences*, 10:239–306, 1971.

[12] D.T. Davy and M.L. Audu. A dynamic optimization technique for predicting muscle forces in the swing phase of gait. *Journal of Biomechanics*, 20:187–201, 1987.

[13] P. de Leva. Adjustments to Zatsiorsky-Seluyanov's segment inertia parameters. *Journal of Biomechanics*, 29:1223–1230, 1996.

[14] P. Gonzalez de Santos, E. Garcia, and Joaqui Estremera. *Quadrupedal Locomotion*. Springer, Germany, 2006.

[15] W.T. Dempster. Space requirements of the seated operator. *Journal of Biomechanics*, 33:1405–1414, 2000.

[16] E. Dounis, G.K. Rose, R.S.E. Wilson, and R.D. Steventon. A comparison of efficiency of three types of crutches using oxygen consumption. *Rheumatology and Rehabilitation*, 19:252–255, 1980.

[17] C.M. Duffy, A.E. Hill, A.P. Cosgrove, I.S. Corry, and H.K. Graham. The influence of abductor weakness on gait in spina bifida. *Gait & Posture*, 4:34–38, 1996.

[18] C.M. Duffy, A.E. Hill, A.P. Cosgrove, I.S. Corry, R.A.B. Mollan, and H.K. Graham. Three-dimensional gait analysis in spina bifida. *Journal of Pediatric Orthopaedics*, 16:786–791, 1996.

[19] H.D. Eberhart, V.T. Inman, and B. Bresler. *Human Limbs and their Substitutes*, chapter The Principal Elements in Human Locomotion, pages 437–471. Hafner Publishing Company, New York, 1954.

[20] J. Eng and D. Winter. Kinetic analysis of the lower limbs during walking; what information can be gained from a three-dimensional model? *Journal of Biomechanics*, 28:753–758, 1995.

[21] S. Fioretti, A. cappozzo, and L. Lucchetti. *Three-dimensional analysis of human locomotion*, chapter Joint Kinematics, pages 173–209. John Wiley and Sons Ltd, Chichester, 1997.

[22] M. Garcia, A. Chatterjee, A. Ruina, and M. Coleman. The simplest walking model: Stability, complexity, and scaling. *Journal of Biomechanical Engineering*, 120:281–288, 1998.

[23] J.W. Grizzle, G. Abba, and F. Plestan. Asymptotically stable walking for biped robots: analysis via systems with impulse effects. *IEEE Transactions on Automatic Control*, 46:51–64, 2001.

[24] J. Hall and A.K. Clarke. An evaluation of crutches. *Physiotherapy*, 77:156–160, 1991.

[25] D.E. Hardt. Determining muscle forces in the leg during normal human walking-an application and evaluation of optimization methods. *Journal of Biomechanical Engineering*, 100:72–78, 1978.

[26] D.E. Hardt and R.W. Mann. A five body - three dimensional dynamic analysis of walking. *Journal of Biomechanics*, 13:455–457, 1980.

[27] H. Hatze. The complete optimization of a human motion. *Mathematical Biosciences*, 28:99–135, 1976.

[28] A.V. Hill. The heat of shortening and the dynamic constants of muscle. *Proceedings of the Royal Society of London. Series B, Biological Sciences*, 126:136–195, 1938.

[29] http://naturenest.files.wordpress.com/2008/10/skeleton.gif.

[30] V.T. Inman, H.J. Ralston, and F. Todd. *Human Walking 3rd edition*, chapter Human Locomotion, pages 1–18. Lippincott Williams & Wilkins, Philadelphia, 2006.

[31] A.T. Johnson. *Biomechanics and exercise physiology, Quantitative modelins.* CRC Press, Boca Raton, USA, 2007.

[32] H.W. Haslach Jr and J.R. Borrelli. Crutch-like mobility assist device with rotatable footer assembly using same. *US patent*, US 7581556, 2009.

[33] H.W. Haslach Jr and J.R. Borrelli. Tiltable underarm support mechanism and crutch-like mobility assist device using same. *US patent*, US 7673640, 2009.

[34] N. Khraief, N.K. M'Sirdi, and M.W. Spong. Nearly passive dynamic walking of a biped robot. Cambridge, UK, September 2003. European Control Conference.

[35] B. Koopman, H.J. Grootenboer, and J. de Jongh. An inverse dynamics model for the analysis, reconstruction and prediction of bipedal walking. *Journal of Biomechanics*, 28:1369–1376, 1995.

[36] A.D. Kuo. The six determinants of gait and the inverted pendulum analogy: A dynamic perspective. *Human Movement Science*, In press. [doi:10.1016/j.humov.2007.04.003]:1–40, 2007.

[37] P.L. Lane and R. LeBlanc. Crutch walking. *Orthopedic Nursing*, 9:31–38, 1990.

[38] H.L. Langhaar. *Energy Methods in Applied Mechanics.* John Wiley and Sons, Inc., New York, USA, 1962.

[39] M.A. LeBlanc, L.E. Carlson, and T. Nauenberg. A quantitative comparison of four experimental axillary crutches. *Journal of Prosthetics and Orthotics*, 5:20–25, 1993.

[40] A.L. McDonough and M. Razza-Doherty. Some biomechanical aspects of crutch and cane walking: The relationship between forward rate of progression, symmetry, and efficiency - a case report. *Clinics in Podiatric Medicine and Surgery*, 5:677–693, 1988.

[41] T. McGeer. Passive dynamic walking. *The International Journal of Robotics Research*, 9:62–82, 1990.

[42] R.B. McGhee and A.A. Frank. On the stability properties of quadruped creeping gaits. *Mathematical Biosciences*, 3:331–351, 1968.

[43] T.A. McMahon. Mechanics of locomotion. *The International Journal of Robotics Research*, 3:4–28, 1984.

[44] D.A. Messuri and C.A. Klein. Automatic body regulation for maintaining stability of a legged vehicle during rough-terrain locomotion. *IEEE Journal of Robotics and Automation*, RA-1:132–141, 1985.

[45] S. Mochon and T.A. McMahon. Ballistic walking: An improved model. *Mathematical Biosciences*, 52:241–260, 1980.

[46] C. Moore, L. Dias, S. Vankoski, R. Lim, and J.F. Sarwark. Valgus stress at the knee joint in lumbo-sacral myelomeningocele: a gait analysis evaluation. *Gait & Posture*, 3:109, 1995.

[47] D.A. Neumann. Hip abductor muscle activity in persons with a hip prosthesis while carrying loads in one hand. *Physical Therapy*, 76:1320–1330, 1996.

[48] D.A. Neumann. *Kinesiology of the Musculoskeletal System: Foundations for Physical Rehabilitation*. Mosby Inc, St. Lois, MO, 2002.

[49] L. Noreau, C.L. Richards, F. Comeau, and D. Tardiff. Biomechancial analysis of swing-through gait in paraplegic and non-disabled individuals. *Journal of Biomechanics*, 28:680–700, 1995.

[50] J. Nyland, T. Bernasek, B. Markee, and C. Dundore. Comparison of the easy strutter functional orthosis system and axillary crutches during modified 3-point gait. *Journal of Rehabilitation Research & Development*, 41:195–206, 2004.

[51] S. Onyshko and D.A. Winter. A mathematical model for the dynamics of human locomotion. *Journal of Biomechanics*, 13:361–368, 1980.

[52] K.A. Opila, A.C. Nicol, and J.P. Paul. Forces and impulses during aided gait. *Archives of Physical Medicine and Rehabilitation*, 68:715–722, 1987.

[53] D. Orin. Supervisory control of a multilegged robot. *The International Journal of Robotics Research*, 1, 1982.

[54] M.G. Pandy and N. Berme. Synthesis of human walking: a planar model for single support. *Journal of Biomechanics*, 21:1053–1060, 1988.

[55] M.G. Pandy and N. Berme. Quantitative assessment of gait determinants during single stance via a three-dimensional model-part 1. normal gait. *Journal of Biomechanics*, 22:717–724, 1989.

[56] M.G. Pandy and N. Berme. Quantitative assessment of gait determinants during single stance via a three-dimensional model-part 1. normal gait. *Journal of Biomechanics*, 22:717–724, 1989.

[57] M.G. Pandy and N. Berme. Quantitative assessment of gait determinants during single stance via a three-dimensional model-part 2. pathological gait. *Journal of Biomechanics*, 22:725–733, 1989.

[58] M.G. Pandy and N. Berme. Quantitative assessment of gait determinants during single stance via a three-dimensional model-part 2. pathological gait. *Journal of Biomechanics*, 22:725–733, 1989.

[59] L. Ren, R.K. Jones, and D. Howard. Predictive modeling of human walking over a complete gait cycle. *Journal of Biomechanics*, 40:1567–1574, 2007.

[60] R. Riemer, E.T. Hsiao-Wecksler, and X. Zhang. Uncertainties in inverse dynamics solutions: a comprehensive analysis and an application to gait. *Gait & Posture*, 27:578–588, 2007.

[61] G.K. Rose. Orthoses for the severely handicapped - rational or empirical choice. *Physiotherapy*, 66:76–81, 1980.

[62] M. Sankarankutty, J. Stallard, and G.K. Rose. The relative efficiency of 'swing through' gait on axillary, elbow and canadian crutches compared to normal walking. *Journal of Biomedical Engineering*, 1:55–57, 1979.

[63] J. Saunders, V.T Inman, and H.D. Eberhart. The major determinant in normal and pathological gait. *Journal of Bone and Joint Surgery*, 35A:543–558, 1953.

[64] T.E. Shoup, L.S. Fletcher, and B.R. Merrill. Biomechanics of crutch locomotion. *Journal of Biomechanics*, 7:11–19, 1974.

[65] M.W. Spong and G. Bhatia. Further results on control of the compass gait biped. pages 1933–1938, Las Vegas, Nevada, October 2003. Proceedings of the IEEE International Conference on Intelligent Robots and Systems.

[66] M. Srinivasan and A. Ruina. Computer optimization of a minimal biped model discovers walking and running. *Nature*, 439:72–75, 2006.

[67] Y. Tagawa, N. Shiba, S. Matsuo, and T. Yamashita. Analysis of human abnormal walking using a multi-body model: joint models for abnormal walking and walking aids to reduce compensatory action. *Journal of Biomechanics*, 33:1405–1414, 2000.

[68] Y. Tagawa and T. Yamashita. Analysis of human abnormal walking using zero moment joint: Required compensatory actions. *Journal of Biomechanics*, 34:783–790, 2001.

[69] A.E. Taylor. Differentiation of fourier series and integrals. *The American Mathematical Monthly*, 51:19–25, 1944.

[70] D.J. Todd. *Walking Machines: An Introduction to Legged Robots*. Chapman and Hall, New York, USA, 1985.

[71] S. Vankoski, C. Moore, K.D. Statler, J.F. Sarwark, and L. Dias. The influence of forearm crutches on pelvic and hip kinematics in children with myelomeningocele: don't throw away the crutches. *Developmental Medicine and Child Neurology*, 39:614–619, 1997.

[72] R.L. Waters, J.S. Yakura, R. Adkins, and G. Barnes. Determinants of gait performance following spinal cord injury. *Archives of Physical Medicine and Rehabilitation*, 70:811–818, 1989.

[73] E.N. Williams, N.S. Broughton, and M.B. Menelaus. Age-related walking in children with spina bifida. *Developmental Medicine and Child Neurology*, 41:446–449, 1999.

[74] D. Winter. *The biomechanics and motor control of human movement*. Wiley, New York, 1990.

[75] Q. Wu and C.Y. Chan. Design of joint angle profiles for a planar five-link bipedal system. *ASME Journal of Dynamic Systems, Measurement, and Control*, 127:192–196, 2005.

[76] C. Zhang and S. Song. Stability analysis of wave-crab gaits of a quadruped. *Journal of Robotic Systems*, 7:243–276, 1990.